Iowa State University
Digital Repository

Retrospective Theses and Dissertations | Iowa State University Capstones, Theses and Dissertations

1997

Capacitive sensor array for nondestructive evaluation applications

Amneh Moh'd Akour
Iowa State University

Follow this and additional works at: https://lib.dr.iastate.edu/rtd

Part of the Electrical and Computer Engineering Commons

Recommended Citation

Akour, Amneh Moh'd, "Capacitive sensor array for nondestructive evaluation applications" (1997). *Retrospective Theses and Dissertations*. 106.
https://lib.dr.iastate.edu/rtd/106

This Thesis is brought to you for free and open access by the Iowa State University Capstones, Theses and Dissertations at Iowa State University Digital Repository. It has been accepted for inclusion in Retrospective Theses and Dissertations by an authorized administrator of Iowa State University Digital Repository. For more information, please contact digirep@iastate.edu.

www.manaraa.com

Capacitive sensor array for nondestructive evaluation applications

by

Amneh Moh'd Akour

A thesis submitted to the graduate faculty

in partial fulfillment of requirements for the degree of

MASTER OF SCIENCE

Major: Electrical Engineering

Major Professor: John P. Basart

Iowa State University

Ames, Iowa

1997

TABLE OF CONTENTS

ACKNOWLEDGMENTS vi

CHAPTER ONE. INTRODUCTION 1

1.1 Overview 1

1.2 Probe capabilities 2

1.3 Probe configurations 4

1.4 Applications 7

1.5 Objectives 8

1.6 Organization 9

CHAPTER TWO. NUMERICAL METHOD 10

2.1 Introduction 10

2.2 Circuit model 11

2.3 Finite-difference method 13

2.4 partial capacitance's calculation 20

2.5 Field and capacitance calculations 22

2.6 Comparison with the analytical solution 23

2.8 Effect of unused conductor 28

CHAPTER THREE. EXPERIMENT SETUPS AND RESULTS 30

3.1 Introduction 30

3.2 General setup 31

3.2.1 The probe 31

3.2.1 Electronics and data acquisition system 34

3.2.1 Test fixture 39

3.2.1 The sample 40

3.3 Defining the best measurement configurations 40

3.3.1 Shielding effect 43

3.3.2 Effect of grounding the bottom metal plate 44

3.3.3 Operating frequency effect 47

3.3.4 Liftoff effect 52

3.3.5 Finger spacing effect 53

3.3.6 Finger dimensions effect 59

3.3.7 Number of fingers effect 63

3.4 Determining the thickness of a dielectric material 68

3.5 Detecting flaws in dielectrics 76

CHAPTER FOUR. DISCUSSION 93

4.1 Introduction 93

4.2 Quantitative analysis of the data 93

4.3 Comparison with measurement 98

CHAPTER FIVE. CONCLUSIONS 101

APPENDIX. SOURCE CODE OF THE NUMERICAL METHOD 106

REFERENCES 111

ACKNOWLEDGMENTS

Nobody can stand alone in a major accomplishment. There have been many people who supported, influenced and helped me to get this final product. It is very difficult to name all of those people. However, I will try to do all of my best.

I wish to express gratitude to Dr. John Basart and John Moulder for their guidance, discussions, and feedback. Their suggestions always help me to improve my performance and look for more complete pictures. They have the true ability to help instill greatness in others.

I wish to thank William Ward for his help in designing the printed circuit board capacitive sensors, and building the electronic circuit on the probes. Also I wish to thank Tauquir Khan for his help running some required software and solving some computer problems. I wish to thank the Westinghouse Company for providing the financial support for this research effort.

Finally, I want to express my warm feelings to my mother, spouse, son, and daughter for providing love, with support, and the environment in which to flourish. They always have had confidence in me, and they always encourage me. Thanks.

CHAPTER ONE

INTRODUCTION

1.1 Overview

Electromagnetic sensors come in different versions: capacitive, inductive, microwave, optics, etc. Eddy current probes (inductive sensors) have been used for decades in nondestructive evaluation (NDE) applications to detect flaws in conducting objects. Inductive probes are discussed by Rosegreen and Cooley (Bahr, and Rosegreen, 1987; Bahr, 1982; Bahr, and Cooley, 1983; Bahr, 1985). Capacitive sensors have been widely used for many decades also, but these applications have been based on extremely simple physical concepts; there has been no attempt to exploit the sophisticated sensing capabilities of generalized electric field probes. In NDE, there is a requirement to know not only how a probe behaves analytically under different probe geometry transformations, but also how a probe interacts with objects of different shapes and material properties.

Eddy current probes can not be used to detect a flaw in dielectric objects, because they are not sensitive to changes in dielectric constants. Therefore, a special technique needs to be used in this case. A number of researchers have extended the usage of the capacitive probes into sophisticated dielctric inspection applications (Auld et al., 1986; Gimple and Auld , 1989; and Shull et al., 1990). The advantages of these sensors have over their eddy-current counterpart, the inductive sensor, is their ability to interrogate

dielectric materials. In addition to inspection of insulators, capacitive probes can also detect surface features of conductive materials.

Capacitive probes can be used to investigate the properties and structures of both conductors and dielectrics. For conductors, only surface features can be extracted, charges which accumulate at the surface blind the capacitive probe to the interior structures. Dielectric materials do not present this problem. Both surface and interior features can be examined. The conventional eddy current probes can analyze sub-surface features of samples, provided the features lie within a skin depth of the surface. Capacitive probes are much less sensitive in this situation.

Studies of flaw detection probes have shown that desirable detection properties can be designed into the capacitive probes by using spatial frequency analysis to determine the optimum probe geometry for the test at hand (Auld et al., 1986). Spatial resolution in this case is determined by the geometry of the probe, rather than the electromagnetic wavelength.

The capacitive sensor is a versatile and promising device for nondestructive evaluation of dielectric materials. It responds to the complex dielectric constant of the interrogated material. The device is sensitive to both surface as well as subsurface defects in dielectric materials and to surface features in conductive materials.

1.2 Probe capabilities

The electromagnetic basis of a sensor allows for multi-parameter sensing. A probe measures electromagnetic coupling with the sample to determine the distance of the probe from an object. It measures changes in the voltage versus current characteristics at

the probe terminal to detect the existence, and the sizes, of flaws. By using differential probes, simple surface features such as edges can be detected. Finally, the changes in capacitances and resistances in known geometry samples can be used to extract material properties such as dielectric constant and conductivity.

Capacitive sensors have been used before by many researchers in the following applications: first, distance ranging, which refers to the ability to detect distance from an object without having to make any physical contact (Gimple, 1987; Gimple and Auld, 1989); second, edge detection capability, which means the ability to locate interfaces of an object and its environment (boundaries), or the ability to find and characterize discontinuities in an object's geometry or material property (Gimple, 1987; Gimple and Auld, 1989; Shull et al., 1990; Shull et al., 1988); third, response optimization which refers to the ability to change the sensor response to a given stimulus in order to enhance the detection of the desired property or feature (Gimple, 1987; Gimple and Auld, 1989); fourth, pattern matching, which is the ability to recognize a certain feature, or features, by configuring the probe to behave as a template. When the pattern is detected (or the template matches the physical feature) the total response is at an extreme (Gimple, 1987; Gimple and Auld, 1989); fifth, monitoring porosity and thickness of a dielectric material, which refers to the ability of the probe to give different responses corresponding to different thickness of the dielectric material or to different density of the material (Shull et al., 1990; Shull et al., 1988). The strategy for separating proximity and material effects in a capacitive probe for dielectric objects can be achieved by operating the probe in a

variable geometry mode; sixth, detection of surface and subsurface flaws and features in insulators (Shull et al., 1990).

1.3 Probe configurations

A common capacitive probe for NDE is essentially a parallel plate capacitor that has been unfolded so that the two plates lie in the same plane against a common substrate. Because of this, the electric field lines, rather than being uniform parallel and are now semielliptical (non-uniform). The probe is operated by feeding the voltage to one of its electrodes (source), and measuring the current from the second element (receiver). Material samples are placed in the lower half space. Changes in the measured current reflect changes in the sample or probe configuration. If we place a grounded metal sample close to the electrodes, the current around the receiver electrode to ground will be shunted, which lowers the output signal. On the other hand, dielectrics will enhance the output. They increase the capacitive coupling between the sensing electrodes without shunting a large amount of current to ground. The basic probe element is shown in Figure 1-1a, with a variation shown in Figure 1-1b. The second probe is similar to the basic element, except that the source, in this case consists of two adjacent electrode fingers excited simultaneously, and the receiver consists of the another two adjacent electrode fingers whose current outputs are added together. This probe element can be used for deeper field penetration and higher sensitivity at a given distance from the probe. It has less lateral resolution because the sample interacts with the probe over a larger distance. This behavior creates more uncertainty in determining the location of the features under examination.

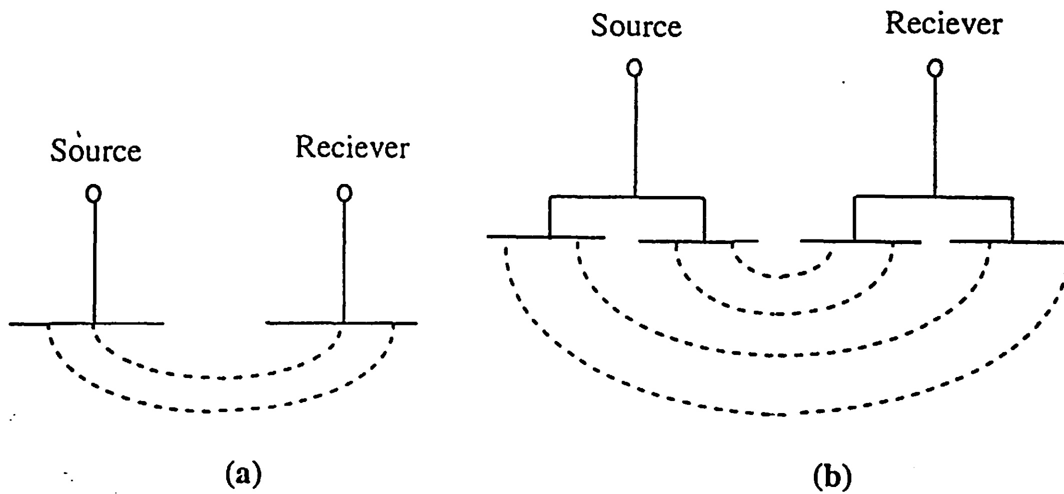

Figure 1-1 (a) 1-finger scaling (b) 2-finger scaling

All of the above probes are sensitive to both the vertical distance between the probe and the sample and horizontal displacements. Separating the two effects from each other cannot be done using a single source-receiver probe. This leads to the third type of probe element. Figure 1-2a displays an electrode configuration that makes use of multiple receivers and a single source electrode. This type of probe together with a differential electronic circuit can be used to eliminate signals from common-mode outputs. Changes that are identically effected on both sides of the differential pair similarly produce zero voltage. Only changes that asymmetrically disturb parts of the probe fields will result in non-zero outputs. The differential configuration is essentially two elementary probes connected in tandem with opposite polarity.

Figure 1-2b displays a slightly more complicated probe than the previous one. It is nothing more than a differential probe that combines two (multi) electrodes together at

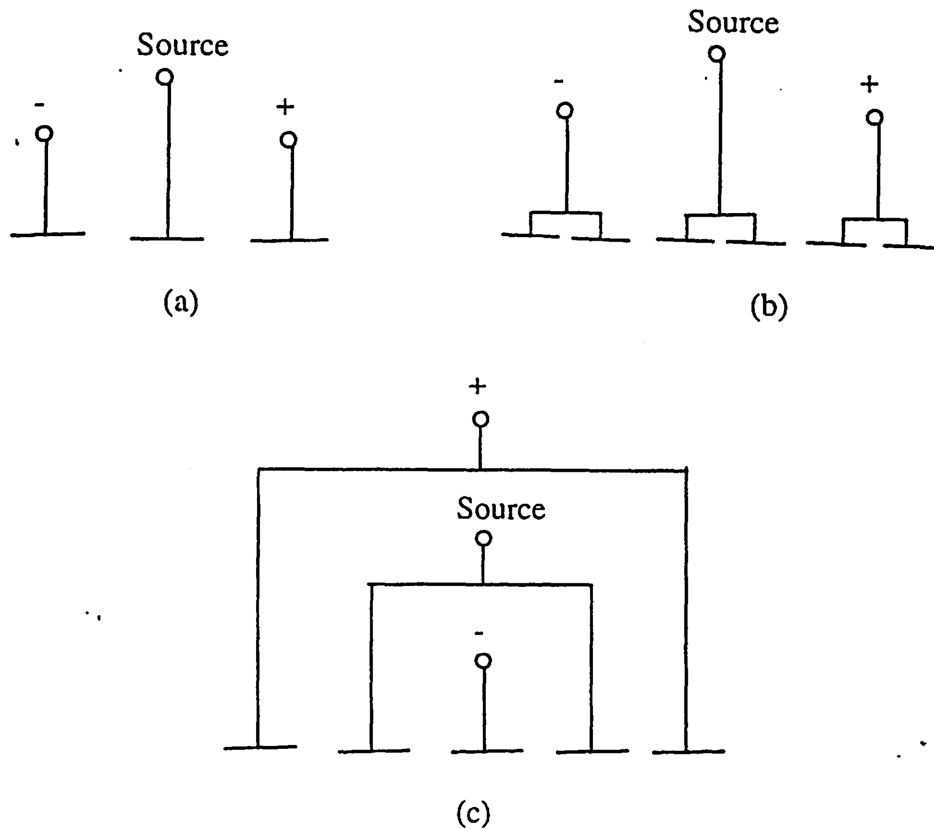

Figure 1-2 Differential probes

both the source and the receiver. It combines the two probe types in Figure 1-2a and 1-1b. Because of that, one can expect an increase in the sensitivity to distance and a decrease in the resolution in the lateral direction.

The last important variant of the simple differential probe is shown in Figure 1-2c. It is just two differential probes connected in tandem with opposite polarity. This probe can be used to look simultaneously at features (edges) that are separated in space (slot) (Gimple, 1987; Gimple, and Auld, 1989). When the spatial separation of the sample edge

matches the spatial separation of the source electrodes, the output signal will be the sum of the two signals at the edges.

The probe sensing ability can be varied by changing the number and geometry of the electrodes, and the size of the sensor. Sensitivity to liftoff, a common problem with electromagnetic sensors, can be reduced by operating the probe in a differential geometry (Shull et al., 1990). In this mode the probe can detect variations that are small in size compared with the probe's sensing area. Although this probe can reduce the effect of the liftoff problem, it reduces the probe sensitivity to a slowly varying parameter. Because of this, we need to connect the probe in the absolute mode (Figures 1-1a, 1-1b) to use it as a proximity sensor or to detect changes in material properties, such as varying thickness, porosity, or dielectric constant. The difficulty with operating in this mode is the extreme sensitivity to liftoff.

1.4 Applications

Capacitive sensors are used in many applications: robotic sensing, nondestructive evaluation (NDE), etc. The most important applications of using the capacitive sensor in the robotics area are in locating the presence and the nature of an object (Gimple, 1987). Gimple mentioned that one advantage of using capacitive sensors is that they are not easily fooled by apparently large imperfections caused by surface effects.

In NDE, the capacitive sensor can provide information about the surface and sub-surface regions of a dielectric material. It also provides information about surface features of conductors. The most important applications of this ability are in monitoring the curing process of epoxy, or the doping a semiconductor. Also, using these sensors,

we can detect surface or sub-surface flaws in a dielectric material. This sensor can be used to detect variations in the thickness or the density of dielectrics. We use these characteristics of the sensor to monitor the integrity of ceramic coatings used in turbines.

1.5 Objectives

The main objective of this research is to study various applications of capacitive sensors for dielectric measurements. We also developed a numerical model for application of the sensor to thickness measurement. The finite difference method was used to develop the numerical model. The effect of various factors in the measurement setups and environment on the response of the sensor were studied. Also, various factors have been studied in designing the probes. These factors affect the output response of the sensor. A technique was developed to determine the thickness of a dielectric material. We used the sensors to detect different types of flaws (surface or subsurface) in a dielectric material. A technique based on the convolution idea was developed to determine the width and the length of slots. Finally, some image restoration techniques were used to restore image obtained from the sensor. Restored images were used to improve estimates of the width and the length of slots.

Most of the research done on capacitive sensors by previous investigators was oriented towards robotic sensing or general NDE applications. In some of this work numerical codes were developed to model the response of this sensor in the presence of flaws using the finite element method, but no models were developed for thickness measurements. Part of the research in NDE was focused on the response of capacitive

sensors in the presence of flaws, but the response was not explained nor were images studied to determine the width or length of cracks or slots.

1.6 Organization

Chapter two discusses a numerical model of the sensor for thickness measurements. It also describes a circuit model for the sensor and the effect of unused fingers in measurements. Chapter three summarizes the most important experimental results we obtained in different areas: studying the effect of different factors on the design of the sensor and in the experimental setups, using the sensor to measure the thickness of dielectrics, using the sensor to detect the presence of a flaw and gauging the dimensions of this flaw. Chapter three also compares experimental results with theory and explains these results. Chapter four discusses some important quantitative results. Finally Chapter five discusses the important conclusions of this work and directions for future developments.

CHAPTER TWO

NUMERICAL ANALYSIS

2.1 Introduction

The most general application of the capacitor sensor uses a parallel plate capacitor that has been opened up so that the two plates lie in the same plane, against a common substrate. Finding a closed form solution for this case, in which all values of the problem parameters can be substituted, is not an easy task. The analytic solution provides the guiding equations, but the numerical solution can provide real quantities. Therefore it is important to develop a numerical model of the sensor that represents the probe's behavior efficiently and correctly because of the number of variables available to tailor the capacitive probe to meet a required applications. This model and the results based on numerical methods have many important uses: they can minimize the spent time in testing a prototype probe, can be used for quantitative comparisons with experimental results, and the numerical and the experimental results can be combined to form a hybrid method of analysis that could be used to determine certain properties of the required material.

In our applications, the capacitor sensor has been used in two major areas. First, it is used to determine some important properties of a dielectric material such as thickness, dielectric constant, and porosity. Second, it is used to detect the presence of a flaw or step change in the dielectric material. The analytic solution in chapter two can provide a good prediction on the behavior of the sensor in the presence of a flaw, but this solution can not predict the behavior of the sensor with an inhomogeneous dielectric material. Therefore,

a numerical solution developed in this research is used to demonstrate the behavior of the capacitor sensor under changing dielectric thickness and geometry.

The particular system that has been examined in this case is a single finger electrode as shown in Figure 3.1, in which one finger is connected to a source and the second finger is connected to a receiver. Also a system of three fingers has been studied in two cases. The first case was connecting the first finger as a source and the third finger as a receiver, while keeping the middle finger floating. The second case was connecting the first and third finger as before, but fixing the voltage on the middle finger to a certain potential which has been calculated from the numerical solution. This system has been examined to check the effect of the left finger placed between the active ones.

2.2 Circuit model

The fundamental operations of the probe sample system can be described by looking at the circuit model of the basic source-receiver-sample system. This model is displayed in Figure 2-2. There are mainly four capacitor components representing the capacitive coupling in the system (Gimple, 1987). These are the capacitive coupling between the source and the receiver, C_{SR}, between the source and the bottom metal plate of the sample, C_{SD}, between the receiver and the bottom metal plate, C_{RD}, between the bottom metal plate and the ground, C_{DG}. The variability of C_{DG} is not due to the change in the dielectric thickness, but it is due to the change in the grounding environment, i.e. the connecting wire with the ground, the connectivity between the grounding wire and the bottom metal plate, etc. The variability in the other coupling capacitances (C_{SR}, C_{SD}, C_{RD}) and is due to the change in the thickness of the dielectric material. The coupling

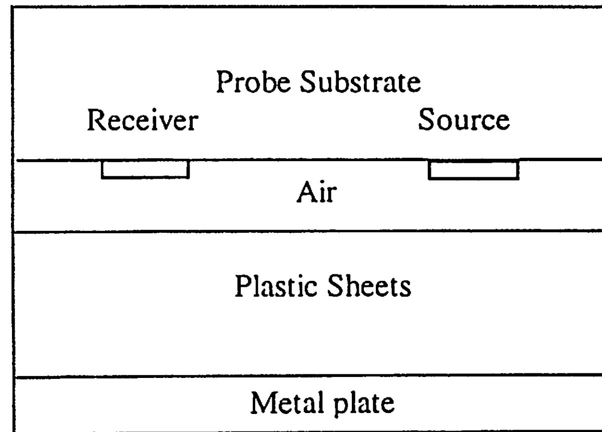

Figure 2-1. Basic numerical field geometry for probe-sample system

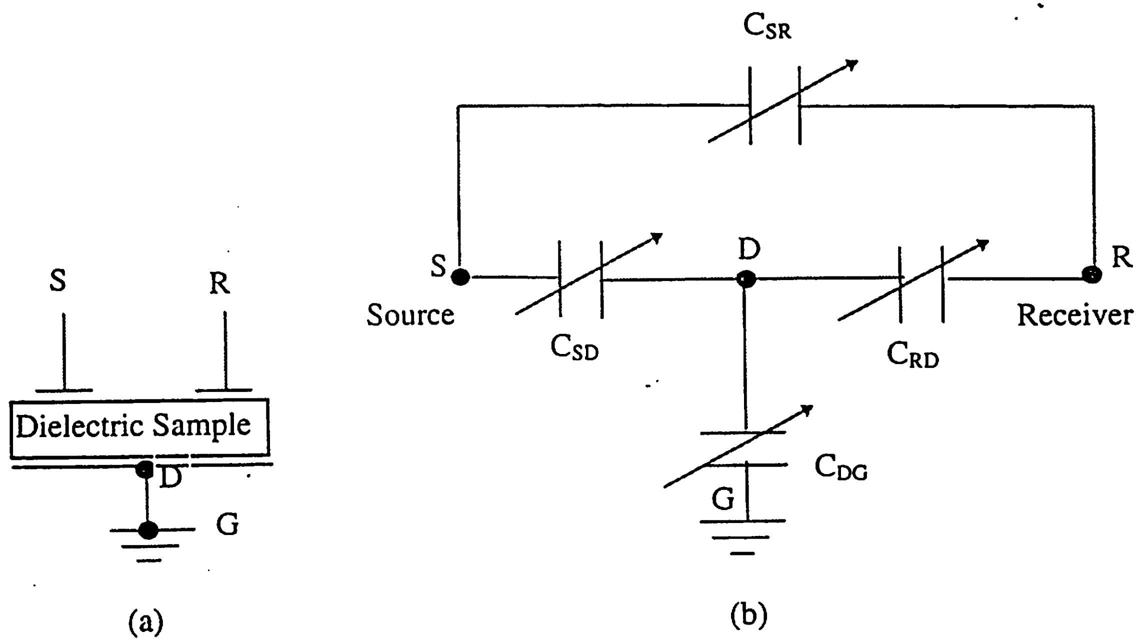

Figure 2-2. Circuit model for a source-receiver-sample system

capacitance between the two electrodes and the ground have been neglected, because they do not have any effect on the output signal assuming that the voltage source and the current meter for the impedance analyzer are near the ideal (Gimple, 1987).

The numerical solution to be discussed later will examine the behavior of the probe-sample system by determining the quality of the effect of each of the capacitors in the circuit model. Then the total response will be calculated as a combination of all of them.

2.3 Finite - difference method

The finite difference method is a simple numerical technique used in solving partial differential equations. The main equation used for solving the fields for the electrodes is the Laplacian. The main step to find the solution by finite-difference method is based on finding field values at discrete points spaced in an ordered way over the whole field region of the function describing the field. The one partial differential equation of the field (Laplace's equation) has been replaced by many simple finite difference equations which take the form of linear equations connecting the potential at each point with the potential at its neighboring points (Binns and Lawrenson, 1973; Sadiku, 1989). The field value at each grid point can be obtained by solving a set of simple simultaneous algebraic equations for potential values.

Of the many techniques available, the square or rectangular mesh or network was chosen. In this case, the five star iterative network was used, Figure 2-3 shows the five star geometry. From the general form for an asymmetrical star, the difference equation for

the potential at the center of certain special star like the square or rectangle was calculated (Binns and Lawrenson, 1973).

The grid used in this calculation has its node points separated by 2 mils in the horizontal direction and by a range of separation from 0.5 mils to 4 mils in the vertical direction. The grid size was determined by repeating the experiment different times and studying the change in the capacitance value in each case. When the difference was less than a certain amount, we stopped decreasing the grid size. The small vertical separation of the nodes is used for all nodes on the sample and up to a point 10 mils above the electrodes. The vertical node spacing doubles for every 20 rows of node points from there on. This variable vertical spacing was used to decrease the computation time and improve the accuracy of the calculated values. The accuarcy improved by using small spacing in the area of a large variation and small steps when the variation is slight.

The finite difference method was used to solve Laplace's equation $\nabla^2\Phi = 0 = \frac{\partial^2\Phi}{\partial^2 x} + \frac{\partial^2\Phi}{\partial^2 y} + \frac{\partial^2\Phi}{\partial^2 z}$. This 3D equation can be changed to a 2D equation by assuming that we have a constant Φ in the z direction. Laplace's equation is valid in static fields. Because we used a frequency with large wavelength campared with the diemnsions of the whole sytem, we can approximate the field in our case as a static field. The general finite difference form of asymmetrical star used to solve Laplace's equation (Binns, and Lawrenson, 1973) can be written as

$$\frac{\Phi_1}{p(p+r)} + \frac{\Phi_2}{q(q+s)} + \frac{\Phi_3}{r(p+r)} + \frac{\Phi_4}{s(q+s)} = \left(\frac{1}{pr} + \frac{1}{qs}\right)\Phi_0 \qquad (2.1)$$

where p, q, r, and s are the distance from points 1, 2, 3, and 4 to the origin 0, respectively. and Φ_o, Φ_1, Φ_2, Φ_3, Φ_4, are the corresponding potentials at the points 0, 1, 2, 3, and 4 respectively. For the points that are centered on a uniform square mesh, the distances becomes $p = q = r = s$, therefore the difference equation reduces to

$$\Phi_0 = \frac{1}{4}(\Phi_1 + \Phi_2 + \Phi_3 + \Phi_4) \tag{2.2}$$

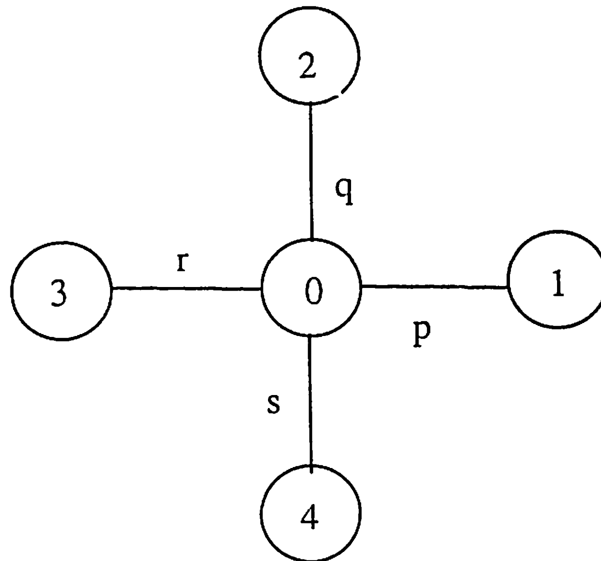

Figure 2-3. The star geometry used for finite difference calculations

For the points that are equally spaced in a rectangular mesh, the difference equation for node 0 is obtained by putting $p = r$, $q = s$. The potential at 0 can be calculated using

$$\Phi_0 = 0.5(\frac{q^2+1}{q^2})(\Phi_1 + \frac{\Phi_2}{q^2} + \Phi_3 + \frac{\Phi_4}{q^2}) \tag{2.3}$$

For the points that are centered at non-uniform stars for which $p = r$, and $q \neq s$, the potential at 0 equals:

$$\Phi_0 = \frac{AB}{1+AB}\left(\frac{\Phi_1}{2} + \frac{\Phi_2}{A^2+AB} + \frac{\Phi_3}{3} + \frac{\Phi_4}{B^2+AB}\right) \tag{2.4}$$

where

$$A = \frac{q}{p}, \quad B = \frac{s}{p}$$

For points at the boundary of the dielectric sample and the air due to the liftoff distance that the probe had when we did the measurements as shown in Figure 3.1, the following implementation was used (assuming a uniform legged star pattern) (Binns and Lawrenson, 1973; Ferziger, 1981; Gimple, 1987).

$$\Phi_0 = \frac{1}{4}\left(X\Phi_1 + \Phi_2 + Y\Phi_3 + \Phi_4\right) \tag{2.5}$$

where

$$X = \frac{2\varepsilon_r}{1+\varepsilon_r} \quad \text{and} \quad Y = \frac{2}{1+\varepsilon_r}$$

The sample used for the calculation consists of polyester plastic sheets placed on a metal plate. The average thickness of each plastic sheet is 4.01 mils. The electrode fingers are 66.67 mils in width, 66.67 mils in spacing, and 355.2 mils in length. The relative dielectric constant of the plastic sheets is 2.3. The voltage source is set to 1 volt for normalization purposes. The metal plate under the plastic sheets is set to 0 volts. The plastic sheets and the metal plate in our numerical model are assumed to be infinite in width, and the metal plate is assumed to be a perfect conductor. These two assumptions approximate the actual system, but not model it exactly. Figure 2-1 displays the basic geometry field with the electrodes and sample shown.

The sample was scanned from the northwest corner to the southeast corner using the Gauss-Siedel method (Binn and Lawrenson, 1973). In this method, the potential at 0 is calculated using the values for the north and west points that had just been previously calculated in the present scan, meanwhile we used the old values from the previous scan for the south and east points. This kind of method requires less memory and speeds up convergence (Binns and Lawrenson, 1973). The new calculated value is substituted the for old value without violating the boundary conditions. The first boundary condition assumed in our case was that the potentials at the points which are far away from the probe or at infinity, equal zero. The second boundary condition was that the potential of the two fingers and the bottom metal plate were fixed to a constant value at every point on them (conductors are equipotential surfaces). The degree of accuracy of the values is measured by the residuals at the nodes. The residual R_0 at node 0 is the amount by which the calculated potential at this node fails to get a constant number which is equal to the actual voltage at this node, and is given by

$$R_0 = V_n - V_0 \tag{2.6}$$

where V_n = new potential calculated by one of the above equations

V_0 = old potential (from the previous scan)

The potential at node 0 is modified by the new calculated value from one of the above equations (2.2, 2.3, 2.4, 2.5) so as to relax (or reduce) the residuals at that node. The relaxation process is repeated at each node and the whole grid is iterated several times until the residuals at any point in our system is reduced to zero or to a sufficiently small value.

The accuracy of the method depends on the fineness of the grid and the amount of time spent in refining the potentials. The computer time can be reduced and the accuracy and the convergence rate can be increased by using the method of successive over relaxation (Binns, and Lawrenson, 1973), by making reasonable guesses of initial values, by taking advantage of symmetry if possible, and by using more complex finite difference methods.

In solving the finite-difference equation, the technique is to continually modify values of potential until all the equations are satisfied to a sufficient degree of accuracy. To increase the rate of convergence of the solution while keeping the equation as simple as possible, the successive over-relaxation (SOR) version of the Gauss-Siedel algorithm has been used (Binns and Lawrenson, 1973). SOR is the most flexible and useful of the rapidly convergent iterative methods. In this case, the new value of potential has been determined as the sum of the old value and α times the difference between the calculated value and the old value. That is,

$$\Phi_0 = \alpha(V_n - V_0) + V_0 \qquad (2.7)$$

$$= \alpha V_n + (1-\alpha)\, V_0$$

where α is a convergence or relaxation factor between 1 and 2 that determines the degree of over-relaxation.

When $\alpha >> 2$ the process becomes unstable. For convenience a value for α of 1.5 was chosen to insure stability. There are a number of other rapidly convergent methods which have been more recently used (Binns, and Lawrenson, 1973), but the SOR method is the best because of its simplicity, flexibility, and relatively rapid rate of convergence.

The boundary elements have initial conditions of zero potential at all points except at the points corresponding to the capacitor plates and the bottom metal plate. The boundary values are chosen as a compromise between computing time, storage requirements, and accuracy of the solution. The number of iterations K, required for the reduction of the largest error at any node to a fraction ε of some previous value, is in general a function of the boundary shape and conditions, the number of nodes, the particular type of difference equation, and the convergence factor. Convergence is determined for the base cases by examining the behavior of three test points. For every iteration, we calculated the residual at each point. When these residuals were reduced to about 0.1 per cent of the mean value of the potentials, the algorithm is terminated. We reduced the complexity of the program by making runs with small incremental changes at a fixed iteration count. As an example, we modeled the parallel plate capacitor with plate area 0.1 m^2 and plate spacing 0.01 m by a grid of size 0.1 mm, and with fixed potentials of 1 volt at the upper plate and 0 volt at the lower plate. We found that by doubling the number of grids, the change in the calculated capacitance did not exceed 0.1 % of the value calculated before (without doubling), but it more than doubled the execution time. We also found that 200 iterations is a good number in this case. Increasing this number by 50 iterations did not change the calculated capacitance by more than 0.07 %. According to our experiments, we found that more iterations were required if the number of grids increased.

2.4 Partial Capacitance Calculation

The measured admittance is directly proportional to the total capacitance between the plates under measurements. The admittance value varies as the total capacitance is changed. To determine this capacitance, the partial capacitance has been used (Boast, 1956). For a system of three conductors as shown in Figure 2.1, with the metal plate as a reference potential node (0), the two charges upon the source and the receiver conductors can be written as :

$$Q_R = B_{RR}\Phi_{0R} + B_{RS}\Phi_{RS} \quad (2.8a)$$

$$Q_S = B_{SS}\Phi_{0S} + B_{SR}\Phi_{SR} \quad (2.8b)$$

where the coefficients B_{RR} , B_{SS} were called by Maxwell the coefficients of capacitance, and B_{RS}, B_{SR} the coefficients of induction (Boast, 1956). Φ_{OR} , Φ_{OS} : are the potentials between the receiver and the reference (bottom metal plate), and between the source and the reference respectively. Q_R ,Q_S : are the charges on the receiver and the source respectively.

To determine the value of these coefficients, the above equation can modified as

$$Q_R = B_{RR}\Phi_{0R}|_{\Phi_{RS} = 0} \quad (2.9a)$$

$$Q_R = B_{RS}\Phi_{RS}|_{\Phi_{0R} = 0} \quad (2.9b)$$

$$Q_S = B_{SS}\Phi_{0S}|_{\Phi_{SR} = 0} \quad (2.9c)$$

$$Q_R = B_{SR}\Phi_{SR}|_{\Phi_{0S} = 0} \quad (2.9d)$$

Then from the above equation one can calculate the value of the coefficients, if the values of the charges and the potentials are known. If Q_S/Φ_{RS} is called the partial capacitance between

source and the receiver, then Q_S/Φ_{RS} is called the partial capacitance between the source and the receiver conductors, and B_{RS} is the negative of this partial capacitance. Consequently, Maxwell's Coefficients of induction B_{RS} and B_{SR} are identical. The interpretation of Maxwell's coefficients of capacitance and induction gives the partial capacitance , then

$$C_{0S} = B_{SS} + B_{SR} \tag{2.10a}$$

$$C_{0R} = B_{RS} + B_{RR} \tag{2.10b}$$

$$C_{RS} = -B_{RS} \tag{2.10c}$$

$$C_{SR} = C_{RS} \tag{2.10d}$$

where C_{0S}, C_{0R} is the partial capacitance between the reference and the source and between the reference and the receiver, respectively. While C_{RS}, or C_{SR} is the partial capacitance between the source and the receiver. By using the partial capacitance method, all of the capacitances in the system can be determined. To calculate the partial capacitance in our case between the source and the receiver conductors C_{RS}, or C_{SR} with plate spacing of 0.01m, we ran our program with zero potential for the receiver conductor and the bottom metal plate, and 1 volt for the source conductor. The calculated Q_R (330.54 pC) corresponds to the coefficient B_{RS} which equals in this case the partial capacitance C_{RS}, and the value of Q_S (83.32 μC) corresponds to the coefficient B_{RR}. To find the total capacitance of the source conductor, we need to add the two coefficients: B_{RS} and B_{RR}. We can repeat the same procedure for the receiver conductor by fixing the source conductor at zero volts and the receiver conductor at 1 volt. We get the same partial capacitances.

2.5 Field and capacitance calculations

The total capacitance of any conductor (receiver or source) is determined by calculating the total flux entering (or leaving) the conductor per unit potential difference between it and all neighboring conducting parts (Binns and Lawrenson, 1973). For the relaxation solution, the potential of the conductor is conveniently set at 1 volt, whilst the remaining conductors are set at zero.

The total flux Φ_e is calculated by integrating the normal component of flux density, determined from the potential gradient, a round a suitable contour enclosing the conductor.

$$\mathbf{E} = -\nabla V = -(\frac{\Delta V}{\Delta x}\hat{i} + \frac{\Delta V}{\Delta y}\hat{j}) \quad (2.11)$$

$$\Phi_e = \oint \mathbf{D} \bullet ds = \varepsilon \oint \mathbf{E} \bullet ds \quad (2.12)$$

$$Q = \int \rho dv = \Phi_e \quad (2.13)$$

where Q is the total charge enclosed by the surface through which the flux is flowing. The contour was chosen to avoid regions with large gradients. A rectangular contour was chosen in the calculation for simplicity. Figure 2-4 shows a simple example of the path used to calculate the capacitance for a parallel plate capacitor. If Φ_i is the potential at the node just inside the contour, and Φ_o is the potential at the adjacent node just outside it, the normal potential gradient on the contour is $(\Phi_i - \Phi_o)/h$ (assuming the same grid size in both vertical and horizontal directions). Thus, if $\varepsilon_r\varepsilon_o$ is the permitivity of the insulating

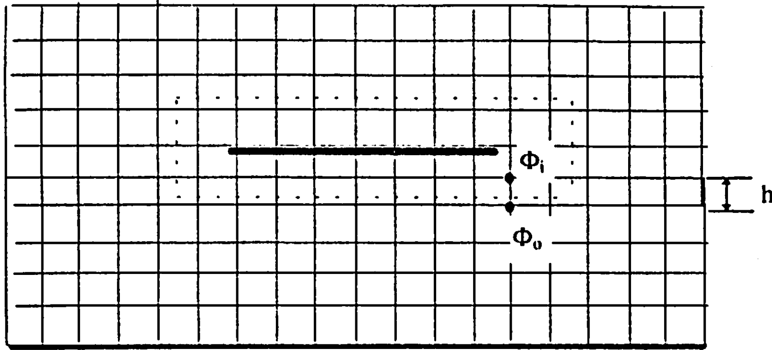

Figure 2-4. Calculating the capacitance of the parallel plate capacitor

material and N is the number of meshes cutting the contour (in the example shown in Figure 2-4 equals N 26 points: 20 points from the horizontal crossing on both sides of the contour and six points from the vertical crossing on both sides of the contour) , the total flux is

$$\Phi_e = \varepsilon_r \varepsilon_o \sum_{n=1}^{N} (\Phi_i - \Phi o) \qquad (2.14)$$

(assuming the gradient is constant over a mesh length h), and the capacitance is

$$C = Q\,/\,\Delta V = \Phi_e\,/\,\Delta V \qquad (2.15)$$

where ΔV= difference in the potential between the two conductors (source and receiver).

2.6 Comparison with the analytical solutions

As a check of the numerical solution code, a parallel plate capacitor was modeled and tested. The analytical solution of the parallel plate capacitor is determined by $C=\varepsilon A/d$, where A is the area of the plate, d is the separation between the two plates. This formula for the parallel plate capacitor neglects the fringing effect of the electric field. Using the numerical solution code, the parallel plate capacitor has been tested for different

plate areas (0.025 to 0.125 m^2) and for different spacings between the plates (0.01 to 0.05 m). The size of grid used in this program was fixed at 0.1 mm, while the number of iterations varied, according to the total number of grids required to model each case, from 200 (in the case of 0.01m spacing) to 600 (in the case of 0.05m spacing). In all cases the upper parallel plate was fixed at 1 volt and the lower parallel plate was fixed at 0 volts. We ran the program on the DEC station 5000. The execution time varied from 6 hours (at 200 iterations) to 18 hours (at 600 iterations). Table 2-1 summarizes these results.

From Table 2-1, it is noticed that the calculated capacitance using the numerical solution is always a little bit higher (in the maximum case equals 3.62%) than capacitance using the analytical formula. This increase is due to the fact that the analytical formula neglects the fringing effect, but the numerical code calculates the capacitance using the total charge without neglecting the fringing effect. Using the results tabulated in this table, the effect of increasing the area of the two plates and the spacing between the two plate has been studied. Figures 2-5, 2-6, 2-7, and 2-8 study this relation.

We see in Figure 2-5 that the analytical solution is a straight line because the relationship between the area and the capacitance using the analytical formal is completely linear, but the numerical capacitances deviate a little bit from the straight line. This is because the numerical solution takes care of the fringing effect and does not assume linearity. We noticed also from Table 2-1 that the difference, between the capacitance calculated using the analytical formula and the one calculated using a numerical solution as the area increases is due to some numerical errors. From Figure 2-7 we notice that the

Table 2-1. Comparison between analytical and numerical solution of the parallel plate capacitor

Plate area (m^2)	Plate spacing (m)	Analytical C[a] (pF)	Numerical C[b] (pF)	Percentage of [c] error
0.1 x 1	0.01	327.44	330.54	0.95
0.1 x 1	0.02	163.72	165.41	1.03
0.1 x 1	0.03	109.15	111.1	1.79
0.1 x 1	0.04	81.9	84.58	3.27
0.1 x 1	0.05	65.49	67.86	3.62
0.125 x 1	0.01	409.5	412.25	0.67
0.075 x 1	0.01	245.7	246.67	0.39
0.05 x 1	0.01	163.8	164.76	0.59
0.25 x 1	0.01	81.9	82.49	0.72

[a] Calculated capacitance using the analytical formula $C=\varepsilon A/d$

[b] Calculated capcitance using the numerical program with 1 volt at the upper plate and 0 volt st the lower plate, the grid size used was 0.1 mm. The number of iterations varied according to the number of grids used to represent each case.

[c] Percentage of error =[(|Analytical C - Numerical C|)/Analytical C] * 100%.

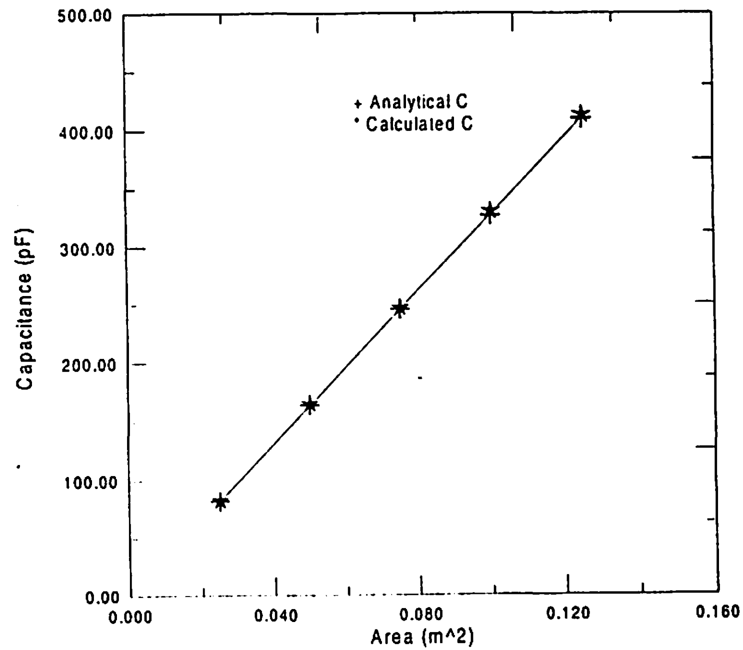

Figure 2-5. Effect of the area of the two plates

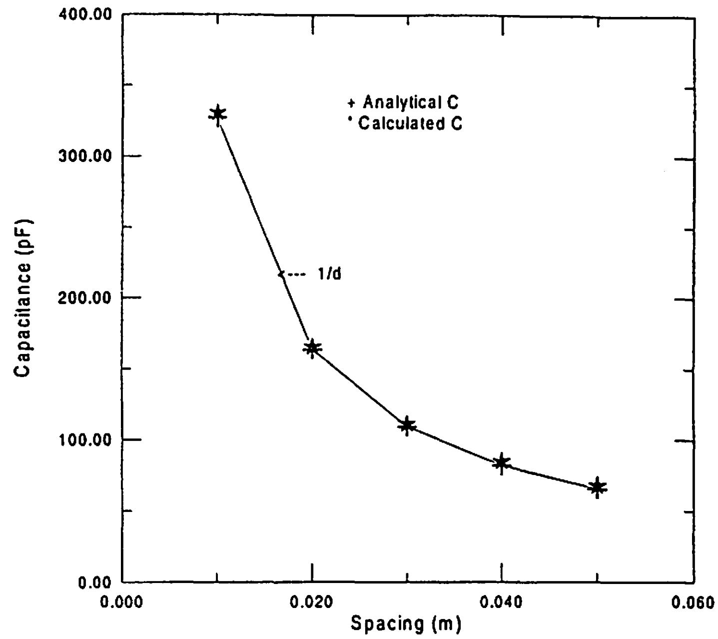

Figure 2-6. Effect of changing the spacing between the two plates

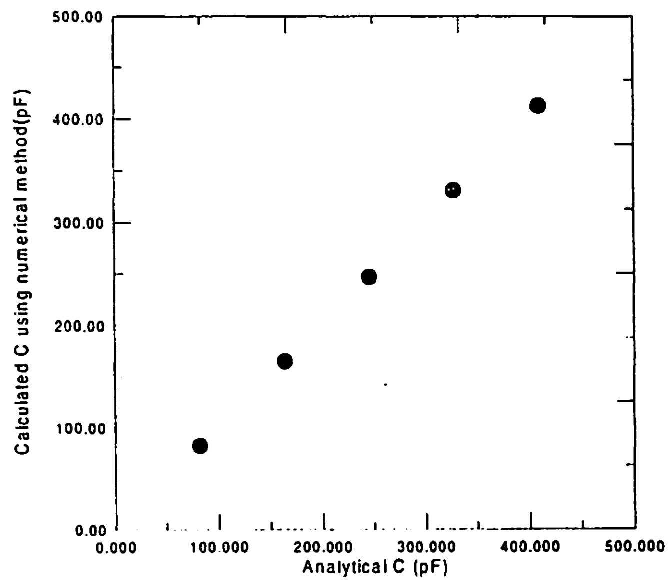

Figure 2-7. Analytical capacitance vs. calculated capacitance using the finite difference method at different plate areas.

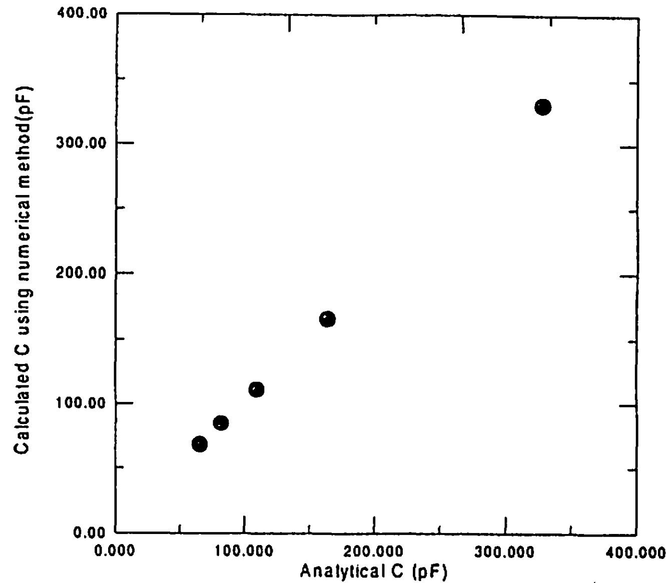

Figure 2-8. Analytical capacitance vs. calculated capacitance using the finite difference method at different plate spacing

relationship between the analytical capacitacnes and the calculated capacitances from numerical solution at different areas is close to a straight line of slope 45°. This indicates that the numerical values approximate the analytical ones very closely. From Figures 2-6 and 2-8, we see that the calculated capacitance from the analytical solution is close to the 1/d curve expected from the analytical relation. We noticed also from the table that the difference between the analytical values and the numerical ones increases as the spacing increases. This is consistent with the neglect of fringing in the analytical case. Also from Figure 2-8, we can get the same relationship we observed from Figure 2-7 between the analytical values and the numerical values at different plate spacing. This kind of behavior can be improved, and this difference can be decreased to the minimum, if the number of iterations increases to improve the accuracy. This solution increases the execution time very much. For example, if we increase the number of iterations by 50

iterations in the case of 0.1 m^2 plate area and 0.05 spacing between the plates, the execution time may increase by more than three hours.

2.7 Effect of the unused conductor

One of the most important steps in making measurements with a capacitive probe is repeating the measurements for different spacings between the source finger and the receiver finger. This can be achieved by using the first finger as a source, then leaving one finger unconnected, then connecting the third finger as a receiver. This is illustrated in Figure 2-9. The spacing between the source and receiver in this case is the sum of the spacing between the left finger and the central one plus the spacing between the right finger and the central one plus the width of the central finger. All fingers have constant potential, i.e. they are equipotential surfaces.

The effect of this central conductor on the value of the capacitance of the probe was calculated numerically with and without fixing the potential on this conductor. The source code of the numerical program was modified to take into consideration this situation. Firstly, we ran the program as usual, so this means that the voltage of the central finger was not fixed. It was found that the value of the capacitance without fixing the potential on this conductor equals 419.4 pF. Secondly, we ran the program with a fixed potential on the central conductor by forcing the potential of all grids related to this conductor to be equal to a calculated value from the program at the first grid point on this conductor. The value of the capacitance when the potential of this conductor was fixed was 418.7 pF. The difference between the two cases is 0.7 pF. Because of the small difference in the two cases we can conclude that there is little effect on the value of the

capacitance of the probe if the potential on the central conductor is not fixed to a certain potential. All of the codes used in this chapter are summarized in Appendix A.

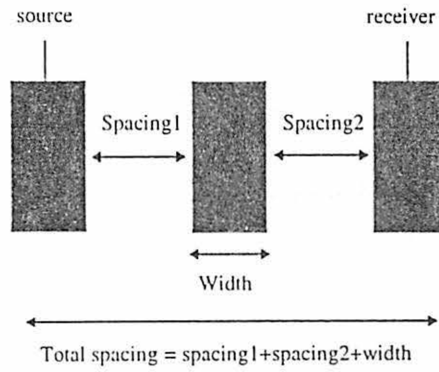

Figure 2-9. Changing the spacing between fingers

CHAPTER THREE

EXPERIMENTAL SETUPS AND RESULTS

3.1 Introduction

In our research we used the capacitive probe in various applications each of which required a different experimental setup. Experimental setups in all applications have four major elements. The first is the probe itself. The probe is the active element in the system. After being excited by a source signal, it converts the source signal into an output signal that is a function of the position, physical surface features, and the material properties of the sample.

The second element is the electronics circuits and the data acquisition system. In some applications, we found that the signal was very noisy and weak. In this case, we amplified the output signal directly before doing any kind of processing. We built an electronic circuit to convert the signal to a usable output. Then following this electronic circuit, we used an HP 4194A Impedance/Gain-Phase Analyzer to measure the output signal. This instrument provided a source signal for the probe. In some applications, a computer was used to capture the data and control both the impedance analyzer and the motor motion. The computer kept synchronization between the motor motion and the measuring system, and recorded both the position of the probe and the corresponding measured value.

The third system component is the text fixture. This is a mechanical device that physically holds the sample and the probe together in a proper orientation and location. It

consists of a test bed and a motor. The motor controlled the motion of the probe. The fourth experemental component is the sample itself.

Overall, the system was built for many purposes: Studying the effect of changing parameters in the probe or the surrounding setups, determining the thickness of the dielectric material, detecting the change in the thickness of the sample, and detecting different types of surface or subsurface features. For this reason, we built our probe with a large degree of freedom to allow the probe to move over the sample in both the x and y directions at a controllable height z. In addition to that, we found that examining pure surface or subsurface features requires determining the distance from the probe to the sample.

In the next section, we discuss the general setup for each of the above four elements. At the beginning of each result section, we mention the specific setups for each element. In section 3.3 we discuss the effect of certain parameters in the designing of the probe or in building the measurement system. In section 3.4, we discuss the use of the probe to determine the thickness of a dielectric material. In section 3.5, we discuss the use of the probe to detect the change in the thickness of the dielectic material. In the last section, we discuss the most popular application of the probe to detect different types of flaws or features.

3.2 General setup

3.2.1 The Probe

In all of our experiments, we used a capacitor probe in two modes: an absolute mode and a differential mode. We built two different types of probes: the interdigitized

(ID) probes and the square directional (SD) probes. The ID probes consist basically of electrode strips in parallel separated uniformly from each other on a dielectric substrate. At the beginning of our research we built prototype probes of the ID type and used them to study the effect of different factors on the output signal and to test the capabilities of the capacitive probe. We Then used printed circuit board (PCB) technology to build new probes from the two types. With PCB technology we can build probes with smaller sizes and smaller spacing between the fingers. These new probes are more flexible when connecting and moving.

Figure 3-1a shows the basic ID probe. In contrast, the SD probes shown in Figure 3-1b consist basically of a square conductor surrounded by four electrodes. The SD probe was used to detect different types of flaws. It is assumed that this probe can detect any flaw in any direction due to the presence of the two pairs of opposite electrodes. The use of this type of probe have not been previously reported in this literature. The inside square was driven by the source signal, while the opposite pair of the electrodes was connected as a differential receiver.

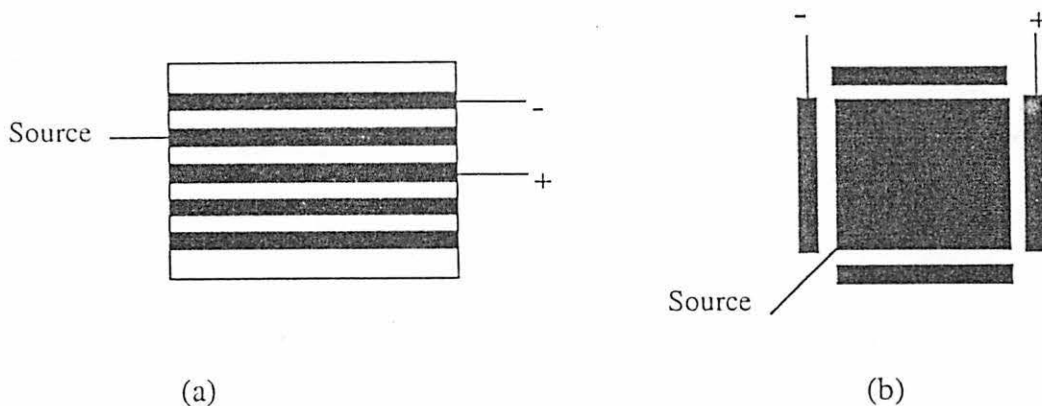

Figure 3-1. (a) Basic interdigitized probe (b) Basic square directional probe

The probes were labled in a manner that gives the user or reader complete dimension information about the probe used. The interdigitized probes were designed the probe with an equal space between the fingers, with the width of the finger and the space between the finger in the permanent probes, the same. Table 3-1 summarizes the names we used for the ID probes. The center column contains a descriptive name with dimensions as specified in the footnote. The SD probes were built with equal lengths of the square sides of the source and the receiver electrodes. Table 3-2 summarizes the naming criteria for the SD probes. The center column also contains descriptive dimensions as specified in the footnote. For the prototype probes, we used only the ID type of the same general geometry as the one shown in Figure 3-1. We had two types that differed in length. The longer one was of length 8.88 mm, while the shorter one was of length 6.96 mm. The widths of the fingers in both cases was 1.67 mm.

Table 3-1. Naming the interdigitized probes

Description	Complete Name[a]	Common Name
8mil, 15 fingers	ID-8-8-200-15	ID-8
20mil, 15 fingers	ID-20-20-500-15	ID-20
40mil, 15 fingers	ID-40-40-1000-15	ID-40

[a] ID-finger width-space between fingers-finger length-number of fingers (dimensions in mils)

Table 3-2. Naming the square directional probes

Description	Complete Name[a]	Common Name
100 mils long fingers	SD-10-10-100	SD-100
200 mils long fingers	SD-8-12-200	SD-200

[a] SD-finger width-space between fingers-finger length

Each type of probes was built with two spacings: the single space was 1.67 mm, and the double space was 3.41 mm. When we used more than one finger as a source or as a receiver, we made the source connections from one side of the probe and the receiver connections from the other side as shown in Figure 3-1. This was done to minimize any possible cross-talk noise.

To change the spacing between the source and the receiver in the PCB interdigitized probes, we changed the connection of the receiver finger by leaving number of fingers near the source unconnected, as explained in Chapter two. The reason for this in the PCB probes is that we can not remove the unused fingers.

3.2.2 Electronics and data acquisition system

The basic source-receiver system can be considered as an admittance-measuring system where the source is a voltage source, and we measured the current to the ground from the receiver side, as shown in Figure 3-2. In some measurements, we used the probe in a differential mode as shown in Figure 1-2. This means that the system becomes more complicated, but it is still an admittance measuring system.

The output signal from the probe was very weak and was strongly affected by parasitic capacitance in the system. Also, we noticed that the measured signal strongly fluctuated if the position of the wires was changed with respect to each other. This behavior affects the stability of the results and the flexibility of the system. To reduce the effect of the parasitic capacitance of the wires, we replaced individual wires with coaxial cables. The inner conductor of the coaxial cable was connected to the source or the receiver with the analyzer, while the outer conductors for all coaxial cables were

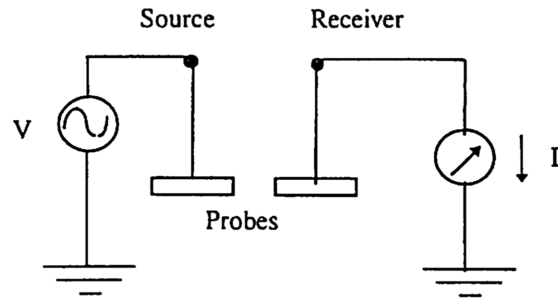

Figure 3-2. Basic source-receiver system

connected with each other and with the ground point in the analyzer. These coaxial cables provided sufficient shielding to reduce the effects of parasitic capcitances.

To make the output signal from the probe stronger, we boosted it with a current amplifier (often called a transistance amplifier) as shown in Figure 3-3. This circuit is a current to voltage converter where the output is related to the input voltage as

$$V_{out} = I_{cap}\ R \quad \text{or} \quad I = \frac{V_{out}}{R} \tag{3.1}$$

where I_{cap} is the current passes through the capacitive probe.

We define

$$Z_c \stackrel{\Delta}{=} \frac{V_{in}}{I_{cap}} \quad \text{or} \quad I_{cap} = \frac{V_{in}}{Z_c} \tag{3.2}$$

$$\text{then} \quad \frac{V_{out}}{R} = \frac{V_{in}}{Z_c} \tag{3.3}$$

$$Z_c = \frac{V_{in}}{V_{our}} R \quad \text{or} \quad Y_c = \frac{1}{Z_c} = \frac{V_{out}}{V_{in}} \frac{1}{R} = \frac{G}{R} \tag{3.4}$$

$$\text{where } G = \frac{V_{out}}{V_{in}}, \quad \text{then} \quad Y_c = 10^{-5} * G \text{ for } R = 100\ k\Omega \tag{3.5}$$

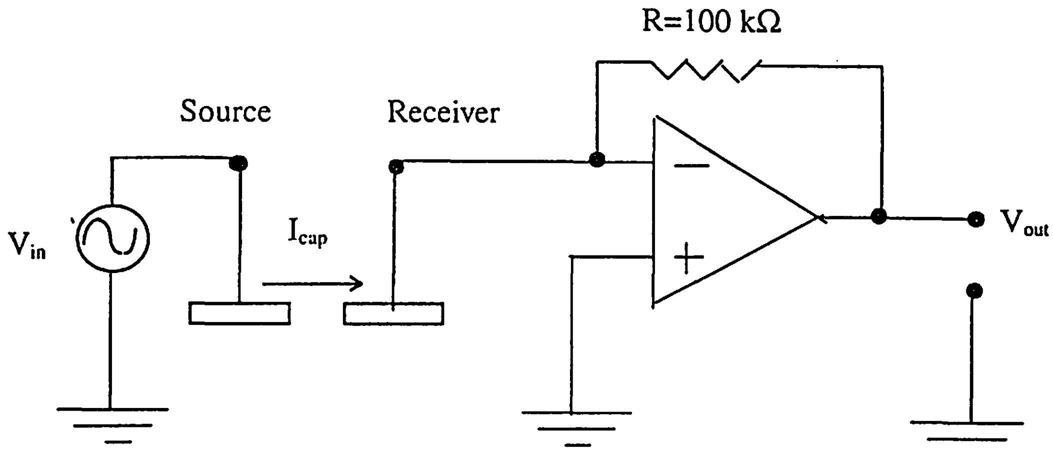

Figure 3-3. Current or transistance amplifier

The complete circuit with the amplifier and the probe were tested with the impedance analyzer. The source electrode was connected to the output channel of the analyzer and to the reference channel while the output of the amplifier was connected with the test channel of the analyzer. The reference channel was set at 50 Ω and 20 dB. The test channel was set at 1 MΩ, and 0 dB. The output channel was set for a single measurement, and the oscillator level set at 15 dBm. The starting frequency was 1 kHz and the stop frequency was 2 MHz. The impedance analyzer was used in Gain-Phase measurement. We measured the characteristic function, or the gain-frequency plot as shown in Figure 3-4. In the area from 0-1200 kHz the amplifier itself has a constant gain, then this gain decreases as the frequency Increases, but due to the presence of the capacitive probe the overall transfer function changes to the one shown in Figure 3-4. For this reason, we noticed that the amplifier was more stable if the operating frequency for

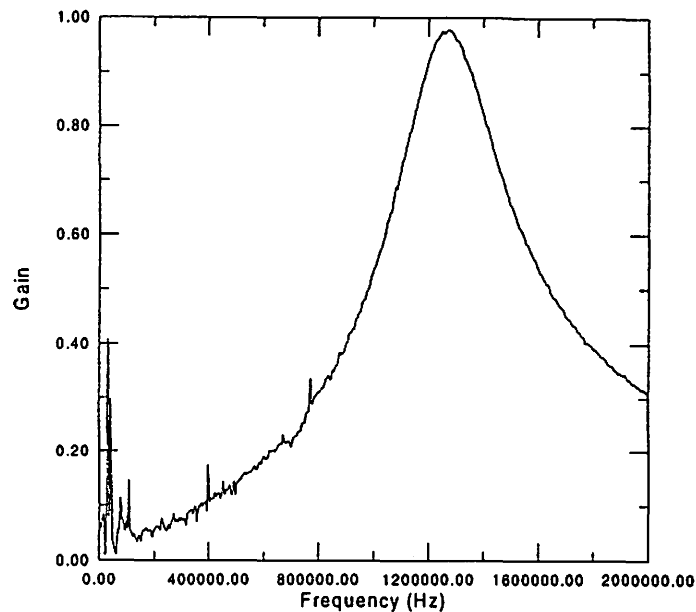

Figure 3-4. Gain-frequency characteristic function for the current amplifier

the system is less than 1.0 MHz. To work in the stable region, we made all of our measurements at 300 or 500 kHz. For the differential mode case, we built a circuit like the one in Figure 3-3 for each receiver finger. Due to the small size of the probe, we could not build a differential amplifier on the same bread board. For this reason, we individually measured the voltages on the probes and then used the computer to calculate the differential signal between the two electrodes. A point to note is that, for a balanced signal (equal electrode voltages), the output of the two amplifiers is not the same due to the small common-mode element and the unbalancing in the amplifier itself.

The overall schematic for the electronic system is shown in Figure 3-5. The voltage source used was the HP 4194A Impedance/Gain-Phase Analyzer operating with a sine wave output mode. The operating frequency was chosen to be high in order that the

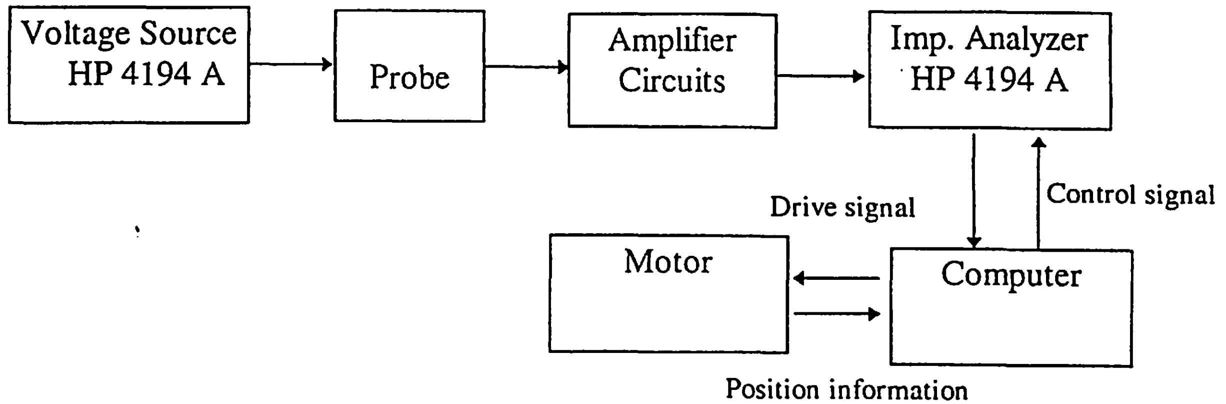

Figure 3-5. Overall schematic for the electronic system

impedance of the source-receiver pair be low enough to produce adequate output current. This frequency was limited at the high end by the bandwidth restrictions of the transistance amplifier as mentioned above.

The output signal from the receiver was fed again to the impedance analyzer HP4194A. The HP analyzer has two modes of measurements: impedance mode and gain-phase mode. When we used the capacitive probe in the absolute mode, we used the analyzer in the impedance mode. On the other hand, when we used the probe in the differential mode, we used the analyzer in the gain-phase mode, except in some cases which we will discuss later. An external power supply was used to power the electronics board. The supply voltage used was a Dual-Tracking DC power supply, Model TPS-4000. It supplied dual dc voltage output of plus/minus 15 volts.

The computer was directly connected to the impedance analyzer. The computer controlled all of the setups required for the impedance analyzer. The computer also controlled the position of the test bed and the motor motion. Using a package software

called MOVER, we controlled the whole system and captured the data from the analyzer together with the position information of this data. Then this software stored the data into a file.

3.2.3 Test fixture

The text fixture includes the test bed used to position the sample on it, the positioner which is the device used to fix the position of the probe and to determine the vertical distance between the sample and the probe, the motor which is used to move the test bed and the sample at the same time. We used the DAEDAL M23 Motor/Drives set to work as a motor in our system. This device has a built-in test bed so we can use the bed to fix the position of the sample. It is a complete microstepping motor drive. The drive operates from a step and directional control input. The set is supplied with an indexer interface input which consists of a 25-pin female "D" type connector. This connector is where pulse and direction inputs are supplied. Then, the device is connected with a PC computer to control the motion of the motor and the position of the bed. The whole set also is supplied by three micrometers working in three directions. These micrometers control the motion or the position of the bed in the three directions: x, y, z. The x and y micrometers are used for slight fixing of the position of the bed with respect to the head which is used to hold the probe. The z micrometer is used to control the vertical distance between the head and the bed, i.e., control the liftoff distance.

In some of our point measurements, we used a separate positioner to hold the probe and the sample. This positioner also has three micrometers to control the distances in the three directions.

3.2.4 The sample

We used two different samples: The plastic sheet sample and a plastic sample machined with slots of varying widths and depths. The plastic sheet sample consisted of a number of plastic sheets, with a thickness of 4.01 mil for each sheet. This sample was used with prototype probes to study the effect of different factors on the output signal from the probe. This sample also was used in measuring the thickness of the dielectric material. The second sample was a thick plastic sample with a thickness of 0.697 inch. We made two types of slots in this sample. The first one was a wide slot of width 0.25 inch, and the second one was a narrow slot of width 0.105 inch. For each width we made five types of slots of different depths: surface breaking (i.e., the depth was 0.697 inch), 0.662 inch, 0.627 inch, 0.522 inch, 0.347 inch slots. Each slot was used as a surface slot or a buried slot except the surface breaking one. Figure 3-6 shows two views of this sample.

3.3 Defining the best measurement configurations

To determine the best measurement configurations, we studied the effect of various factors on the measurements. From the probe side, we studied the effect of the number of fingers used as a source or as a receiver, the spacing between neighboring fingers, and the dimensions of each finger. From the system side, we studied the effect of the shielding, the operating frequency of the system, the liftoff problem, and the grounding of the bottom metal plate under the dielectric sample. According to the effects of all of these factors, we selected the best configurations. In this part of our study, we used the plastic sheet sample of ten sheets. Using the impedance analyzer in the impedance mode, we selected the admittance measurement type.

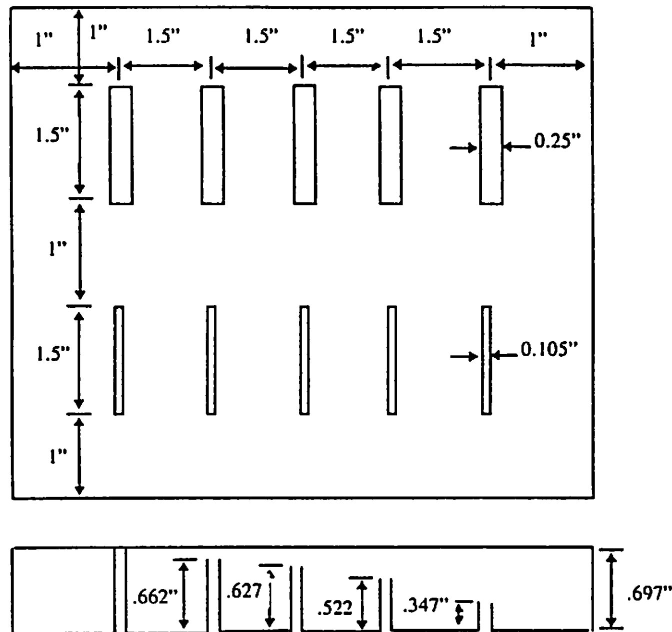

Figure 3-6. The top and side views of the plastic sample

We set it at short integration time and 32 averaging. We used two frequencies (50 kHz and 100kHz) in all of our measurements. Also we used the prototype probes of both widths: the wide one of width of 8.88 mm, and the narrow one of width 6.96 mm. In some of our measurements we used both kinds of probes with different spacing between fingers (single spacing is 1.67 mm and double spacing is 3.41 mm), and with different number of fingers (single finger or double finger for the receiver or for the source). However, in all of our measurements in this case, we used the probes in the absolute mode. We studied all of these factors in two main types of connection of the fingers as a source or receiver. Connection number one was performed by connecting one side of the probe with the high potential connector of the impedance analyzer and the second side connected to the low potential connector of the analyzer while keeping the bottom metal

plate either floating or connected to the general ground of the analyzer. This connection is illustrated in Figure 3-7a. Connection number two was done by connecting both sides of the probe with same point (high potential) of the analyzer while connecting the bottom metal plate to the other connector of the analyzer. Figure 3-7b illustrates this connection. In the case of using more than one finger as a source or a receiver, we used two different ways to connect these fingers. These two ways are illustrated in Figure 3-8.

To study the effect of each factor, we repeated the measurements with different combinations of the other factors. For example to study the effect of the operating frequency, we took measurements at two frequencies with a different number of fingers, different spacings between fingers, different areas of the fingers, and different grounding environments for the bottom metal plate. We did the same thing for the other factors except for the shielding and the lift off factors.

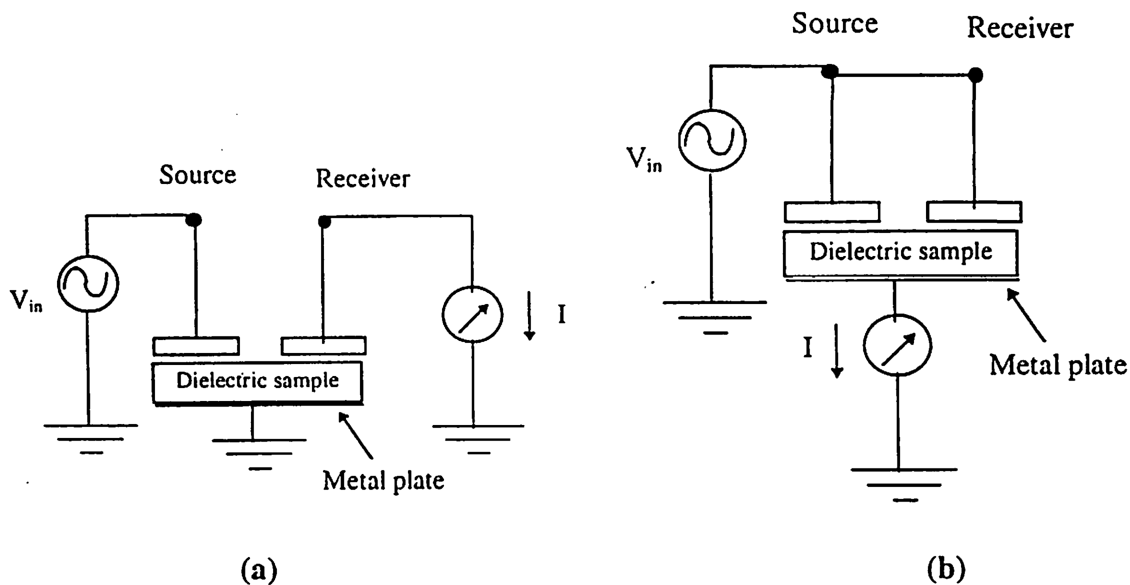

Figure 3-7. Basic connection of the probe with the analyzer
(a) Connection number one (b) connection number two

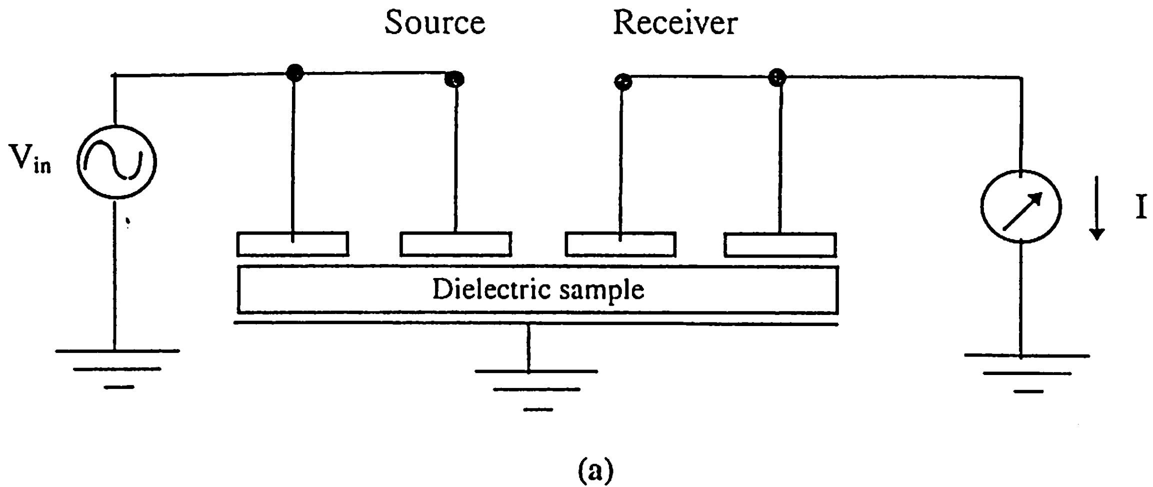

(a)

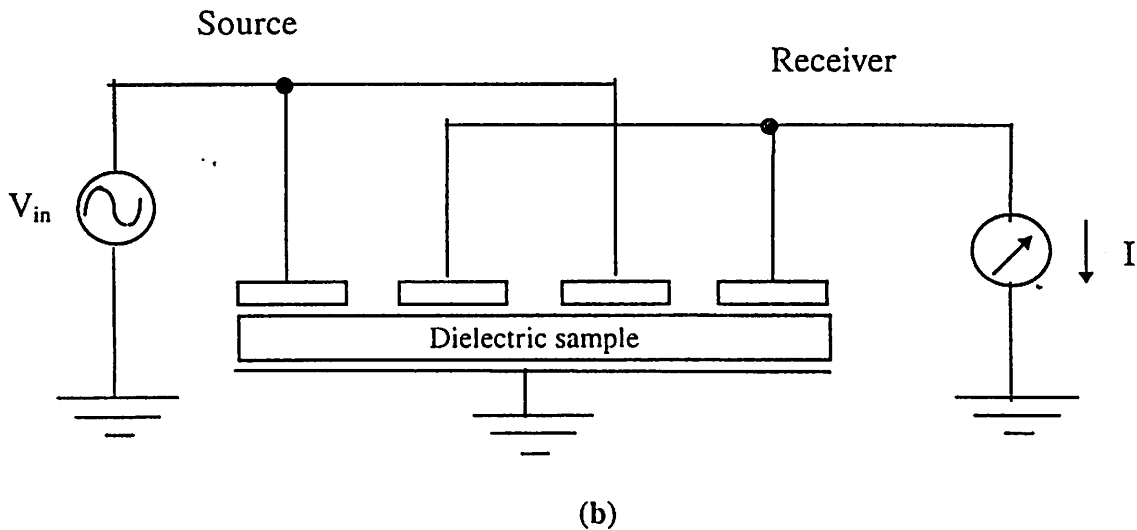

(b)

Figure 3-8. The two possible ways to connect the double finger probe. We denote the connection in (a) as + + - - and the connection in (b) as + - + -.

3.3.1 Shielding effect

As we mentioned in section 3.2.3, the wiring geometry had a great effect on the measurements. The parasitic capacitances of the wires have values similar to the output capacitance from the probe or more, therefore any changes in these values affect the overall result very much. From our experiments, we observed that sometimes the output

did not respond to the changes in the sample, because changes dominated the fluctuating stray capacitance. The length of the wires, their position relative to each other, and any motion in the whole system, produced a large change in the parasitic capacitance, and gave an erroneous response from the probe.

To decrease the effect of the relative position of the wires, we tried fixing their position at the beginning by bundling them. Although this solution decreased the effect of the relative position and the motion in the system, it increased the absolute value of the parasitic capacitance of each wire. This solution made the value of the parasitic capacitances much larger than the output capacitance from the probe. This means that any changes in the output response due to changes in the sample cannot be seen, because this change is much smaller than the overall response.

To solve this problem properly, we used coaxial cables to make all of the connections in our system. The coaxial cable has lower parasitic capacitance than open wires, and also provides good shielding. With the coaxial cable, the overall response improved very much, and it became more stable and flexible to any changes in the position.

3.3.2 Effect of grounding the bottom metal plate

As we mentioned before, our measurement system consisted of an opened flat parallel plate capacitor lying against a common substrate. Most of the industrial samples have a dielectric material lying against a metal material. We modeled these samples by a plastic sheet sample lying on a metal plate. This bottom metal plate may work as one plate of a capacitor which consists of the receiver or the source as a second plate,

especially if the thickness of the dielectric material is not large. In the latter case, the electric field generated at the source may penetrate the whole dielectric material and terminate on the bottom metal plate. One of the most important points needing to be studied in this case is how much the output capacitance is affected if this metal plate has been grounded or kept floating. In practice, the grounding of the base of the dielectric material can be difficult, therefore we need to study this effect especially with thin dielectric material.

We built our system to study this effect with ten sheets of plastic material with a thin metal plate underneath the sheets, and used prototype capacitor sensors. We used this set-up just with connection number two because with connection number one the metal plate could not be connected to ground. We collected data by varying the number of fingers, finger spacings, finger dimensions, and operating frequencies.

Figures 3-9, 3-10, and 3-11 summarize the experimental results. All of these figures show the effect of grounding the bottom metal plate under different circuit configurations in order to show that the overall results apply to any system configuration. For instance, Figure 3-9 shows the effect of grounding the metal plate using a double wide finger probe connected in connection number two with single spacing between fingers at 100 kHz operating frequency. In Figure 3-10, the number of fingers has been changed. while in Figure 3-11, the type of connection has been changed. We notice that although the figures have some differences in the system setup, the overall behavior due to grounding the bottom metal plate is still the same. It is noticed from these figures that the difference between keeping the metal plate grounded or floating decreases as the thickness of the

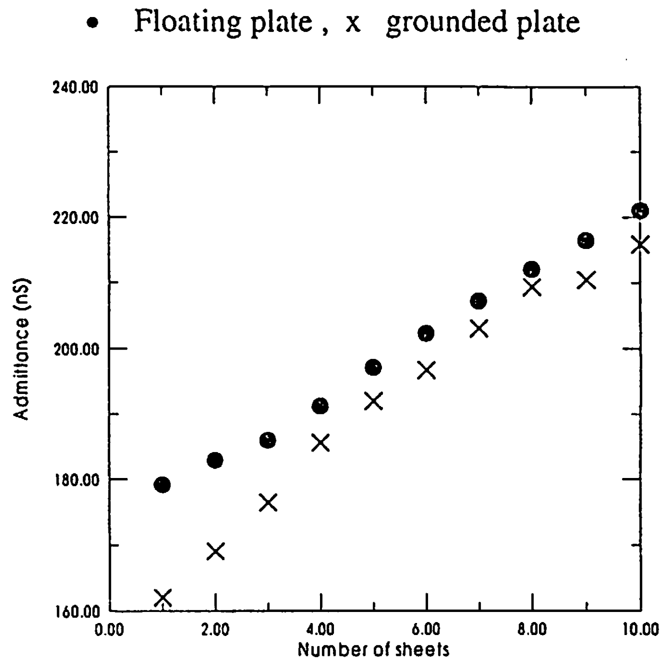

Figure 3-9. Effect of grounding the bottom metal plate using a double wide finger probe with single spacing between fingers, connection ++--operating frequency 100kHz

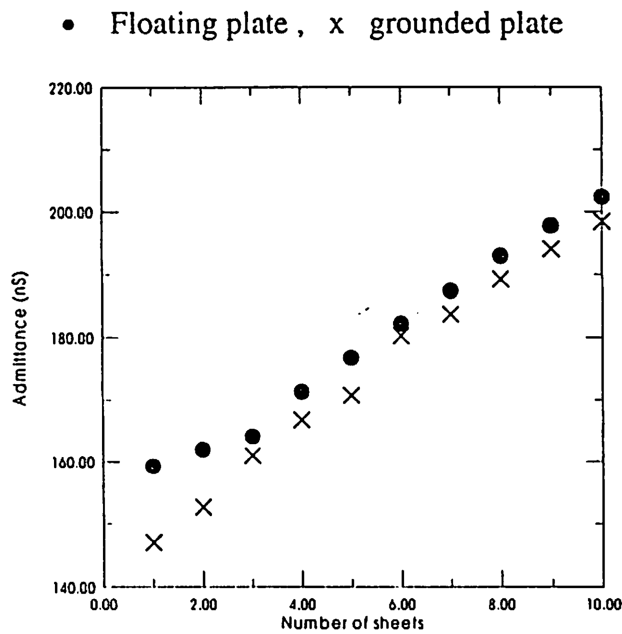

Figure 3-10. Effect of grounding the bottom metal plate using single wide finger probe with single spacing between fingers, operating frequency 100 kHz

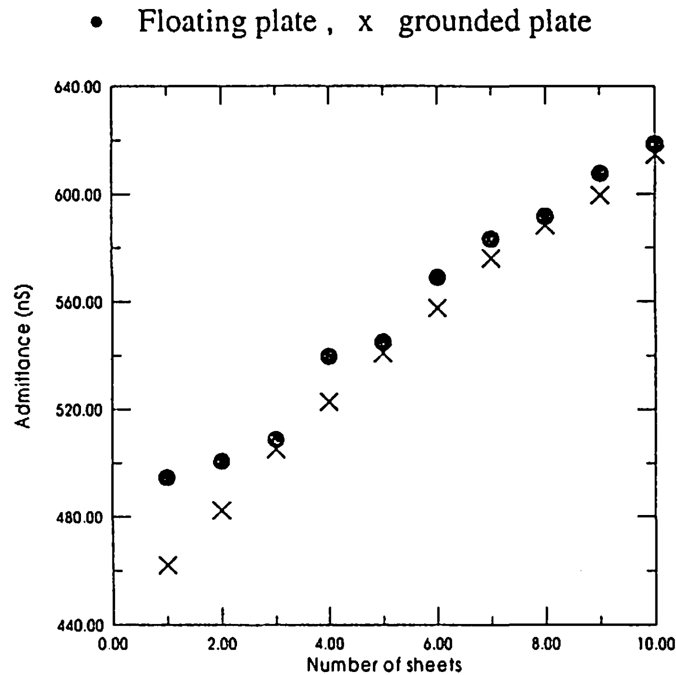

Figure 3-11. Effect of grounding bottom metal plate using double wide finger probe with single space between fingers, connection + - + - operating frequency 100 kHz

dielectric material increases. This may be due to the small value of admittance when the thickness is small, therefore this small value is more sensitive to any changing in the setup. This result is independent of any other factors, and will help simplify future measurements of industrial samples in which it may be difficult to ground the base metal.

3.3.3 Operating frequency effect

The operating frequency of the system means the input frequency supplied to the source electrode using the HP 4194A. As mentioned in section 3.2.2, we measured the admittance between the source and the receiver. The admittance value is related to the capacitance between the source and the receiver by

$$Y = j\omega C = j2\pi f\, C \qquad (3.6)$$

This equation illustrates that the linear relationship between the admittance and the frequency. To test our experiment for this relationship, we measured our prototype capacitors at two different frequencies: 100 kHz, and 50 kHz. We tested the effect of the frequency factor with various circuit connections, number of fingers, finger spacing, and finger areas. The values of admittance corresponding to different thickness of the plastic sheets were measured with the impedance analyzer. The analyzer was set to a short integration time with a data average of 32. The probe was connected in the absolute mode. Figures 3-12, 3-13, 3-14, 3-15, 3-16, and 3-17, show the main results. All of these figures show that the effect of changing the operating frequency on the admittance does not depend on any configuration of the system. For instance, Figures 3-12 and 3-13 show the effect of changing the frequency at different finger dimension using circuit connection number one. Figures 3-12 and 3-14 show the effect of changing the frequency at different spacing between the fingers, while Figures 3-12 and 3-15 show the effect of different circuit connections in a single space case. Figures 3-16, and 3-17 show the effect of double fingers with two different combinations. From all of these figures, we observed that the values of admittance doubled, as the frequency was doubled. This means that the admittance also increases as the frequency increases, therefore to get better response from the probe, it is better to operate it at higher frequency. The practical limit of operating the system at a high frequency is controlled by the gain-bandwidth of the electronic devices: the current amplifier and the impedance analyzer. For this reason, we tried to operate our system at the maximum frequency allowed according to the gain-bandwidth curve of the amplifiers.

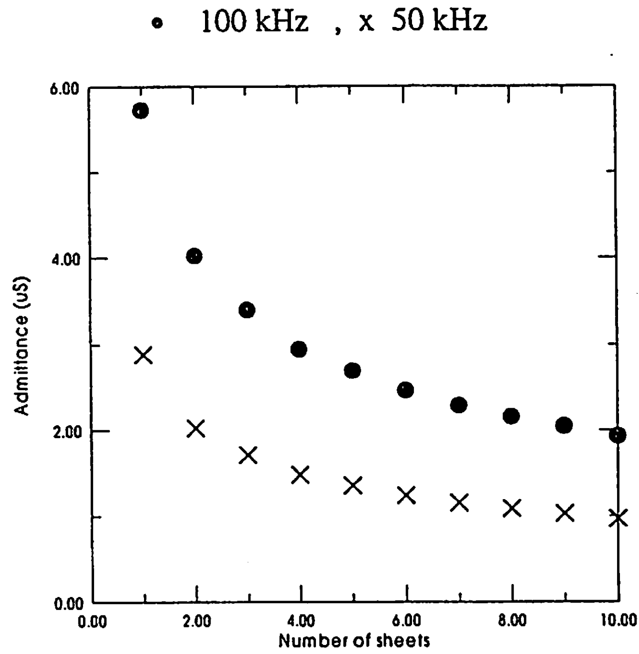

Figure 3-12. Effect of changing the operating frequency using single narrow finger, single space between fingers, connection one

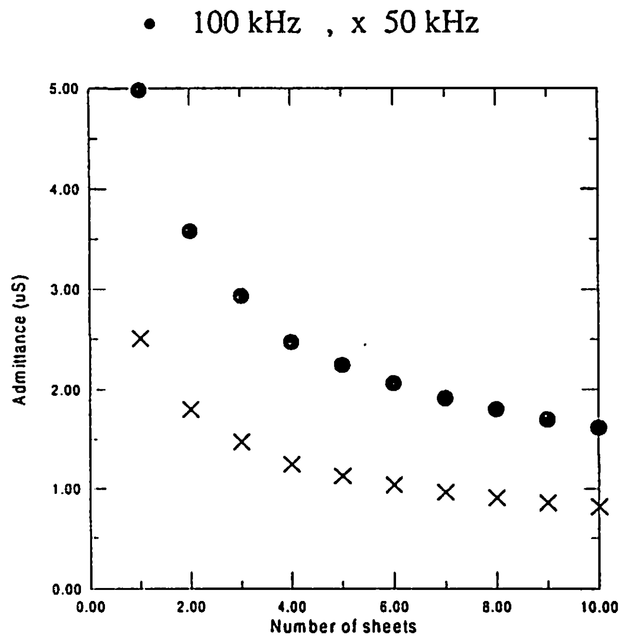

Figure 3-13. Effect of changing the operating frequency using single wide finger, single space between fingers, connection one

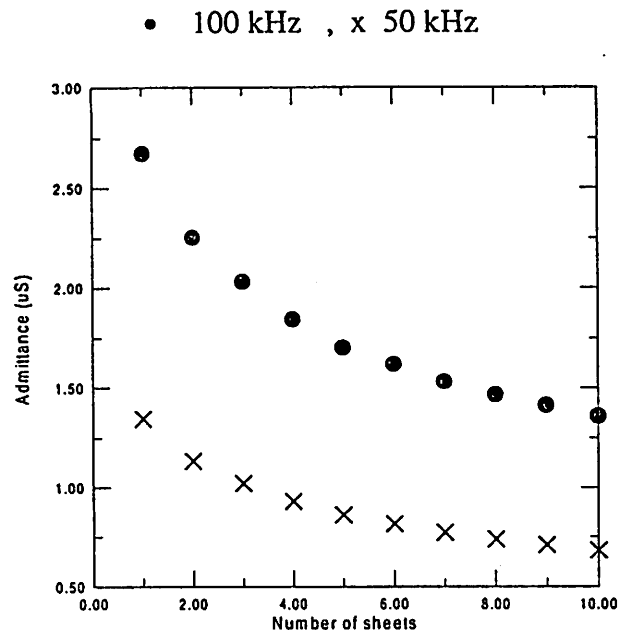

Figure 3-14. Effect of changing the operating frequency using single narrow finger, double space between fingers, connection one

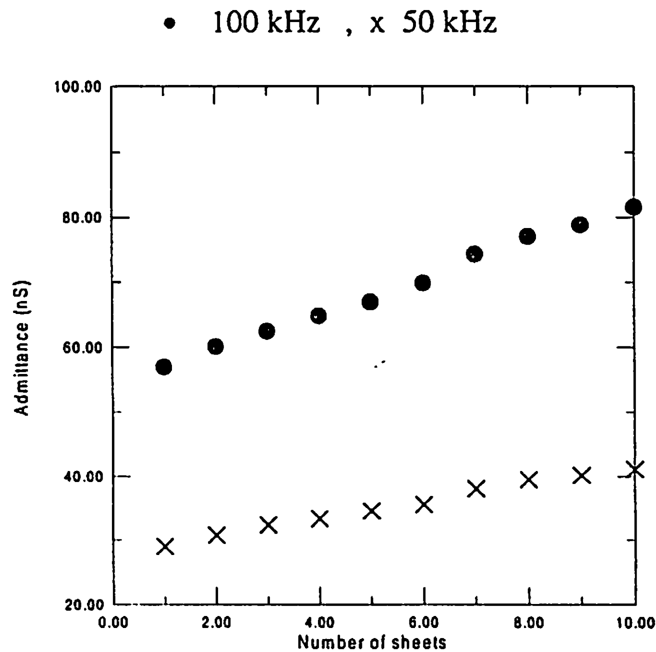

Figure 3-15. Effect of changing the operating frequency using single narrow finger, single space between fingers, connection two

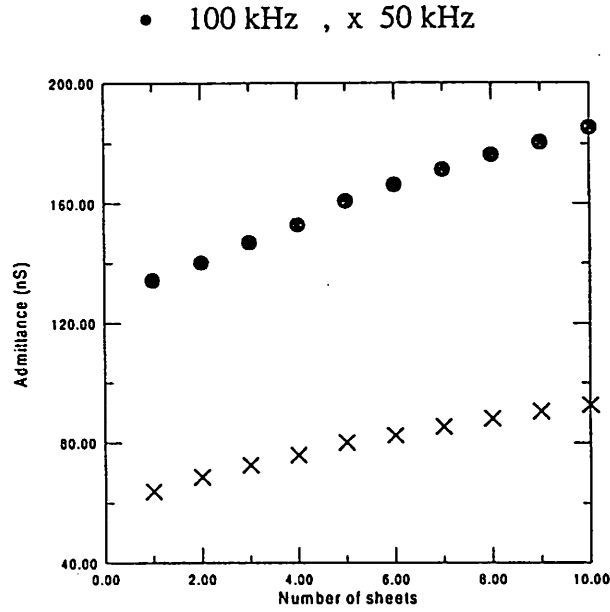

Figure 3-16. Effect of changing the operating frequency using double narrow finger, single space between fingers, connection two ++ --

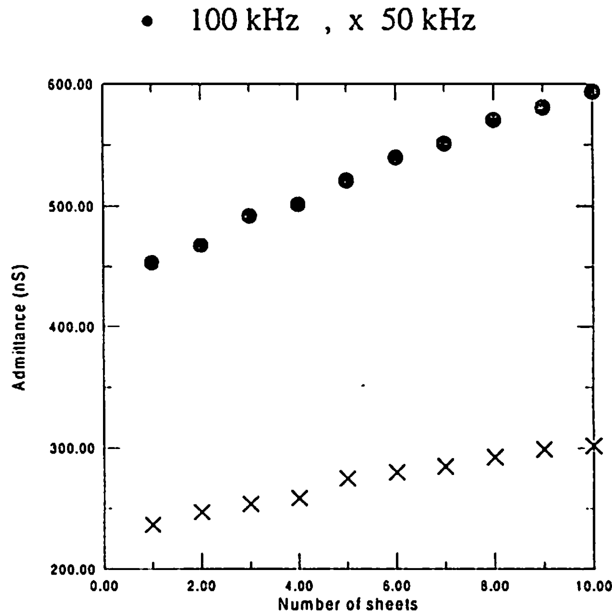

Figure 3-17. Effect of changing the operating frequency using double narrow finger, single space between fingers, connection two +-+-

3.3.4 Liftoff effect

The liftoff distance is defined as the vertical distance between the probe and the sample. This distance affects the admittance value especially if we use the probe in the absolute mode. We studied this factor using the plastic sheet sample with a bottom metal plate under the sheets. We used a prototype probe of length 6.96 mm , width 1.67 mm, and 1.67 mm spacing between fingers and set the impedance analyzer to short integration time and 32-point averaging. A general gage was used to measure the liftoff distance. Figure 3-18 displays the output signal responses from a single electrode source/receiver probe as a function of the liftoff distance. As indicated in Figure 3-18, the experimental admittance versus liftoff curve initially decreases rapidly followed by a recovery. This recovery was discussed by other investigators (Gimple, 1987; Shull et al., 1990). Gimple

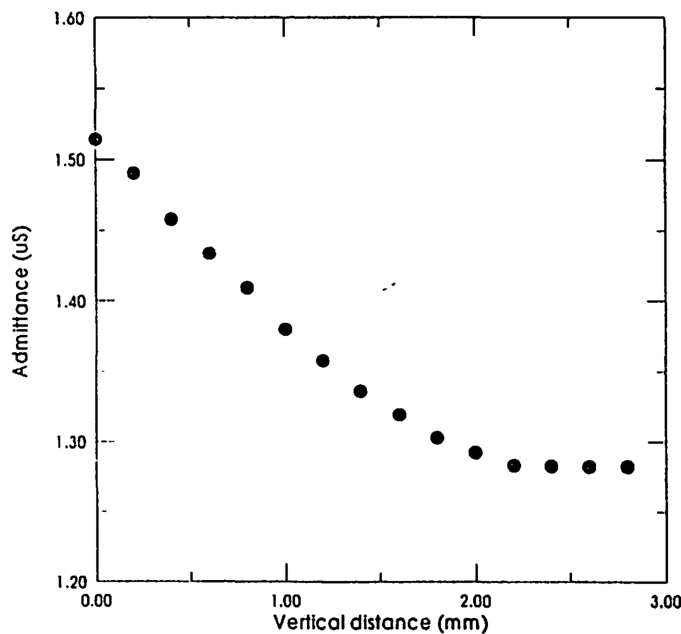

Figure 3-18. Effect of the liftoff on the admittance

conjectured that the recovery was caused by parasitic capacitive coupling between the probe and grounding points in the environment. Shull assumed that this recovery effect was caused by the capacitive coupling to any conducting planes in the probe vicinity. They reduced this recovery effect by placing the workpiece on a nonconductive pedestal above the ground plate. The response of the probe with the liftoff can be modeled by two capacitors in series. One of these capacitors due to the liftoff, C_{lift}, and the second one is the capacitance of the dielectric material and the parasitic capacitances, C_c. The second capacitor is constant when the liftoff distance changes, while the first one varies with the liftoff. The measured capacitance is the equivalent of the two capacitors in series as given in the following equation

$$C_{eq} = \frac{C_{lift} C_c}{C_{lift} + C_c} \tag{3.1}$$

From the above equation, we notice that if C_{lift} is small compared to C_c (this happens when the liftoff distance becomes big the equivalent capacitance reduces to fixed number equals C_{lift} which is small. But, when C_{lift} is in the range of C_c the equivalent capacitance decreases by decreasing the value of C_{lift} (this corresponds to the first region in Figure 3-18). In our experiments we can minimize the effect of the liftoff and the recovery by taking all of our measurements with a small liftoff.

3.3.5 Finger spacing effect

The spacing between fingers mainly means the spacing between the source and the receiver fingers. To study the effect of the spacing between fingers on the admittance

value, we tried the main connections under different variations of the other factors. We used the same plastic sheet sample with the metal plate, and used the probe in the absolute mode with the same setup of the impedance analyzer. We tried two different spacings: 1.67 mm, and 3.41 mm. We noticed that in connection number one the admittance changed slightly or sometimes did not change with change in the spacing between the source and receiver fingers (shown in Figure 3-19). This is because the capacitances (C_1 and C_2) in connection number one are formed between one of the electrodes of the probe and the metal plate. Each capacitor is a parallel plate capacitor. The system in this case can be modeled by two capacitors in parallel as shown in Figure 3-20. These two parallel capacitances are not effected by changing the separation between them as long as there is no coupling between capacitors. Therefore, there is a minimal relation between these two capacitances and the space between the fingers.

On the other hand, we notice in Figures 3-21, 3-22, 3-23, 3-24, and 3-25 that the admittance value decreases as the spacing between the finger increases. All of these figures study the effect of changing the admittance in a circuit of connection number two. They show that the effect of changing the spacing between fingers in connection number two is almost the same. For instance, Figures 3-21 and 3-22 show that the effect of spacing is the same at different frequencies. Figures 3-22 and 3-23 show the same thing at different width of the probe. Figures 3-21, 3-24, and 3-25 show the effect at different number of fingers and different connection of the double fingers. Although the space between the fingers was doubled, the admittance values did not decrease by one half. This means that the relation between the admittance and the spacing is not exactly $Y=k/d$,

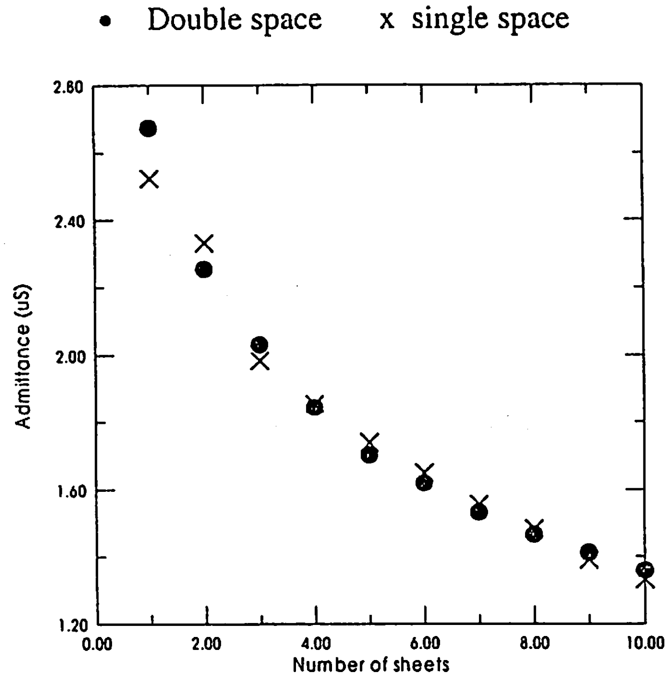

Figure 3-19. Effect of changing the space in connection one narrow single finger probe, 100 kHz

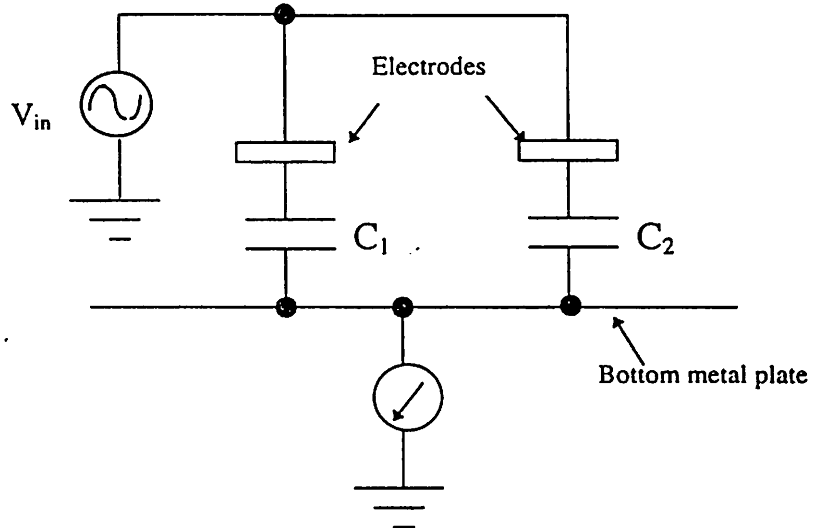

Figure 3-20. The model of the probe in connection number one

where d is the spacing between the fingers, and k is a proportionality factor. This can be explained in different ways: firstly, the admittance in the open flat capacitor does not obey the simple theory of parallel plate capacitors. The spacing between fingers, which was represented by symbol a the spatial frequency, related to the capacitance in an exponential form. Secondly, the measured admittance is coming from two capacitances: the capacitance of the source and the receiver, and the parasitic capacitance of the system. The first capacitance is the one that is changed by changing the spacing between fingers, but the second capacitance is constant under the same wiring system and devices. For this reason, the admittance value has two components, one variable and one constant. Because of this, if we want to suppress the constant admittance, we need to subtract this value from all measurements. In practice, the important thing that needs to be taken under

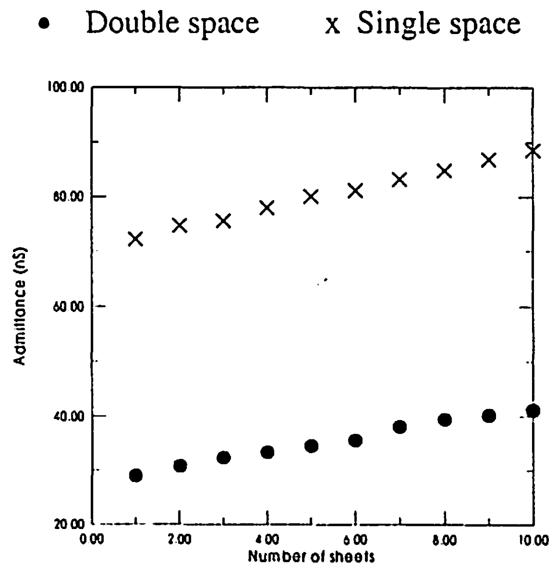

Figure 3-21. Effect of finger spacing using single narrow finger connection two, operating frequency 50 kHz

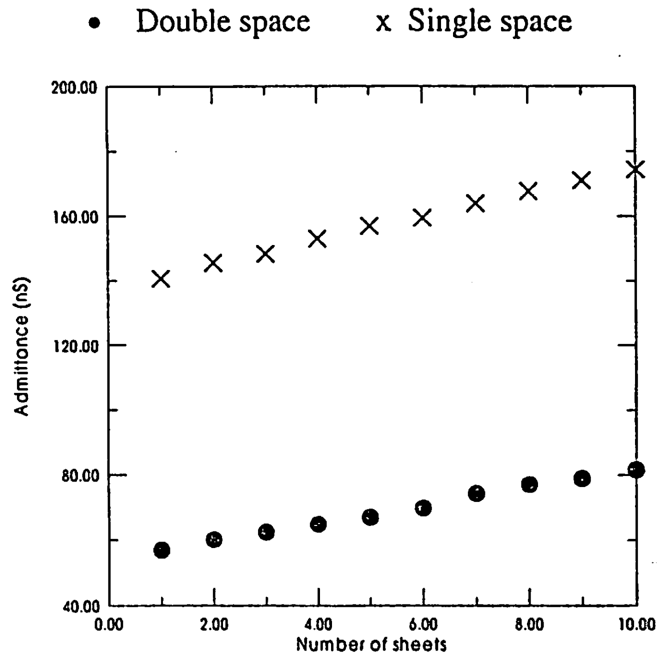

Figure 3-22. Effect of finger spacing using single narrow finger connection two, operating frequency 100 kHz

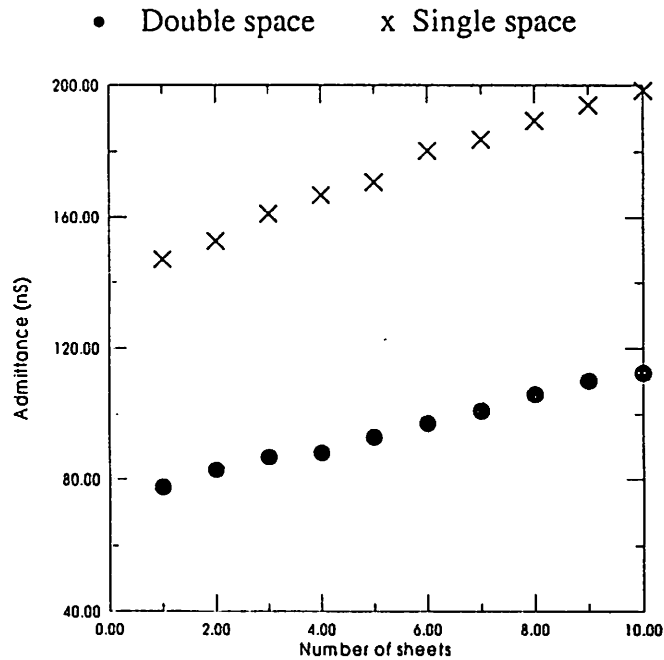

Figure 3-23. Effect of finger spacing using single wide finger connection two, operating frequency 100 kHz

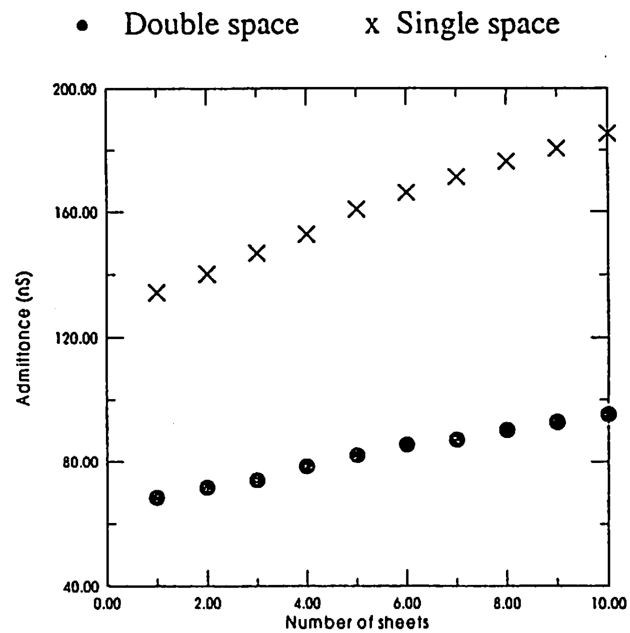

Figure 3-24. Effect of finger spacing using double narrow finger connection two + + - -, operating frequency 100 kHz

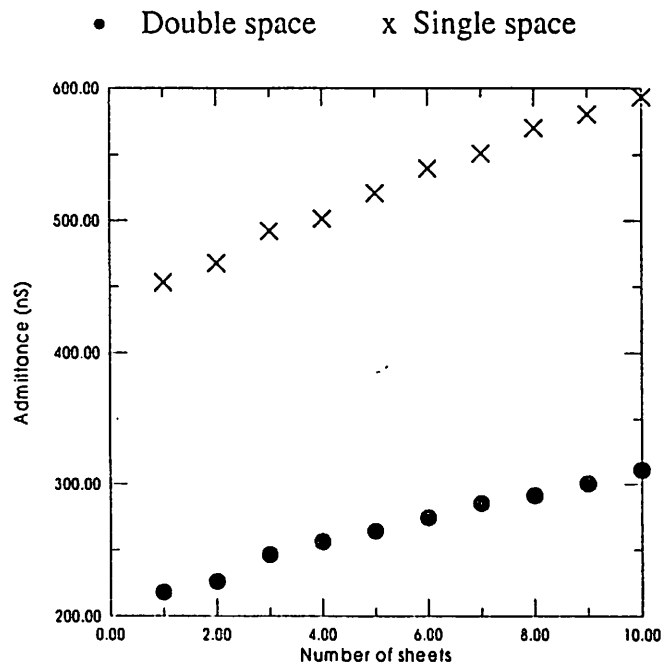

Figure 3-25. Effect of finger spacing using double narrow finger connection two + - + -, operating frequency 100 kHz

consideration is that the admittance value of the capacitor probe decreases as the spacing between fingers increases.

3.3.6 Finger dimensions effect

The area of the source finger or the receiver finger is the second important parameter on the probe side that affects the measurements. We studied this factor under the same setup of the analyzer and used the same sample and probe. We tested the effect of this factor under different variations of the other factors. Figures 3-26, 3-27, 3-28, 3-29, 3-30, 3-31 summarize the most important results. These figures show that the response of the probe due to changing in the probe dimension is not effected by other system setups. For instance, Figures 3-26 and 3-27 show the effect of changing the dimension of the fingers at different frequencies. Figures 3-26, 3-28, and 3-29 show this

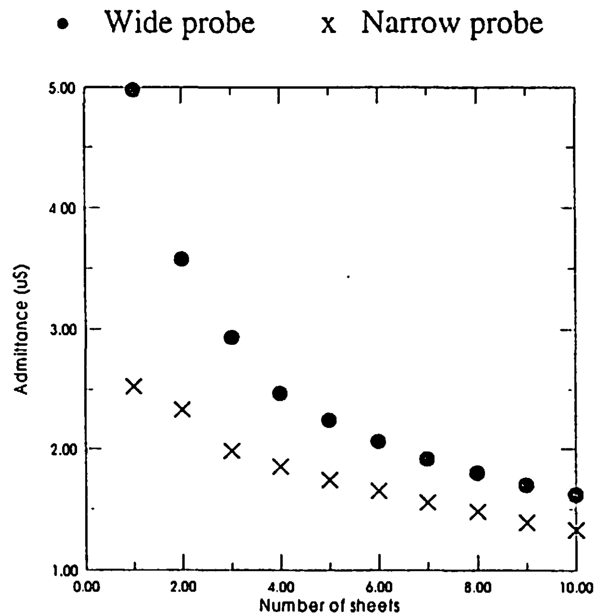

Figure 3-26. Effect of finger dimensions using single finger probe, single space, connection one, operating frequency 100 kHz

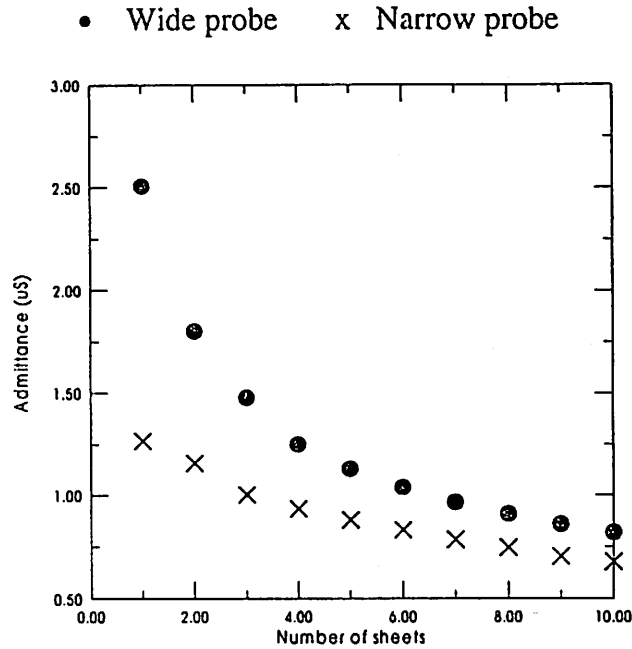

Figure 3-27. Effect of finger dimensions using single finger probe, single space, connection one, operating frequency 50 kHz

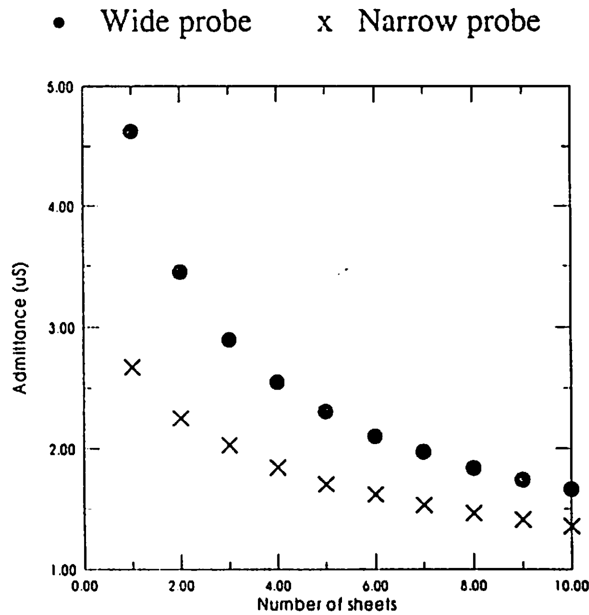

Figure 3-28. Effect of finger dimensions using single finger probe, double space, connection one, operating frequency 100 kHz

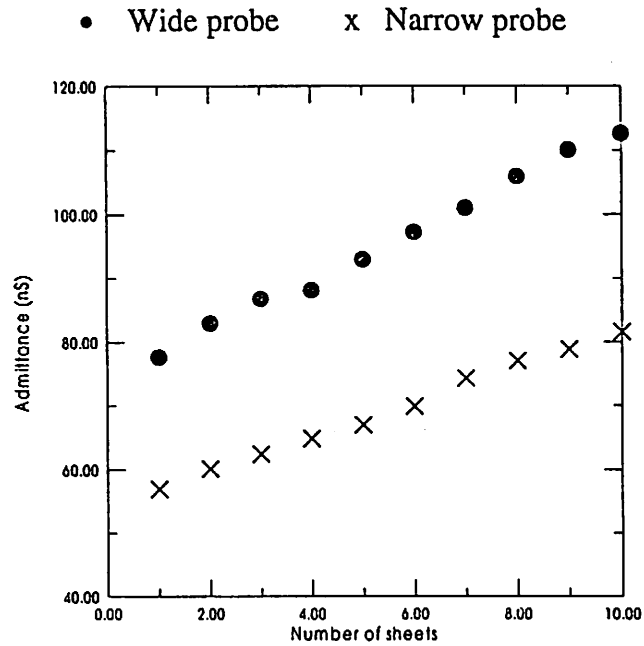

Figure 3-29: Effect of finger dimensions using single finger probe, double space, connection two, operating frequency 100 kHz

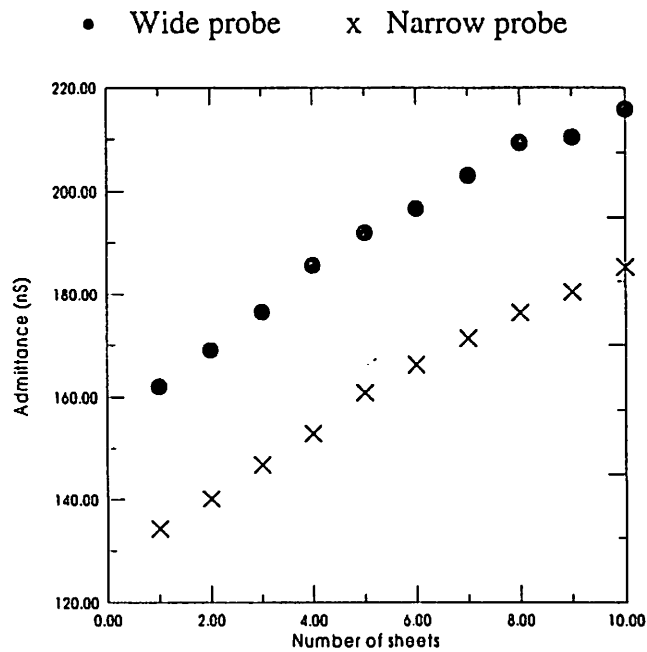

Figure 3-30. Effect of finger dimensions using double finger probe, single space, connection two + + - -, operating frequency 100 kHz

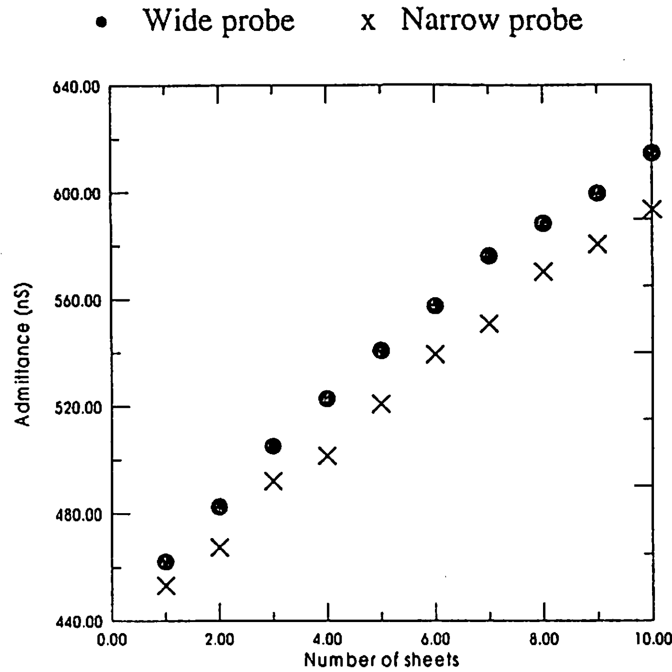

Figure 3-31. Effect of finger dimensions using double finger probe, single space, connection two + - + -, operating frequency 100 kHz

effect at different spacing between fingers and for different types of connections. While Figures 3-30 and 3-31 show this effect at double number of fingers at the two different connections. From these figures, we notice that the admittance value increases as the area of the fingers increases. But the admittance value does not increase by the same factor as the area increases. This can be explained by the second reason we discussed in the spacing effect. The admittance value consists of a variable value related to the capacitance of the probe and a constant value related to the capacitance of the system. We notice from the Figure 3-26, 3-27, and 3-28 that the admittance almost increases by the same factor as the area increases. This is due to the fact that the constant admittance value in this case is small compared with the variable admittance, therefore the change in the variable value

due to the change in the area seems to be dominant. In the other cases, the constant and the variable admittances are in the same range.

3.3.6 Number of fingers effect

Number of fingers means the number of fingers which are connected as a receiver or as a source, not the total. We studied this effect using prototype probes in two cases: with a single finger on each side of the source or the receiver and with double fingers on each side. We used the same setups for the analyzer as the ones we used in the previous parts. We tested this factor also under different variations of the other factors. In the case of double fingers, we have two options to perform the connection: firstly, connect the two adjacent fingers as a receiver or as a source (connection ++--); secondly, connect the first finger as a source, then the neighboring one as a receiver, then the next one as a source again, and the last one as a receiver again (connection +-+-) (shown in Figure 3-8). Figures 3-32, 3-33, 3-34, 3-35, 3-36, 3-37, and 3-38 display the most important results. These figures show that the effect of the number of fingers is not changed with different system setups. For instance, Figures 3-32 and 3-33 show this effect at different finger dimension. Figures 3-32 and 3-34 show this effect at different frequencies. Figures 3-32 and 3-35 show this effect at different spacings while Figures 3-36, 3-37, and 3-38 show this effect using connection number two in its two possibilities. In general, we notice that the admittance value increases as the number of fingers increases. This is because an increase in the number of fingers means an increase in the area of the probe, and we found in the last section that the admittance increased by increasing the area of the probe, which increases the current (see Figure 3-7), we also notice from the Figures that connection +-+-

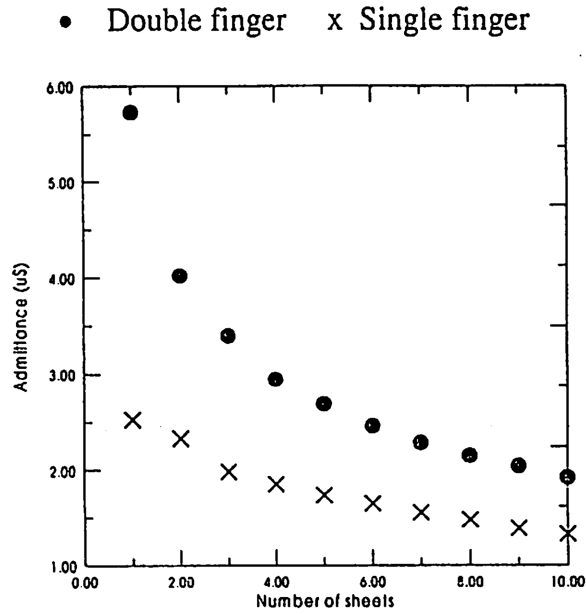

Figure 3-32. Number of finger effect, using narrow probe, single space, connection one, operating frequency 100 kHz

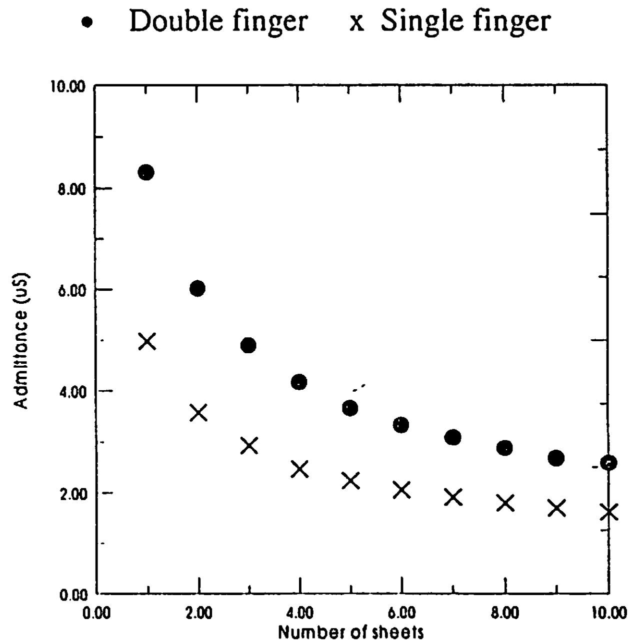

Figure 3-33. Number of finger effect, using wide probe, single space, connection one, operating frequency 100 kHz

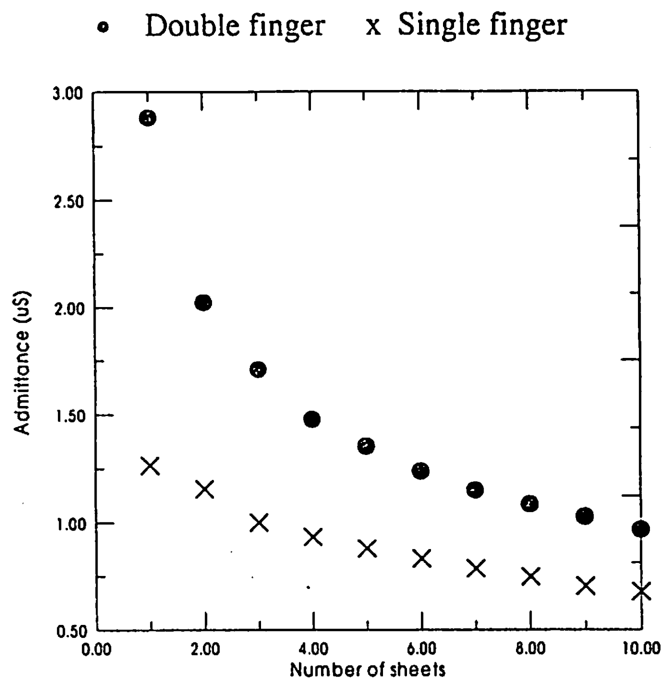

Figure 3-34. Number of finger effect, using narrow probe, single space, connection one, operating frequency 50 kHz

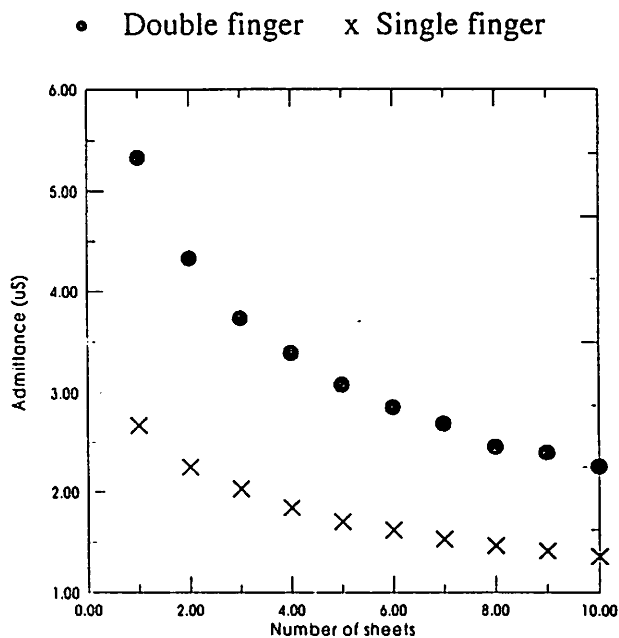

Figure 3-35. Number of finger effect, using narrow probe, double space, connection one, operating frequency 100 kHz

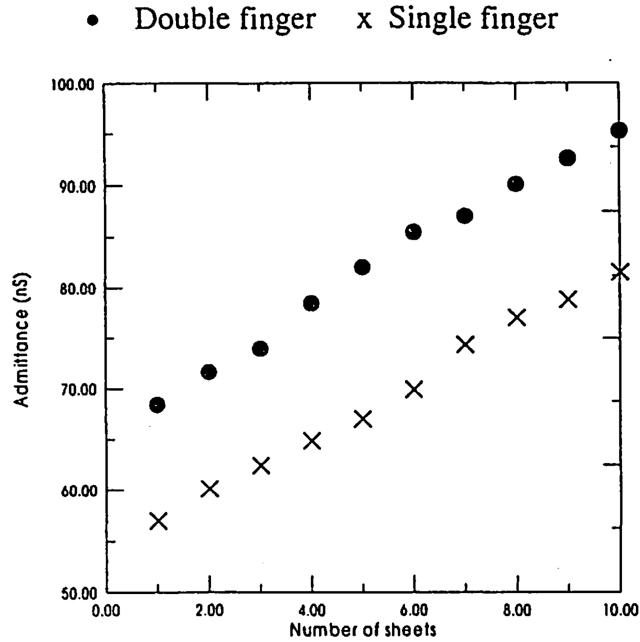

Figure 3-36. Number of finger effect, using narrow probe, single space, connection two + + - -, operating frequency 100 kHz

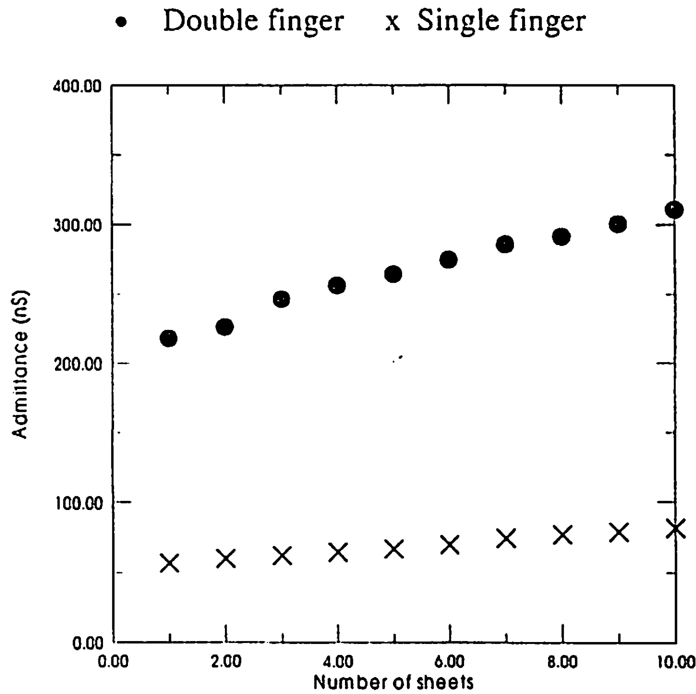

Figure 3-37. Number of finger effect, using narrow probe, single space, connection two + - + -, operating frequency 100 kHz

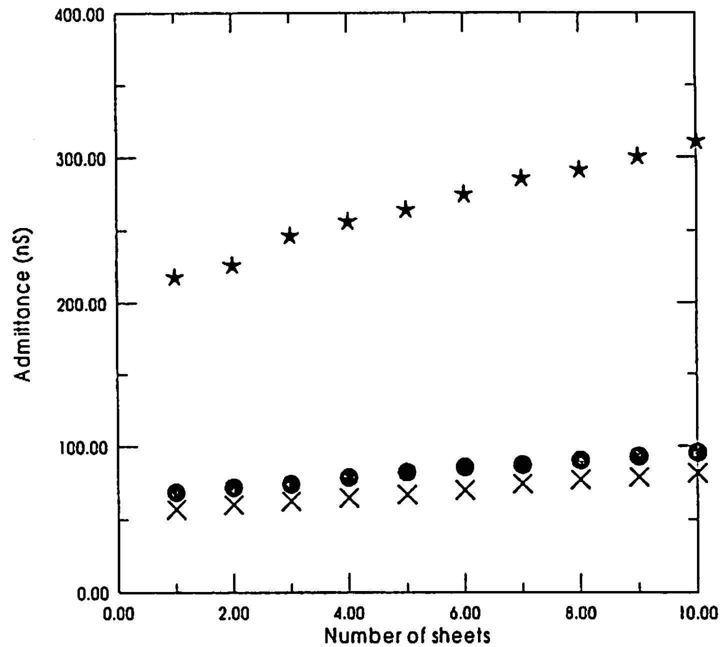

Figure 3-38. Number of finger effect, using narrow probe, single space, connection two, operating frequency 100 kHz

has an admittance value larger than that of connection ++--. This is due to the long distance between the last finger of the source and the last finger of the receiver. As mentioned in section 3.3.5 the capacitance decreases as the spacing between fingers increases. This means that the fingers at the ends have less capacitance than the fingers in the middle, but in the second connection, all fingers contribute with the same capacitance. According to this, the total capacitance in the first connection is less than the one in second connection.

3.4 Determining the thickness of a dielectric material

One of the main objectives in our research is determining the thickness of a dielectric material. It is known that the capacitance value of the probe differs from one dielectric material to another which is not like eddy current probes. In eddy current probes, we can determine the thickness of a dielectric coating on a conductor easily because the impedance of the probe is not sensitive to the type of the dielectric material. The impedance of the probe, in the eddy current probes, is just sensitive to the thickness. In capacitive probes, the problem becomes more difficult because the value of the capacitance depends on the dielectric constant of the material between the probes, as well as on the liftoff distance. One of the ways we reduced the effect of the liftoff was to make all of our measurements of the thickness with zero liftoff, i.e., putting the probe directly in touch with the sample.

To measure the dielectric thickness, an interdigital probe with a length of 200 mil, a width of 8 mil, and a space between fingers of 8 mils, ID-8 (see table 3-1), was used in the absolute mode. An amplifier was placed near the receiver output to boast the small signal. Data was gathered with the impedance analyzer in the Gain/Phase mode with medium integration time and a data average of four. We connected the source finger with the output channel of the analyzer, and the output of the amplifier with the test input channel. We connected the output channel also with the reference input channel, because we only had one output from the probe in this case, and because we needed to measure the gain with respect to the input channel of the probe as shown in Figure 3-39. With this connection, the measured values from the analyzer in this case were the gain and the phase

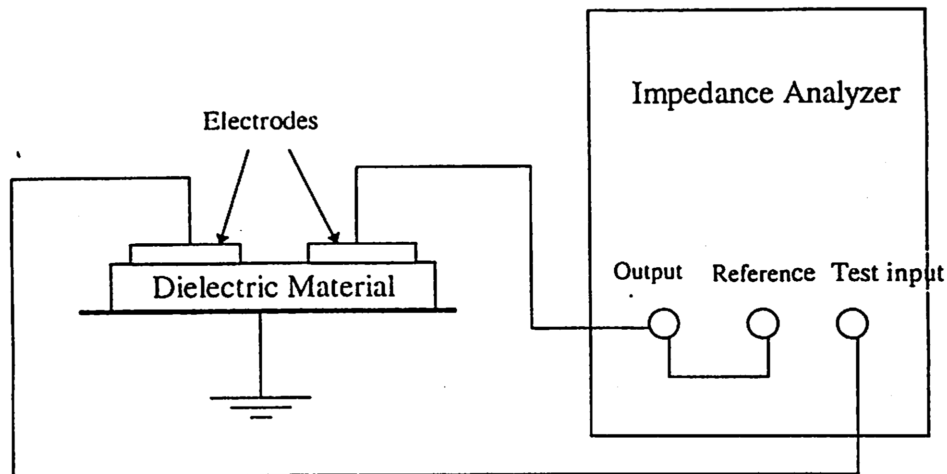

Figure 3-39. The connection of the probe with impedance analyzer

of the output of the probe relative to the input of the probe. From these measured values, we can find the admittance value using equation (3.5). We set the test channel at 1MΩ impedance and 0 dB attenuation, and set the reference channel at 50Ω impedance and 20dB attenuation. We set the output channel of the analyzer at single mode measurements, and the oscillator level to 15 dBm. The positioner controlled the vertical distance between the sample and the probe. A zero liftoff distance (vertical distance) of the probe was maintained by a spring force on the probe.

Because the capacitance of the probe depends upon the dielectric material, there is no unique relationship between the admittance and the thickness. Our approach was to build a look-up table or graph for each material that related the admittance values with the corresponding thicknesses of the same kind of material at different operating frequencies and different probe configurations. Then, to determine the thickness of an unknown

sample from this material, we measure the admittance and look up the corresponding thickness of this admittance from the corresponding graph. To get a more accurate value, we can repeat this measurement using different graphs of the same material (these graphs can be built by repeating the measurements of the admittance at different probe and system configurations), then calculate the average of all of these readings.

We applied this approach to the plastic sheets sample of ten sheets. First, we built the look-up graphs using measurements we had at 300 kHz and 500 kHz operating frequencies and at different spacings between the source and the receiver fingers. The measurements were repeated for five different spacings between the fingers of ID-8: 8 mil, 24 mil, 40 mil, 56 mil, and 72 mil. The spacings were selected according to the allowable spaces between the fingers as discussed in section 3.8. Figures 3-40, 3-41, 3-42, 3-43, 3-44, 3-45, 3-46, 3-47, 3-48, and 3-49 display the look-up graphs for this material. We can improve the accuracy of these graphs if we use many measurements. As the number of measurements used to build these graphs increases, the accuracy of these graphs increases. The accuracy of these graphs increases also, if the measurements are repeated at different times and setups and the average taken of the whole set measurements. To get better accuracy in measuring the unknown thickness, it is important to increase the number of points in the look-up table by making more measurements on the thicknesses in between the values shown. In this way the percentage of error in the approximation decreases.

After creating the look-up graphs we used them to determine the thickness of an unknown sample. The same probe was used with the same spacings and operating frequencies to measure the admittance of this sample. After that we used the look-up

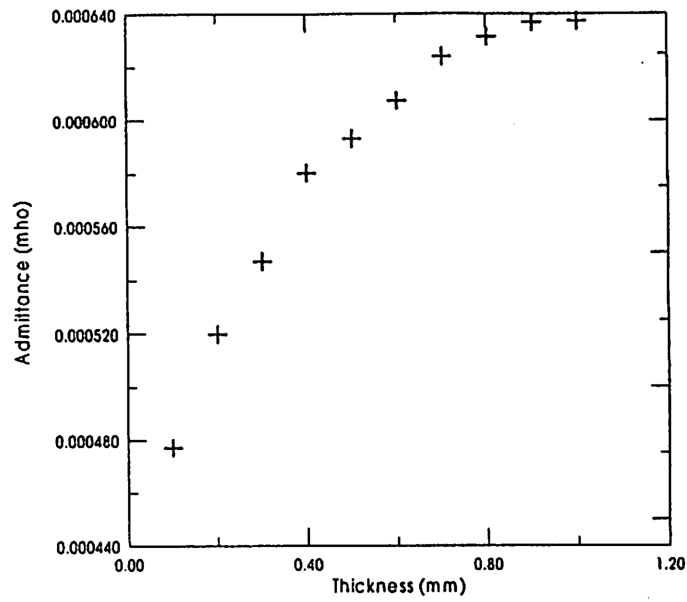

Figure 3-40. Admittance vs. thickness of the polyester plastic sheets using ID-40 with spacing of 8 mil and at 300 kHz

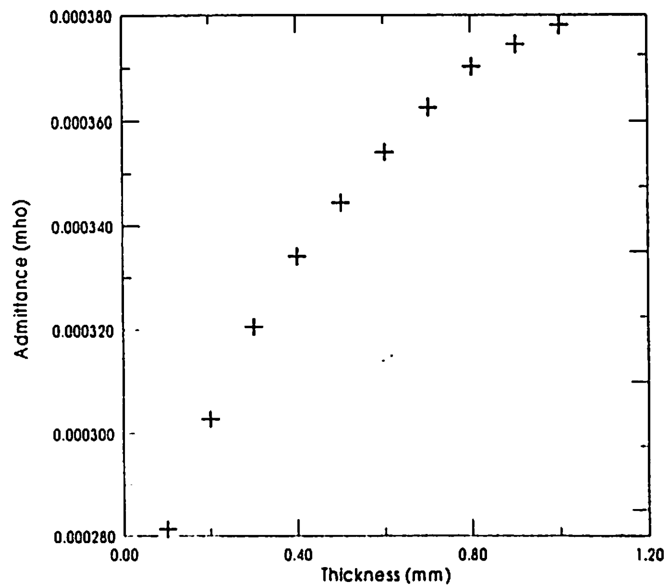

Figure 3-41. Admittance vs. thickness of the polyester plastic sheets using ID-40 with spacing of 24 mil and at 300 kHz

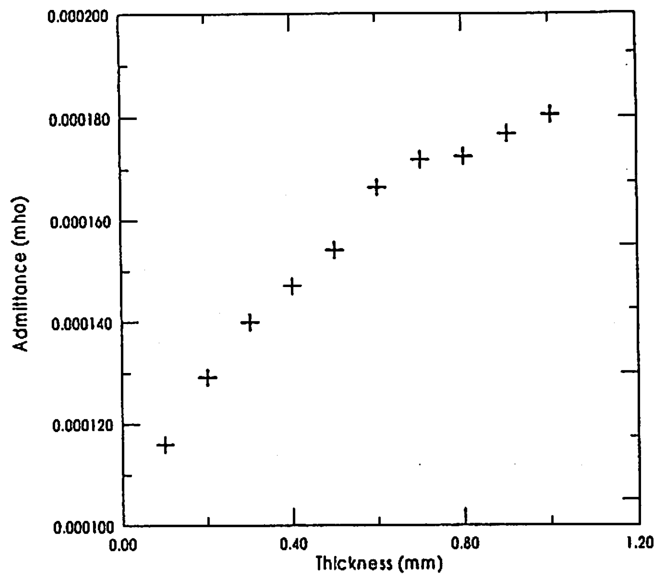

Figure 3-42. Admittance vs. thickness of the polyester plastic sheets using ID-40 with spacing of 40 mil and at 300 kHz

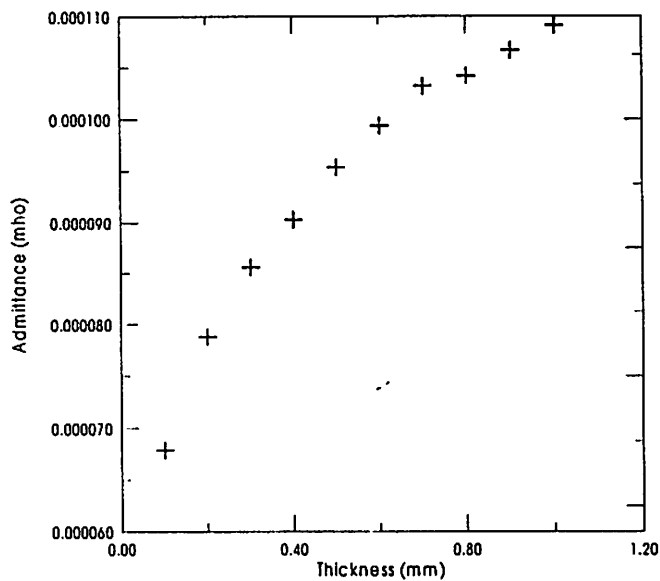

Figure 3-43. Admittance vs. thickness of the polyester plastic sheets using ID-40 with spacing of 56 mil and at 300 kHz

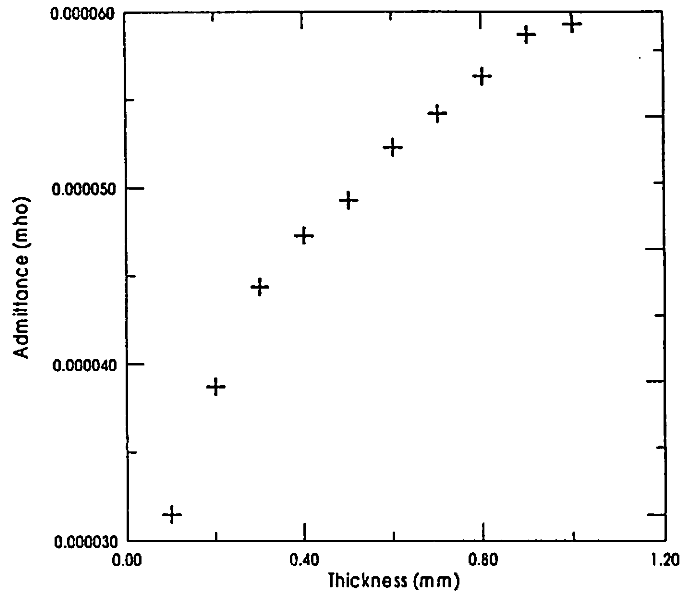

Figure 3-44. Admittance vs. thickness of the polyester plastic sheets using ID-40 with spacing of 72 mil and at 300 kHz

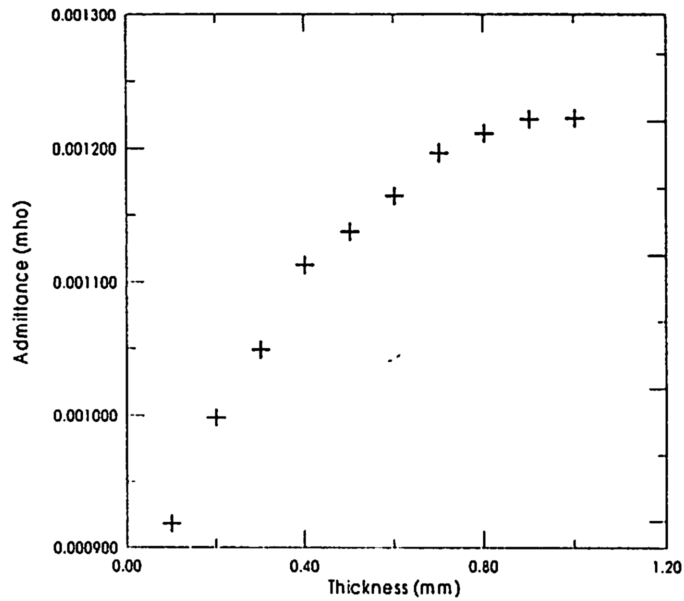

Figure 3-45. Admittance vs. thickness of the polyester plastic sheets using ID-40 with spacing of 8 mil and at 500 kHz

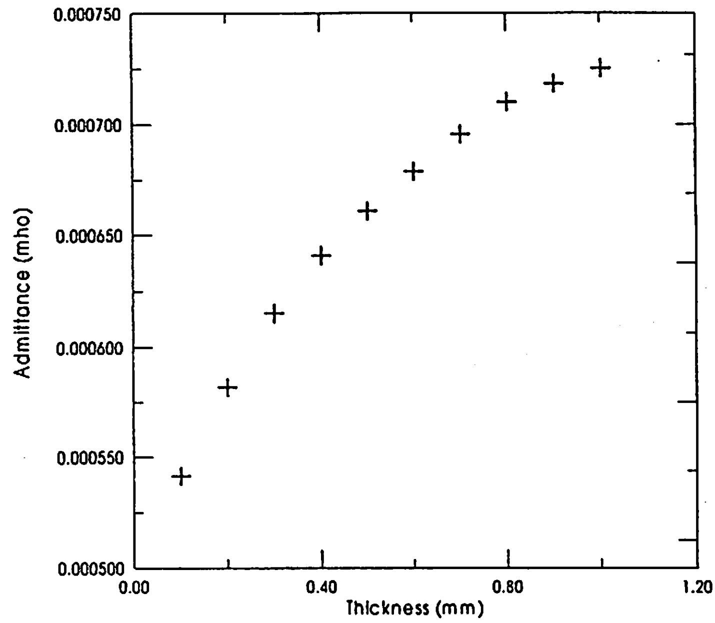

Figure 3-46. Admittance vs. thickness of the polyester plastic sheets using ID-40 with spacing of 24 mil and at 500 kHz

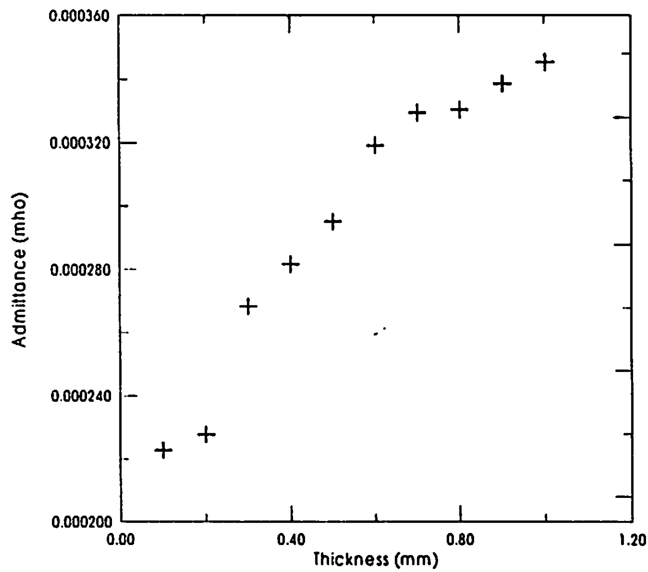

Figure 3-47. Admittance vs. thickness of the polyester plastic sheets using ID-40 with spacing of 40 mil and at 500 kHz

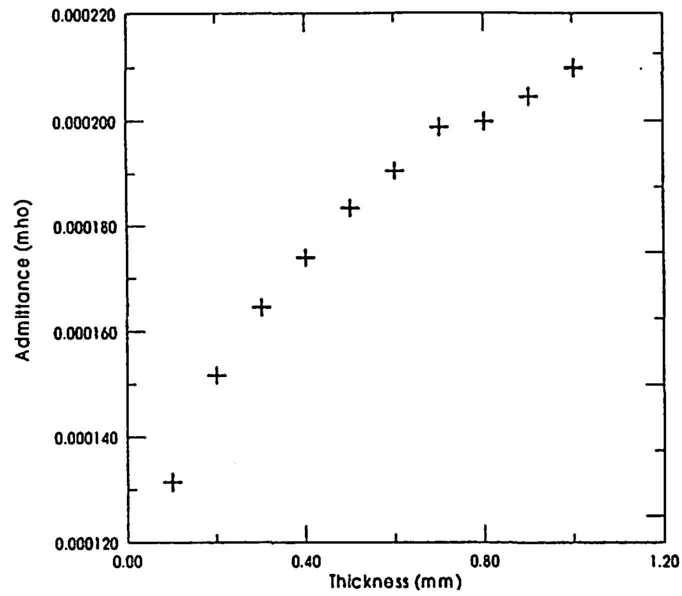

Figure 3-48. Admittance vs. thickness of the polyester plastic sheets using ID-40 with spacing of 56 mil and at 500 kHz

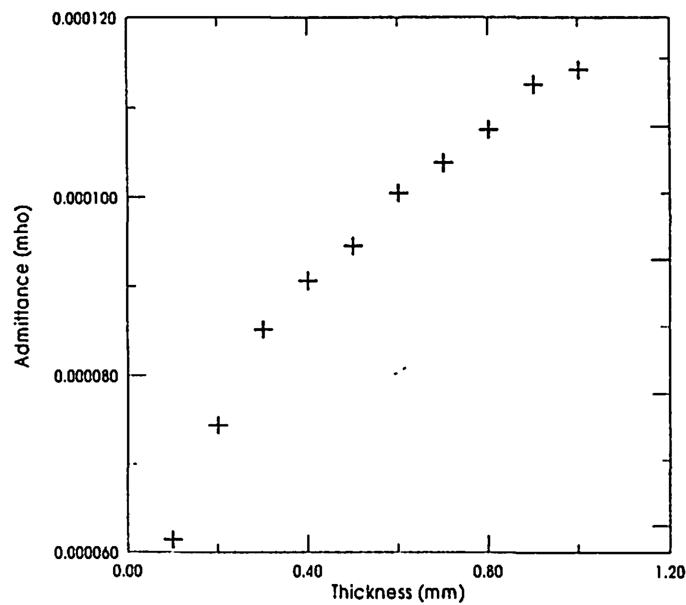

Figure 3-49. Admittance vs. thickness of the polyester plastic sheets using ID-40 with spacing of 72 mil and at 500 kHz

graphs to determine the corresponding thickness for each admittance value. Finally we measured the actual thickness of the sample using a digital micrometer. Table 3-3 summarizes the results and also shows a comparison between the actual measured thickness from the micrometer and the one calculated from the look-up graphs. The maximum percentage of error in this case less than or equal 4.7% of the actual thickness if we assume that the measured thickness from the micrometer is 100% accurate and there is no error in this measurement.

The error in the measurement of the thickness is caused by several factors. Firstly, the measured thickness from the micrometer was not exact. Secondly, we measured the thicknesses in the x-axis of the look-up graph by using a number of sheets and measuring the corresponding thickness using the micrometer and then divided this value by the number of sheets to get the average value of the thickness of the sheet. To get the thickness of n sheets, we multiplied the average thickness by the number of sheets n, assuming that each sheet has the same thickness. Actually, this is impossible. This factor can be reduced if we used a better technique to measure the thickness of the dielectric material. Thirdly, we built our look-up graphs using limited measurements. This cause of error can be reduced, if we use more measurements to build the look-up graphs.

3.5 Detecting flaws in dielectrics

Detecting flaws in a dielectric is one of the most important applications of the capacitive sensor in NDE. We tested this application by using a plastic sample of thickness 0.697 inch with different types of slots. This sample has mainly two widths of the slots: 0.25 inch and 0.105 inch. Each type has five different slots of different depths:

Table 3-3. Determining the thickness of unknown sample

Spacing (mils) /Frequency (kHz)[1]	Measured Admittance[2] (mS)	Expected thickness[3] (mils)	% Error[4]
8 /500	1.1624	23.69	+0.70
24 /500	0.6613	24.09	+2.40
40 /500	0.2992	24.04	+2.25
56 /500	0.1815	23.16	-1.54
72 /500	0.0989	22.93	-2.50
8 /300	0.6118	24.05	+2.25
24 /300	0.3506	22.52	-4.30
40 /300	0.1616	22.42	+4.70
56 /300	0.095	23.69	+0.71
72 /300	0.0516	24.73	+3.80

1 Spacing between the source and the receiver of the probe / Operating frequency of the system
2 Measured admittance using the probe
3 Expected thickness using the previous look-up graphs
4 Percentage of error = (expected thickness-actual thickness)/actual thickness * 100% , actual thickness measured by the micrometer was 23.52 mil (0.588 mm).

surface breaking slot of depth 0.697, 0.662, 0.627, 0.522, 0.347 inch. Figure 3-6 displays different views of this sample. This sample was used in two ways: one of them was by using the slots as surface slots, the second way was to flip it over so the slots became sub-surface slots. Each slot was scanned separately from the bottom to top and from left to right. Two types of probes (SD-200 and ID-40) were used to perform this scanning. Both of them were used in the differential mode. The impedance analyzer was used in the Gain Phase mode with medium integration time and 32 point averages. A current amplifier was installed on each receiver finger. Because of the small size of the probe, we could not build a differential amplifier on the top of it, therefore, we used the analyzer and the software on the computer to find the differential signal between the two electrodes. The source of the probe was connected with the output terminal of the analyzer. The receiver

electrodes were connected with the reference and test channels of the impedance analyzer. The impedance analyzer was set to 1MΩ and 20 dB for both input channels, while the output channel was set at single measurement mode.

The computer was used to control the position of the sample and the motion of the motor. Also, the computer was used to capture the data and store it in a file. To get the differential signal between the two receiver electrode signals, a certain processing technique, developed at the NDE center called **process 2** (developed by Mr. Nakagowa), was used to perform the subtraction between the two captured outputs. In some cases, we used this processing technique to reduce the effect of the noise. Two types of softwares have been used to analyze the data: Surfer16 and Grapher for windows. Surfer16 was used to analyze the 2D data, while Grapher was used to analyze the 1D data. Each type of slot has been analyzed using 3D plot, contour plot, image response, and 1D plot. We noticed from our experiment that the two types of sensors did not give good responses for sub-surface slots of depth more than 0.627 inch. To improve the penetration depth of the probe, we need to increase one of the previous factors: the number of fingers, the dimension of the finger, or the spacing between fingers.

The following figures display the most important results. Figures 3-50 to 3-53 show the response of SD-20 due to the narrow slot of depth 0.697 inch (surface breaking slot). Figure 3-50 show a 1D plot of this response. Figures 3-51, 3-52, 3-53 show the 2D plots of the response in different forms: a contour plot, an image, and a 3D plot. From these figures, it is noticed that the probe response due the surface breaking slot is a valley followed by a peak. In the differential mode, the probe has two capacitances: first,

between the source and the positive electrode of the receiver (C_+). Second, between the source and the negative electrode of the receiver (C_-). The displayed response is the difference between the two capacitances. The valley or the peak is produced due to the unbalance in the capacitances C_+ and C_-. These two capacitors are not equal due to the difference in the dielectric constant of the material between the plates. We notice from Figure 3-50 that the positive peak and the negative peak are not identical. This is due to two factors: first, the difference in the amplifier circuit for each electrode due to the difference in the common-mode signal for each amplifier and each value of resistor in each circuit. Second, it is assumed that the sample has the same thickness before and after the slot, but in fact the sample has a slight difference in the thickness.

Figures 3-54, 3-55, 3-56, and 3-57 show the response of the probe due the presence of a surface breaking wide slot. We notice from these figures that the overall response of the probe in this case is the same as the one for narrow slot. There are some slight differences in the response of the wide slot. For instance, the positive or the negative peaks in the wide case becomes a little bit flat. This is because the unbalance in C_+ and C_- remain longer due to the increase of the width of the slot. The relationship between the 1D response of the probe in this case and the position of the probe above the slot is explained in detail in Figure 3-58.

Figure 3-59, 3-60, 3-61, 3-62 show the response of the probe due to buried slot of depth 0.662 inch. We notice from our experiments that the two probes (SD-200 and ID-40) can not detect a buried slot of depth more than 0.627". After this depth the probe can give a weak response that is difficult to analyze, and the noise becomes large so that the

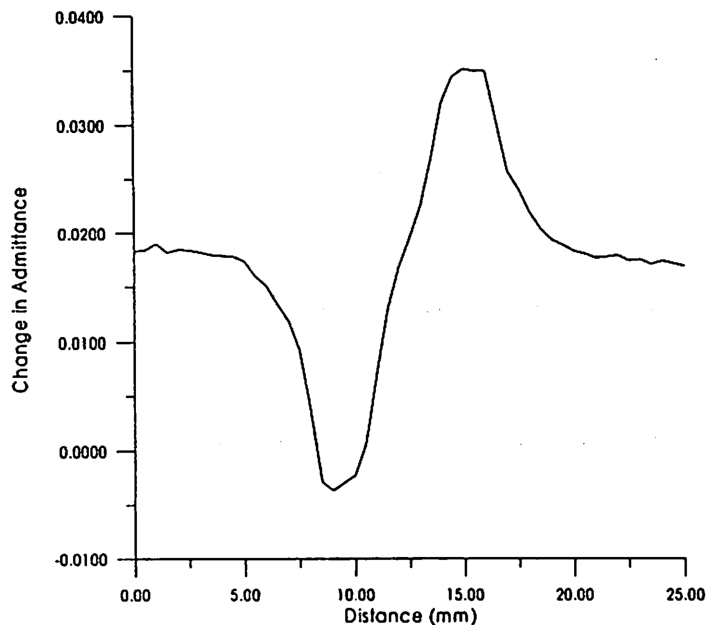

Figure 3-50. Change in the admittance due to the narrow surface breaking slot using a SD-200 capacitive probe

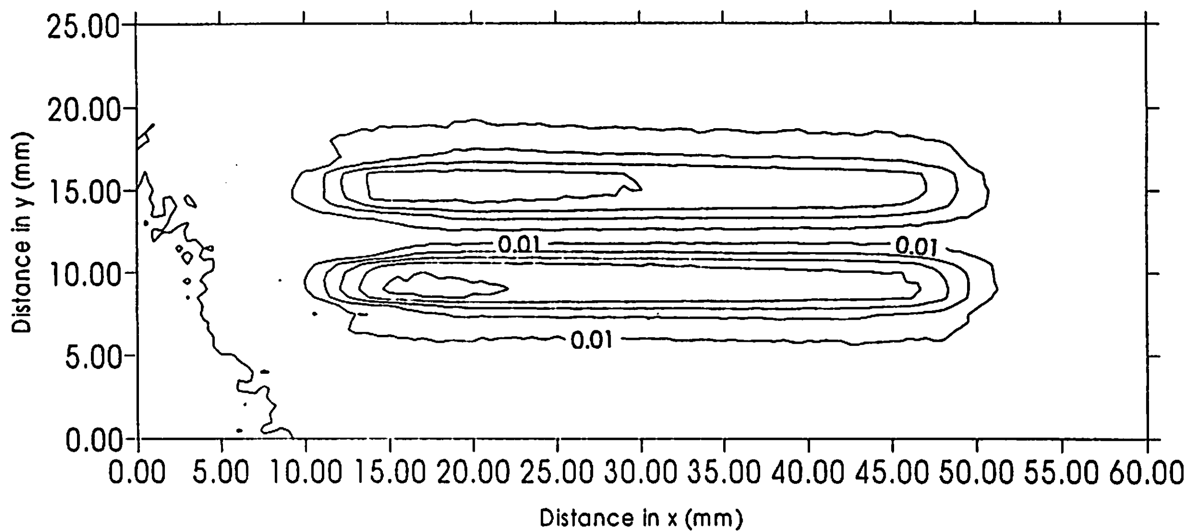

Figure 3-51. Contour plot of the response of SD-200 capacitive probe to the narrow surface breaking slot

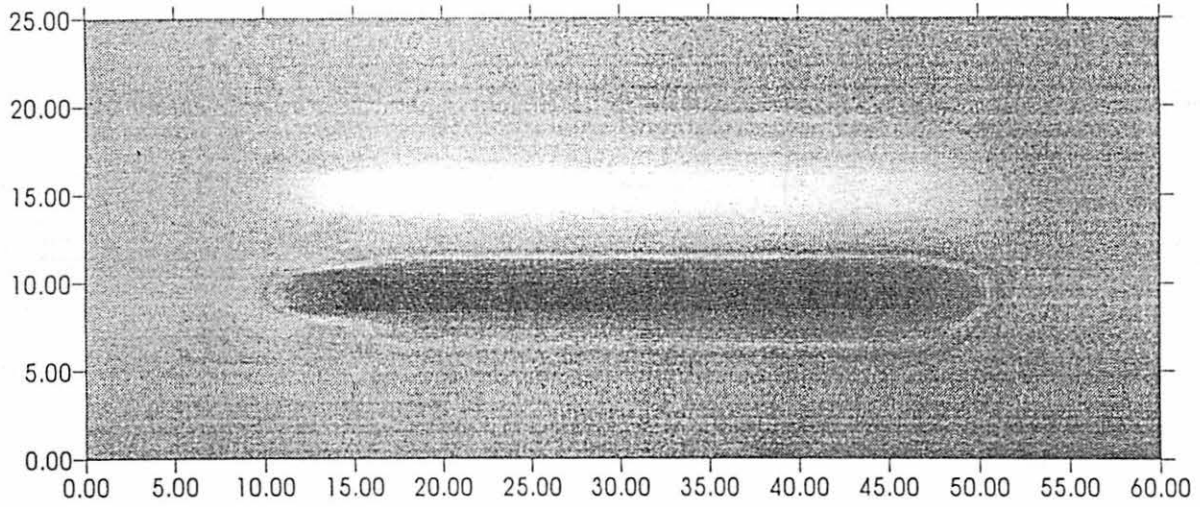

Figure 3-52. The image response of SD-200 capacitive probe to the narrow surface breaking slot

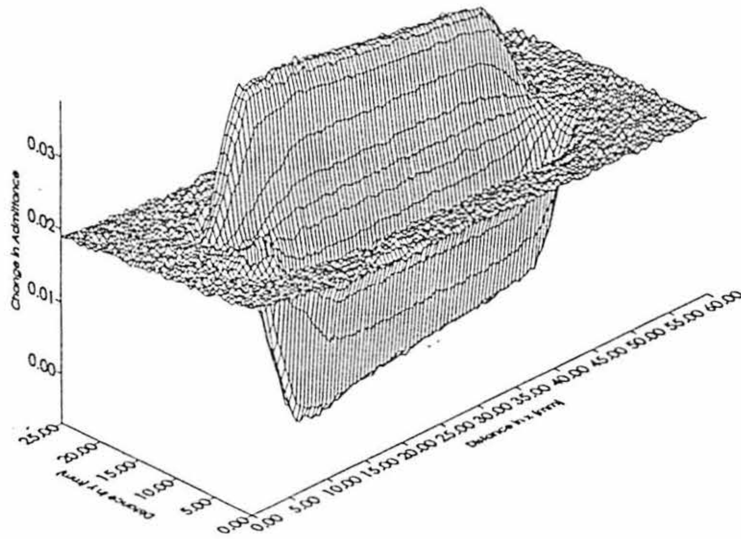

Figure 3-53. 3D plot of the response of SD-200 capacitor probe to the narrow surface breaking slot

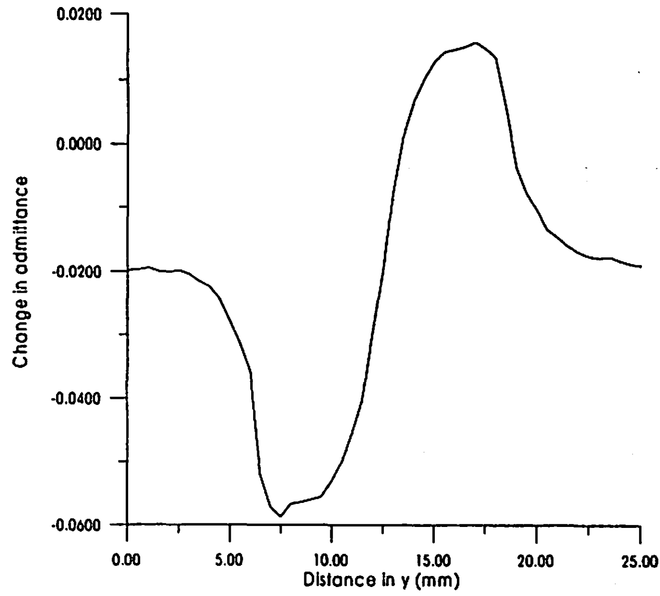

Figure 3-54. Change in the admittance due to the wide surface breaking slot using SD-200 capacitor probe

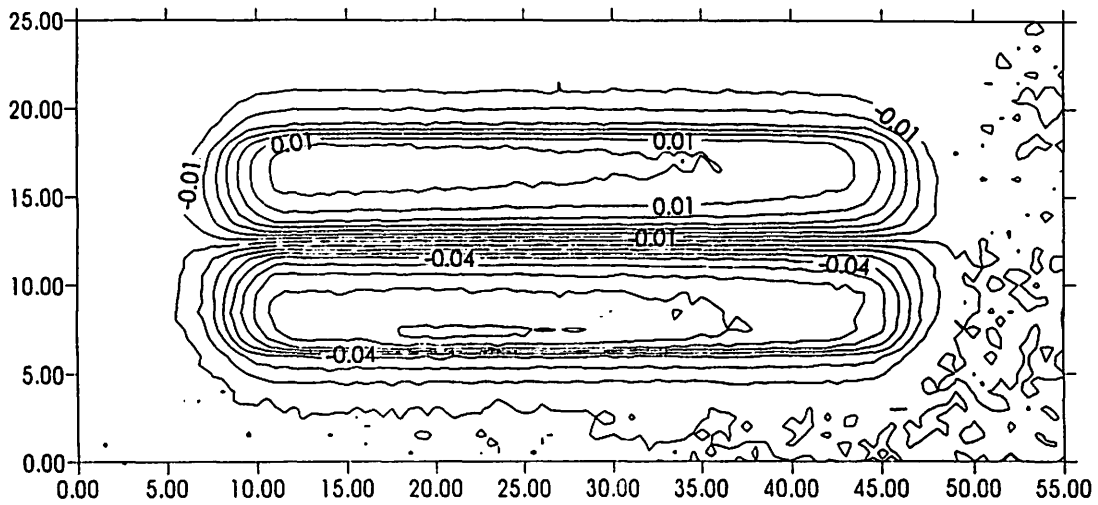

Figure 3-55. Contour plot of the response of SD-200 capacitor probe to the wide surface breaking capacitor probe

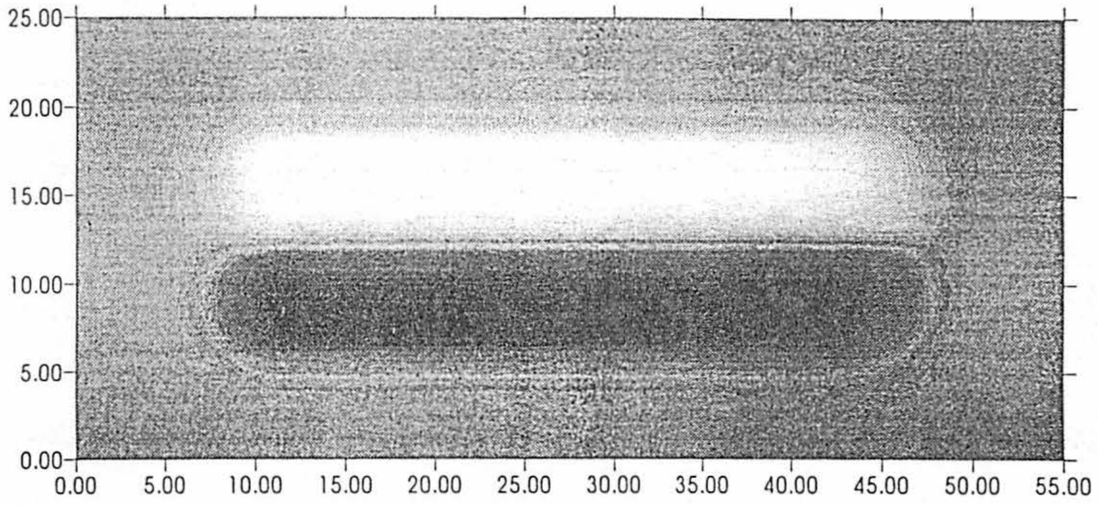

Figure 3-56. Image plot of SD-200 capacitor probe
to the wide surface breaking slot

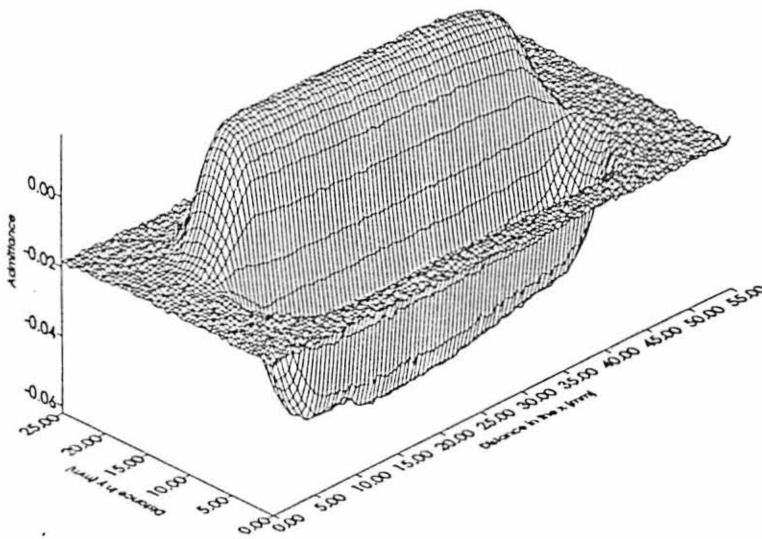

Figure 3-57. 3D plot of the response of SD-200 capacitor probe
to the wide surface breaking slot

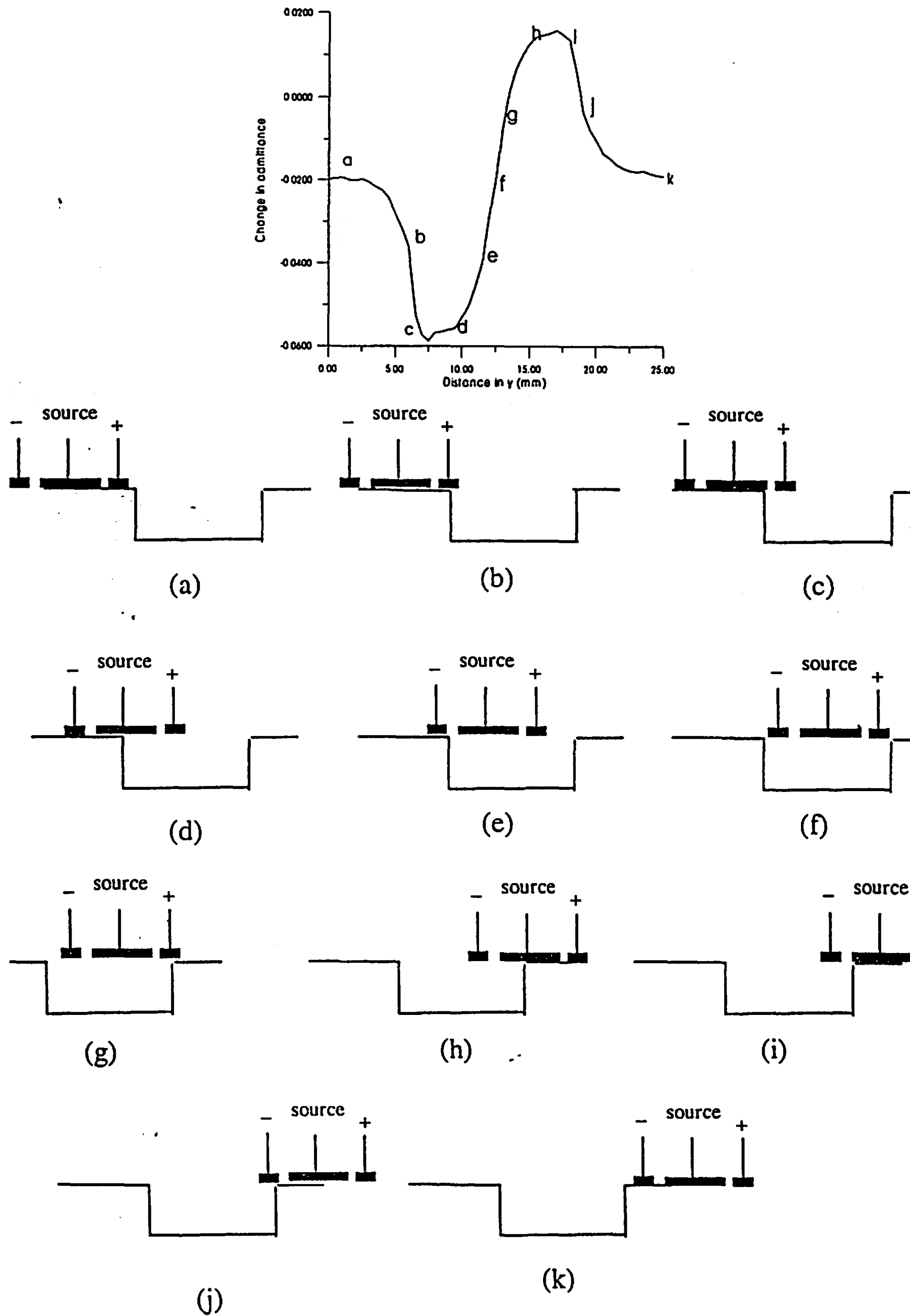

Figure 3-58. The relationship between the response of the SD probe and its position to the wide surface breaking slot

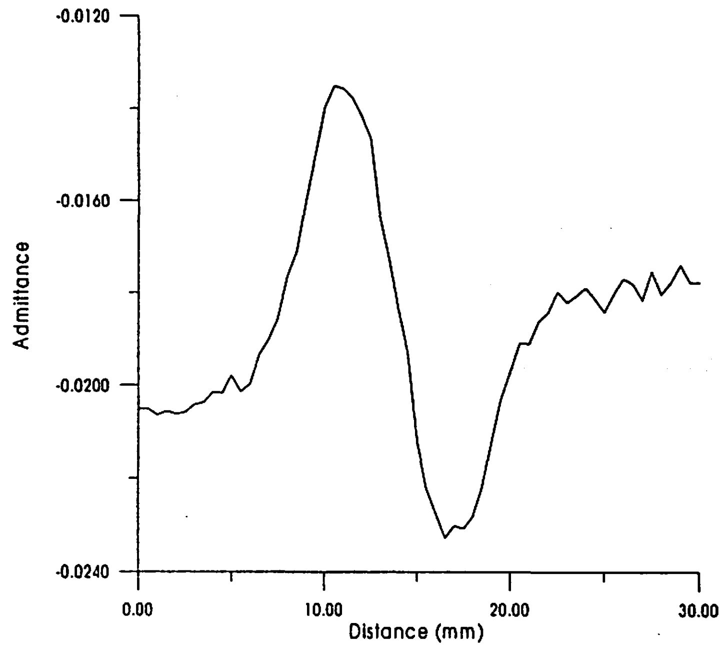

Figure 3-59. Change in the admittance due to the narrow buried slot of depth 0.662 inch using probe SD-200

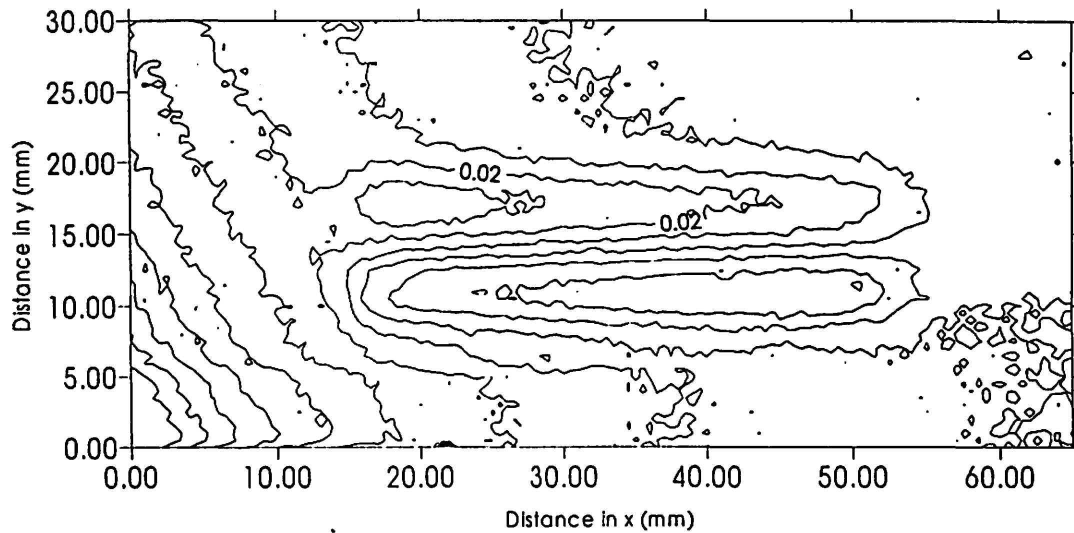

Figure 3-60. Contour plot of the response of SD-200 capacitor probe to narrow buried slot of depth 0.662 inch

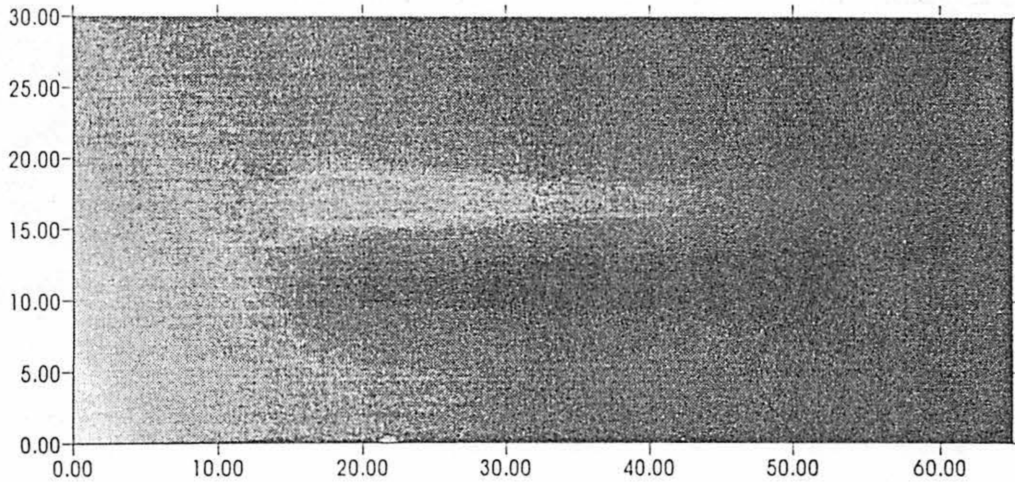

Figure 3-61. Image of the response of SD-200 capacitor probe to the narrow buried slot of depth 0.662 inch

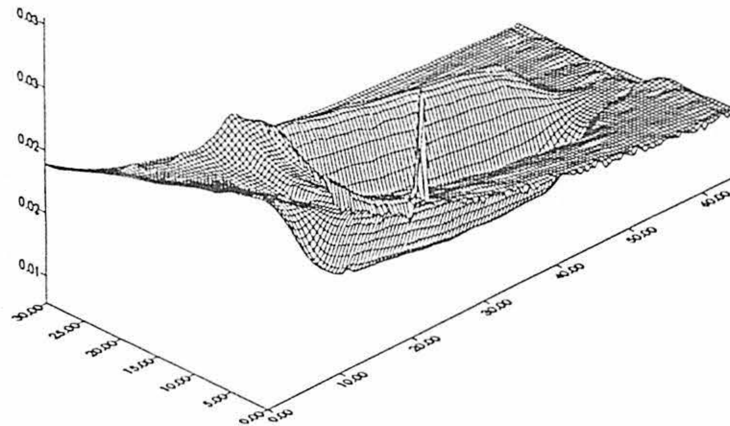

Figure 3-62. 3D plot of the response of SD-200 capacitor probe due to the narrow buried slot of depth 0.662 inch

signal to noise ratio decreases. In the buried slots, the response starts with the peak instead of the valley. This difference is due to the variation in the dielectric material (plastic above the air) between the electrode plate above the slot and the source.

Figures 3-63, 3-64, 3-65, and 3-66 display the response of the interdigitized probe ID-40 due to the wide surface breaking slot. From these figures, we notice that the response of the probe is almost the same as the one from the square directional probe. The slight difference in this case is due to the differences in the dimensions of this probe and the spacing between the fingers.

Our next step is using the above response to determine the width and the length of the slot. From Figure 3-58, we notice the response of probe starts decreasing when the edge of the first electrode approaches the slot. It returns to the neutral level after the last edge of the first electrode approaches the slot. The process repeats with the opposite sign as the probe exits the slot. This shows the measured signal is the convolution of the transfer function of the probe and a square rectangular signal corresponding to the width of the slot. The width of this signal approximately equals the width of the slot plus the width of the transfer function of the probe. Because of that, we need to determine the transfer function of the probe. Figure 3-67 displays the transfer function of the probe using a thin wire. From this figure, the width of the transfer function is 19-6.5=12.5 mm (0.5 inch). As an example of calculating the width of a slot consider Figure 3-54. From this figure, the signal starts decreasing at 3.5 mm and returns to the neutral value at 22 mm. The width of the response is 22-3.5 = 18.5 mm (0.74 inch). The calculated width of the slot in this case is 0.74 - 0.5 = 0.24 inch. There is a slight difference between the

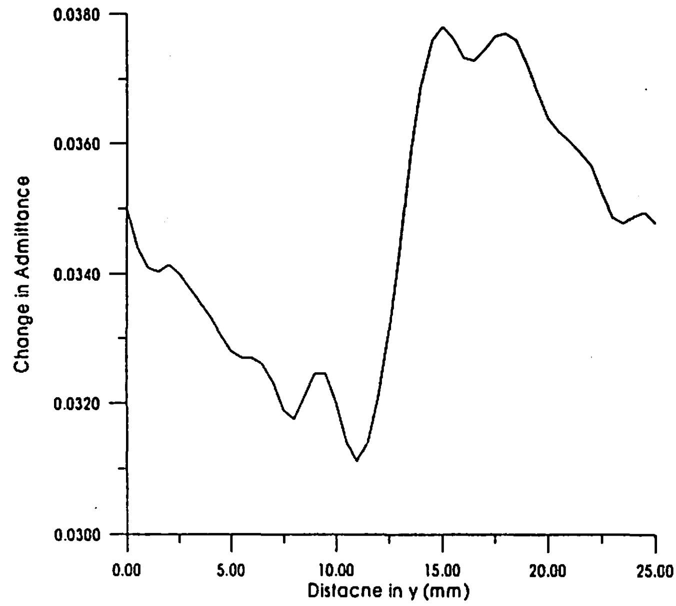

Figure 3-63. Change in the admittance due to the wide surface breaking slot using ID-40 capacitor probe

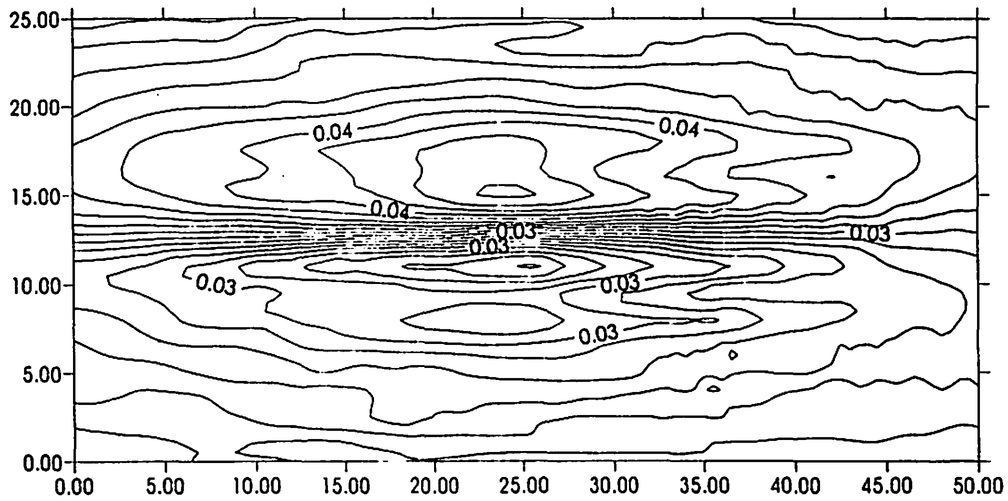

Figure 3-64. Contour plot of the smoothed response of ID-40 capacitive probe due to the wide surface breaking slot

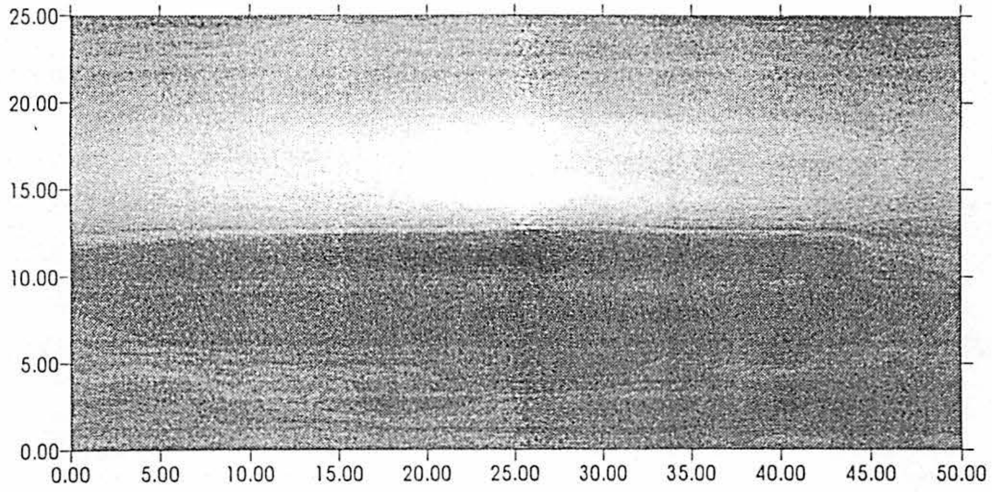

Figure 3-65. Image of the smoothed response of ID-40 capacitor probe due to the wide surface breaking slot

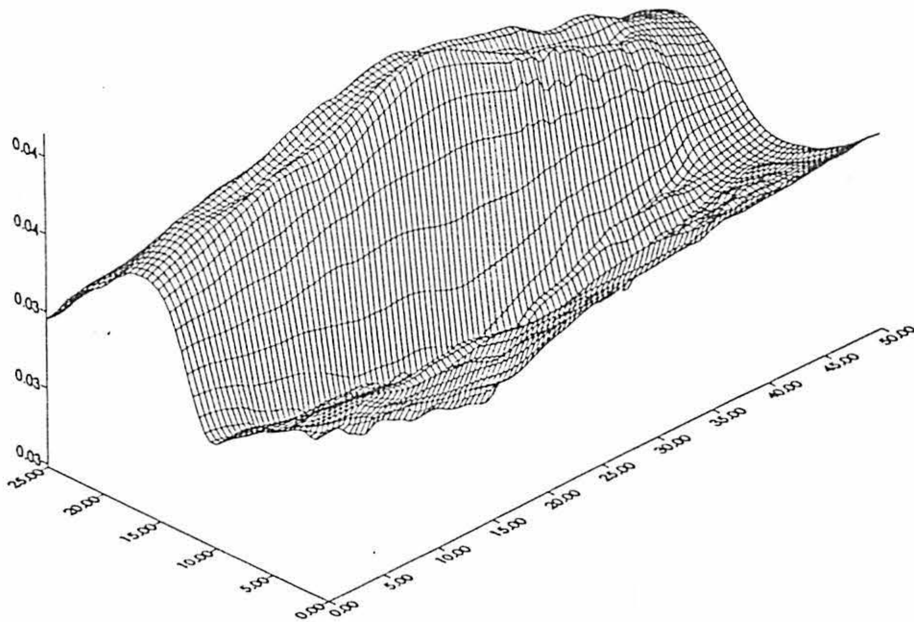

Figure 3-66. 3D plot of the response of the ID_40 capacitor probe to the wide surface breaking slot

measured width (0.25 inch) and the calculated width due to: firstly, the effect of fringing, secondly, some measurement error of the width of the slot, thirdly, approximation error in our calculations, and fourthly, experimental errors.

To determine the length of the slot, we use the same approach with some modifications. One of these modifications is using the length of the probe instead of the width. Also we need to use either a slot in the y-direction to do the calculations or use the image response.

To determine the width and length more accurately, we restored the image, then calculated the dimensions of the slot from the restored image. To restore the image, the transfer function of the probe needs to be determined. We used a thin wire of thickness 0.0065 inch to represent the delta function required to find the impulse response. Figure 3-67 displays the impulse response of the SD-200 probe. This impulse response represents a slice from 2D plot. We placed both the transfer function and the response of the probe due to the slot in a DEC computer and restored the image with MATLAB. Two techniques were tried for restoration. The first technique was inverse filtering, while the second one was Wiener filtering. Wiener filter has the following form:

$$F(u,v) \approx \left[\frac{H^{*}(u,v)}{|H(u,v)|^{2} + K}\right]G(u,v) \tag{3.7}$$

where H(u,v) is the Fourier transform of the transfer function.

F(u,v) is the Fourier transform of the restores image.

G(u,v) is the Fourier transform of the measured image.

The G(u,v) is the fourier transform of the 2D image shown in Figure 3.56. The H(u,v) was calculated using the 2D image of the transfer function shown in Figure 3.67. Different values for K were tried, the best value was 500. The output result of inverse filtering was bad and could not be used at all. While the output result of the Wiener filter was not so bad, but also it did not restore the image correctly. Figure 3-68 show the results of the restoration of the image with a Wiener filter. From Figure 3-68c, we used a slice of a 2D image to measure the width of the probe. The width of the slot was determined by measuring the maximum and minimum variation in the intensity, then using the middle point from both sides of the image to calculate the width. From the restored data, the width of the slot equals 0.24 inch with a percentage of error equals 4%. A better restoration can be obtained by improving the transfer function of the probe. In the future, we will work more on restoring the output image from the probe using better techniques and control the parameters that effect the restoration.

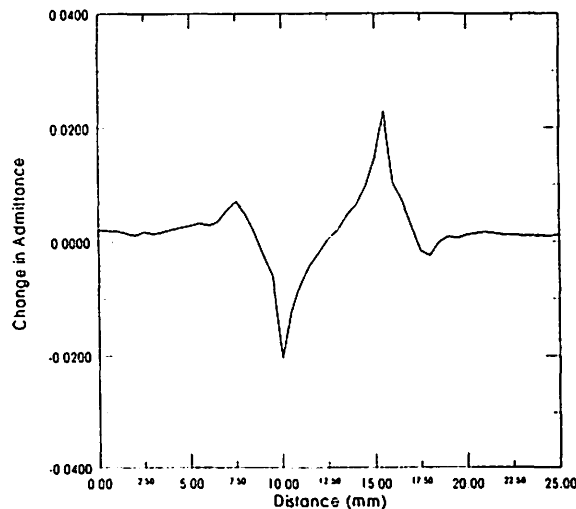

Figure 3-67. Transfer function of the SD-200 probe due to thin wire (0.0065 inch)

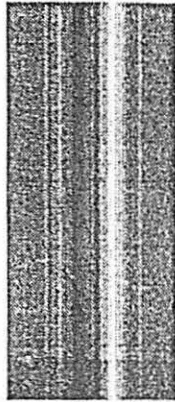

(a)

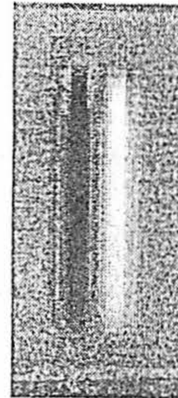

(b)

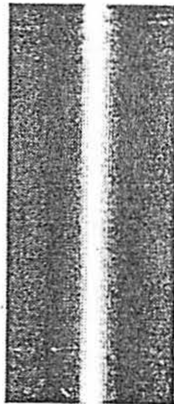

(c)

Figure 3-68 The restoration of the image using MATLAB
a) the transfer function b) the original data c) restored data

CHAPTER FOUR

DISCUSSION

4.1 Introduction

In the last chapter we summarized the most important results obtained using different capacitor probes. The overall response of the probes due to various factors has been studied. In this chapter, we will analyze these data quantitatively. Also in Chapter three, the numerical method was discussed. A numerical method was used to check the strange behavior of the probe by varying the thickness of the dielectric material. In this chapter, we tie the experimental work with the numerical work especially after we discussed the experimental work completely in the last chapter.

4.2 Quantitative analysis of the data

As we discussed previously, the measured admittance of the capacitive probe is affected by various factors: grounding the bottom metal plate, finger spacing, etc. The general relationship between the admittance value and these factors has been studied in the last chapter. In this section, we will try to study the quantitative relationships between the admittance and these factors.

The first factor is the effect of grounding the bottom metal plate. As shown in Figures 4-9 to 4-11 and discussed in section 4.3.2, the grounding of the metal plate had little effect on the measured admittance especially when the thickness of dielctric is larger a certain number (12 mils), and this result is helpful in simplifying the measurements of industrial samples. Table 4.1 summarizes quantitatively the effect of this factor on the

Table 4-1. The effect of grounding the metal plate using double narrow finger probe with single space between fingers, connection + - + - and at 100 kHz

Number of sheets	Measured Y (nS) with floating plate	Measured Y (nS) with grounded plate	Percentage of diff* %
1	179.12	162.02	9.5
2	182.82	169.42	7.3
3	185.91	176.43	5.1
4	191.20	185.55	3.0
5	197.06	191.96	2.5
6	202.30	196.66	2.7
7	207.20	203.07	2.0
8	211.95	209.32	1.2
9	216.42	210.40	2.7
10	220.98	215.83	2.3

* Percentage of diff. = (column two-column three)/column two * 100%

admittance value. This table shows the data represented in Figure 4-9.

We notice from Table 4-1 that the effect of grounding the metal plate does not exceed 10 % in the worst case. From table 4-1 and Figures 4-9 to 4-11 we see that the effect of keeping the bottom metal plate floating is large when the thickness is small, but when the thickness of the dielectric material increases this effect decreases. This is because when the thickness is small, the admittance value is small. Therefore, the admittance is sensitive to any change in the system. It is also clear in Table 4-1 that the general behavior of the admittance due to the change in thickness of the dielectric material is the same. Therefore, we can study some ungrounded industrial samples with small amount of error in the results especially if it is difficult to ground these samples.

The second factor is the effect of the operating frequency of the system. It was observed in section 4.3.3 that the admittance increased by the same factor as the

frequency increased. The relationship between the admittance and the frequency applied in all cases at different connections, spacings, number of fingers, and finger dimensions. To study this effect quantitatively, Table 4-2 shows the measured admittance value at 100 kHz and at 50 kHz. Column four shows the ratio between the measured admittance at the

Table 4-2. The effect of changing the operating frequency using narrow single finger probe single space, connection number one.

Number of sheets	$\lvert Y \rvert$ (μ) at f = 100 kHz	$\lvert Y \rvert$ (μ) at f = 50 kHz	Ratio = column 2/ column 3
1	4.757	2.387	1.993
2	3.336	1.681	1.985
3	2.733	1.316	2.076
4	2.403	1.210	1.985
5	2.150	1.081	1.989
6	1.895	0.986	1.923
7	1.817	0.875	2.077
8	1.709	0.860	1.987
9	1.600	0.806	1.985
10	1.525	0.768	1.986

above two frequencies. We notice in Table 4-2 that changing the operating frequency by a factor two changes the measured admittance by a factor that varies from 1.923 to 2.077. The average of column four equals 1.999 which is almost two. This indicates that the admittance has a linear relationship with the frequency.

The third factor is the spacing between fingers. As discussed in section 3.3.5, the admittance decreased as the spacing between fingers increased. We found from Figures 4-23 to 4-27 that the admittance did not decrease by the same factor as the spacing increased. This is due to the nonlinear relationship between the admittance and the

spacing as discussed in chapter one, and also due to the presence of two types of capacitance. One of these capacitances, the parasitic one, is constant and is not effected by changing the spacing. While the second one, the probe capacitance, is variable and is changed by changing the spacing. To study the relationship between the measured admittance and the spacing between the fingers quantitatively, we need to subtract the constant admittance from the total admittance, then determine the ratio between the variable admittances at different spacings to get the exact relationship. To calculate the constant capacitance, we used the following equations:

$$KV_1 + C = X_1 \tag{4.1}$$

$$V_1 + C = Y_1 \tag{4.2}$$

$$KV_2 + C = X_2 \tag{4.3}$$

$$V_2 + C = Y_1 \tag{4.4}$$

where C is the constant capacitance, K is the assumed ratio between the variable capacitance with single space and double space, V_1 and V_2 are the variable capacitances at two different thickness of a dielectric. X_1 and X_2 are the calculated capacitances from the measured admittances at double space, Y_1, Y_2 are the calculated ones from the measured admittances at single space. Table 4-3 shows one case of the variable admittance at the two spacings: 1.67 mm and 3.41 mm. Column four shows the ratio between the column 2 and column 3. The ratio varies from 2.36 to 2.01. As explained previously, this is due to the nonlinear relationship between the admittance and the spacing between the fingers.

The fourth factor is the dimension of the probes. As discussed in section 4.3.6, the admittance increased as the dimension of the probe increased. The relationship

Table 4-3. The effect of the spacing between fingers using single narrow finger probe, connection number two, at 100 kHz.

Number of sheets	I Y I (nS) spacing = 1.67 mm	I Y I (nS) spacing = 3.41 mm	Ratio = column 2 / column 3
1	110.69	46.97	2.36
2	115.55	50.11	2.31
3	118.33	52.42	2.16
4	123.02	54.83	2.24
5	126.99	56.97	2.30
6	129.49	59.87	2.16
7	133.99	64.31	2.08
8	137.64	67.03	2.05
9	140.99	68.83	2.05
10	144.34	71.56	2.01

between the admittance and the dimension of the probe was not linear due to the presence of the constant admittance, which was related to the parasitic capacitance. To study the effect of the dimension of the probes, it is better to subtract this constant capacitance first. Table 4-4 shows this relation for one of the measured cases. This table shows the variable admittance for two different dimensions with the ratio between these two admittances in column four.

As shown in column four, the ratio between the admittance in the two dimensions varies from 1.28 to 1.33. The average value of these is 1.30, while the expected ratio, which equals the ratio between the two dimensions, equals 1.28. There is a slight difference between the expected ratio and the measured one. This is due to some errors in measuring the admittance value and in measuring the dimension of the probe.

According to all of the above quantitative discussions, we find that the admittance of the

Table 4-4. The effect of changing the dimension of the probe using single finger probe, double space, connection two, at 100 kHz.

Number of sheets	| Y | (nS) length = 8.88 mm	| Y | (nS) length = 6.96 mm	Ratio = column 2 / column 3
1	67.62	52.97	1.28
2	72.87	56.11	1.31
3	76.77	58.42	1.28
4	78.16	60.83	1.32
5	82.93	62.97	1.32
6	87.19	65.87	1.32
7	91.00	70.31	1.29
8	95.96	73.03	1.31
9	100.05	74.83	1.33
10	102.58	77.56	1.32

probe has a linear relationship with the operating frequency and the dimension of the probes, while it has a nonlinear relationship with the spacing between the fingers. Also there is a slight change in the admittance value due to the grounding of the bottom metal plate. Therefore, to increase the admittance value of the probe for penetration, we can increase the operating frequency, the dimension of the probe, or the number of fingers.

4.3 Comparison with the measurements

One of the most important objectives of the numerical solution is checking the behavior of the probe due to the change of the thickness of the dielectric material. This objective can be achieved by comparing the results obtained from the numerical solution and the ones measured by the probe. As found from the measurements (shown in Chapter four), capacitance of the open plate capacitor increases by increasing the

thickness of the dielectric material. This kind of behavior seems to be in contradiction with the simple theory for the parallel plate model, therefore, a numerical program was used to test this behavior by finding the capacitance for different thicknesses.

The open-flat capacitor sensor, which was illustrated in Figure 3-1, has been modeled in a numerical code. The source plate was fixed to 1 volt, the receiver plate was fixed to -1 volt, while the bottom metal plate was fixed to zero volts. The size of each grid was 0.02 mm, the number of iterations varied from 200 (at 0.1 mm) to 700 (at 1 mm). The program was run on the DEC station 5000. The execution time varied from 10 hours (at 200 iterations) to 24 hours (at 700 iterations). This code has been run for five different thicknesses. Table 4-5 summarized these results. The average thickness of the plastic sheets (column one) was calculated by summing the thickness of ten plastic sheets (1.0025 mm or 40.1 mil), then dividing this number by ten. As noticed in the table, the numerical result shows the same kind of behavior for the open-flat capacitive probe as the measured result. As shown from column three, the calculated capacitance increases as the thickness of the dielectric material increases. This means that the measured response is almost correct. By comparing the numbers in columns two and three (see column four), it is noticed that there is a slight difference between these numbers which vary in a rather systematic way as the thickness increases. This difference may occur for various reasons: firstly, the numerical program used the ideal measurements of the thicknesses, i.e. it used the thickness of a number of plastic sheets by multiplying the average thickness of one of them by the number used. In fact the actual thickness of each individual sheet may vary from the average thickness calculated above. On the other

hand, the measured values used the actual thicknesses. Secondly, there might be a slight error in the dimensions of the probe which was modeled. Thirdly, there might be a small error in the modeling of the receiver-source-sample model. Figure 4-1 shows a comparison between measured values and the calculated values using a numerical method. We notice the same slight difference between both of these values.

Table 4-5. Comparison between the measured capacitance and the numerically calculated capacitance from numerical solution for different thicknesses of dielectric material

Thickness (mils)	Measured Capacitance (pF)	Calculated Capacitance (pF)	Difference Meas.-Cal.
8	145	139.56	4.43
16	153.02	150.53	2.49
24	159.49	162.31	-2.82
32	167.64	171.85	-4.21
40	174.34	176.23	-1.89

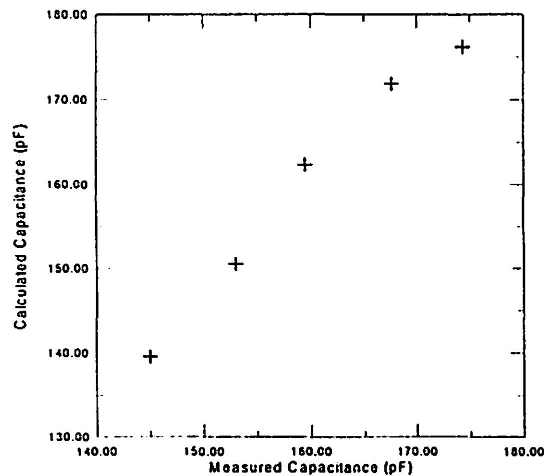

Figure 4-1. Caparison between measured capcitances and calculated ones from numerical method

CHAPTER FIVE

CONCLUSIONS

The capacitive probe is a very useful device for nondestructive evaluation of dielectric materials. It is sensitive to both surface and subsurface features in dielectric materials. From the characterization studies we have shown, we found that the capacitive probe is capable of determining absolute values (such as thickness) in insulating materials, as well as detecting flaws or discontinuities of different types in the dielectric materials.

As the configuration of the capacitive probe becomes more complicated, the study of its behavior analytically becomes more difficult. For this reason, developing a numerical model for the probe and the system is very important. In our case, we used the finite difference method to model an opened flat capacitive probe and the system used to measure the thickness of a dielectric material. From this model, we found that the admittance of the probe increased as the thickness of the dielectric material increased (it varied from 145 pF to 174 pF when the thickness varied from 8 mils to 40 mils). These results from the numerical method were close to those measured by the probe (the maximum percentage of error was less than 3.1%). The numerical method (finite difference method) used to model this system is sensitive to the grid size, the number of iterations, and the boundary conditions in the system. If the grid size decreases or the number of iterations increases to improve the output results, the execution time to run the program increases very much. The numerical results can be improved by using other

numerical methods to model the system, such as the finite element method. It is less sensitive to the grid size and the number of iterations, and it is more suitable for complicated boundary conditions. On the other hand it is more complicated than the finite difference method.

The capacitive probe has two modes of operation: absolute and differential. Each mode has advantages and disadvantages according to the applications. The absolute mode is very sensitive to the liftoff distance. Therefore, we need to control this distance when making any measurements. We usually use the probe in this mode to measure some absolute values of a dielectric material, such as thickness, porosity, dielectric constant, and density. On the other hand, the differential mode reduces the effect of the liftoff, but it reduces also the sensitivity of the probe to the slowly varying features. It was used in this case to detect variations in the sample that are small in size compared with the probe's sensing area, such as slots or voids.

This thesis studied the effect of various factors on the probe response. From our measurements we noticed the following points: first, shielding the wires was necessary to maintain a suitable signal-to-noise ratio and to get consistent results. Second, the admittance of the probe decreased rapidly as the liftoff distance increased. This decrease was followed by a recovery. The recovery was caused by parasitic capacitance coupling between the probe and the grounding points in the environment (Gimple, 1987). To reduce the effect of liftoff on measurements, measurements were taken with zero liftoff. Third, grounding the bottom metal plate, or in general grounding the sample, had little effect on the probe response especially when the thickness of the dielectric material larger

than 12.0 mils, but the grounded sample gave more stable and consistent results. Fourth, the admittance had a direct linear relationship with frequency. We found that the larger the admittance value, the better the response obtained; therefore, it is better to operate the system at a higher frequency. On the other hand, the operating frequency was constrained by the gain-bandwidth of the current amplifier and the impedance analyzer. For this reason, we used the maximum allowable frequency of the system to get a better response. Fifth, the admittance of the probe increased as the dimensions or the area of the probe increased, the number of fingers increased, or as the spacing between the fingers in the probe decreased. So that to get more depth penetration it is better to increase the probe area or the number of fingers for the receiver and the source.

This work demonstrated several capabilities of the capacitive probes. These capabilities include measuring thickness of a dielectric material and detecting flaws or slots in a dielectric material. In measuring the thickness, the measured admittance is affected very much by the liftoff distance. therefore, it is important to control the liftoff distance before doing the measurements to get more accurate results. Because the capacitance value depends on the dielectric constant of the dielectric material, the measured admittance varies from one material to another. To measure the thickness of the material, which is related to the measured admittance, we suggested using look-up tables or graphs for this material to determine an unknown thickness of a sample from this material. These look-up graphs can be built under various configurations for more accuracy in the measurements, but it is required to control the liftoff distance in both the look-up graphs and the present measurements of the unknown sample.

The next application we discussed was detecting a flaw in a dielectric material. We found that the capacitive probe could detect the presence of both surface and sub-surface features (such as slots). The probe could detect the surface slots better than the sub-surface ones. In the sub-surface slots, the probe did not give a good response for slots of depth more than 0.07 mil from the top. The ability of the probe to detect deeper sub-surface slots can be improved either by increasing the area of the probe or by increasing the spacing between the fingers of the probe. In this case, the penetration depth of the probe increases allowing the detection of a deeper flaw. By using the probe response, we measured the width and the length of the slots. Two attempts of measuring the slots was tried. The first technique using the raw data gave a good approximation of the dimensions. The second one used the restoration of the image by the Wiener filter. This technique needs more improvement to get better results.

Various possibilities exist for future work. In terms of modeling, future possibilities are numerous. For instance, rather than modeling the system using a simple finite difference method, one can use other complicated methods such as the finite element methods. By using an advanced method, one can model complicated systems, and get better accuracy. Up to this point, all numerical work was focused on two-dimensional features. In the future, three dimensional features can be modeled.

From all of our results, various probes can be built for various applications. In the future, one can build the electronic circuit with the probe board itself. This kind of design will decrease the effect of the parasitic capacitance of the system, because the signal is

directly amplified. Also in this case, we could make a portable probe which can be used easily.

In NDE, capacitive sensors can be used widely for dielectric materials. We can use these sensors for a variety applications. For instance, they can be used to detect the changes in dielectric constant of dielectric material, or they can detect the change of the density of this material. In the future, we may develop a new technique to measure the thickness of the dielectric material with different densities. Also we may try to develop a new technique to measure the depth of the slot using the response of the sensor.

APPENDIX A.
SOURCE CODE OF THE NUMERICAL METHOD

```
%       ************************************************************
%       Program to calculate potential function using finite
%       difference technique
%       Initialize the required parameters
%       ************************************************************
POT1=1.0;
POT2=0.0;
POT3=0.0;
ER=3.7;
ALPHA=1.5;
H=2.0;
%       ************************************************************
%       Initialize the potential matrix
%       ************************************************************
for i=1:121
    for j=1:385
        POT(i,j)=0.0;
    end
end
%       ************************************************************
%       Model the probe plates and the ground metal plate
%
%       ************************************************************
for i=111:112
    for j=67:150
        POT(i,j)=1.5+POT2;
    end
    for j=233:316
        POT(i,j)=1.5+POT1;
    end
end
i=121;
for j=1:385
    POT(i,j)=1.5+POT3;
end
%       ************************************************************
%       Begin scan the array
%       Scan from northwest corner to southeast corner
%       ************************************************************
for k=1:600
k
for ia=2:120
    for ja=2:384
        i=ia;
        j=ja;
        if(i<51)
            A=4.0/H;
            B=2.0/H;
            W=POT(i-1,j);
            X=POT(i+1,j);
            Y=POT(i,j-1);
```

```
         Z=POT(i,j+1);
         P=POT(i,j);
         POT(i,j)=FUN2(POT(i,j),A,B,W,X,Y,Z,ALPHA);
      elseif((i>=52)&(i<=70))
         A=2.0/H;
         W=POT(i-1,j);
         X=POT(i+1,j);
         Y=POT(i,j-1);
         Z=POT(i,j+1);
         POT(i,j)=FUN1(POT(i,j),A,W,X,Y,Z,ALPHA);
      elseif(i==71)
         A=2.0/H;
         B=1.0/H;
         W=POT(i-1,j);
         X=POT(i+1,j);
         Y=POT(i,j-1);
         Z=POT(i,j+1);
         POT(i,j)=FUN2(POT(i,j),A,B,W,X,Y,Z,ALPHA);
      elseif((i>=72)&(i<=90))
         A=1.0/H;
         W=POT(i-1,j);
         X=POT(i+1,j);
         Y=POT(i,j-1);
         Z=POT(i,j+1);
         POT(i,j)=FUN1(POT(i,j),A,W,X,Y,Z,ALPHA);
      elseif(i==91)
         A=1.0/H;
         B=0.5/H;
         W=POT(i-1,j);
         X=POT(i+1,j);
         Y=POT(i,j-1);
         Z=POT(i,j+1);
         POT(i,j)=FUN2(POT(i,j),A,B,W,X,Y,Z,ALPHA);
      elseif((i>=92)&(i<=110))
         A=0.5/H;
         W=POT(i-1,j);
         X=POT(i+1,j);
         Y=POT(i,j-1);
         Z=POT(i,j+1);
         POT(i,j)=FUN1(POT(i,j),A,W,X,Y,Z,ALPHA);
      elseif(i==111)
         A=0.5/H;
         B=0.5/H;
         W=POT(i-1,j);
         X=POT(i+1,j);
         Y=POT(i,j-1);
         Z=POT(i,j+1);
         POT(i,j)=FUN3(POT(i,j),A,B,W,X,Y,Z,ALPHA);
      elseif(i>111)
         A=0.5/H;
         W=POT(i-1,j);
         X=POT(i+1,j);
         Y=POT(i,j-1);
         Z=POT(i,j+1);
         POT(i,j)=FUN1(POT(i,j),A,W,X,Y,Z,ALPHA);
      end
   end
end
end
```

```
%        *****************************************************
%        Calculate the charge
%        *****************************************************
sum0h1=0.0;
sum1h1=0.0;
sum2h1=0.0;
sum1h2=0.0;
sum2h2=0.0;
sum0v1=0.0;
sum1v1=0.0;
sum2v1=0.0;
sum1v2=0.0;
sum2v2=0.0;
%        *****************************************************
%        Define the actual potential at the plates
%
%        *****************************************************
for i=111:112
     for j=67:150
          POT(i,j)=POT(i,j)-1.5;
     end
     for j=233:316
          POT(i,j)=POT(i,j)-1.5;
     end
end
i=121;
     for j=1:385
          POT(i,j)=POT(i,j)-1.5;
     end
%        *****************************************************
%        Calculate the electric field at each side of the rectangle
%
%        *****************************************************
i=114;
for j=67:150
     sum2h1=sum2h1+(POT(i,j)-POT(i+1,j));
end
for j=233:316
     sum1h1=sum1h1+(POT(i,j)-POT(i+1,j));
end
i=109;
for j=67:150
     sum2h2=sum2h2+(POT(i,j)-POT(i+1,j));
end
for j=233:316
     sum1h2=sum1h2+(POT(i,j)-POT(i+1,j));
end
i=119;
for j=1:385
     sum0h1=sum0h1+(POT(i,j)-POT(i+1,j));
end
j=65;
for i=110:113
     sum2v1=sum2v1+(POT(i,j+1)-POT(i,j));
end
```

```
j=151;
for i=110:113
    sum2v2=sum2v2+(POT(i,j+1)-POT(i,j));
end
j=231;
for i=110:113
    sum1v1=sum1v1+(POT(i,j+1)-POT(i,j));
end
j=317;
for i=110:113
    sum1v2=sum1v2+(POT(i,j+1)-POT(i,j));
end
%       ****************************************************
%       Calculate the total charge
%
%       ****************************************************
sum2h=sum2h2+sum2h1;
sum2v=sum2v2+sum2v1;
sum1h=sum1h1+sum1h2;
sum1v=sum1v1+sum1v2;
Q2=sqrt(sum2h^2+sum2v^2);
Q1=sqrt(sum1h^2+sum1v^2);
Q0=sum0h1;
save phi0210
%       ****************************************************
%       Calculate the node value when the north and south legs
%       of the star are equal but differ from the east and west legs
%       ****************************************************
function [Q]=FUN1(P,A,W,X,Y,Z,ALPHA);

if(P<=1.2)
   if (W>1.2) W=W-1.5;
        elseif (X>1.2) X=X-1.5;
        elseif (Y>1.2) Y=Y-1.5;
        elseif (Z>1.2) Z=Z-1.5;
   end
   G=A^2;
   Q=(G/(G+1))*((Y+Z)/2+(W+X)/(2*G))*ALPHA+(1-ALPHA)*P;
else
   Q=P;
end

%       ****************************************************
%       Calculate node value when north and south legs of the
%       star are different
%       ****************************************************
function [Q]=FUN2(P,A,B,W,X,Y,Z,ALPHA);

if(P<=1.2)
   if (W>1.2) W=W-1.5;
        elseif (X>1.2) X=X-1.5;
        elseif (Y>1.2) Y=Y-1.5;
        elseif (Z>1.2) Z=Z-1.5;
   end
   G=A^2;
   E=B^2;
```

```
   F=A*B;
   Q=(F/(F+1))*((Y+Z)/2+(W/(F+G))+(X/(E+F)))*ALPHA+(1-ALPHA)*P;
else
   Q=P;
end

%       ****************************************************
%       Calculate the node value when all legs of the star
%       are equal but the north leg is in dielectric material
%       ****************************************************
function [Q]=FUN3(P,A,B,W,X,Y,Z,ALPHA)

if(P<=1.2)
ER=3.7;
   if (W>1.2) W=W-1.5;
        elseif (X>1.2) X=X-1.5;
        elseif (Y>1.2) Y=Y-1.5;
        elseif (Z>1.2) Z=Z-1.5;
   end
   G=A^2;
   E=B^2;
   F=A*B;
   T=2*ER/(1+ER);
   U=2/(1+ER);
   Q=(F/(F+1))*((Y+Z)/2+(T*W/(F+G))+(U*X/(E+F)))*ALPHA+(1-ALPHA)*P;
else
   Q=P;
end
```

REFERENCES

Auld, B. A., Jefferies, S., Moulder, J. C. and Gerlitz, J. C. Semi-Elliptical Surface Flaw EC Interaction and Inversion Theory. *Review of Progress in Quantitative Nondestructive Evaluation*, Vol. 5A, D. O. Thompson and D.E. Chimenti, Plenum Press, New York. 1985, pp. 345-356.

Auld, B. A., Kenny, J. and Lookbaugh, T. Electromagnetic Sensor Arrays—Theoretical Studies. *Review of Progress in Quantitative Nondestructive Evaluation*, Vol. 5, D. O. Thompson and D.E. Chimenti, Plenum Press, New York. 1985, pp. 681-690.

Auld, B. A. and Riaziat, M. Using Capacitive Probes in Electromagnetic Nondestructive Testing. *G. L. Report 3161*. Edward L. Ginzton Laboratory, Stanford Univeristy, Stanford, California, August 1980.

Bahr, A. J. System Analysis of Eddy-Current Measurements. *Review of Progress in Quantitative Nondestructive Evaluation*, Vol. 1, D. O. Thompson and D.E. Chimenti, Plenum Press, New York. 1982, pp. 375-386.

Bahr, A. J. Electromagnetic Sensor Arrays – Experimental Studies. *Review of Progress in Quantitative Nondestructive Evaluation*, Vol. 5, D. O. Thompson and D.E. Chimenti, Plenum Press, New York. 1985, pp. 691-697.

Bahr, A. J. and Cooley, A. Analysis and Design of Eddy-Current Measurement System. *Review of Progress in Quantitative Nondestructive Evaluation*, Vol. 2A, D. O. Thompson and D.E. Chimenti, Plenum Press, New York. 1983, pp. 225-244.

Bahr, A. J. and Rosegreen, A. Inductive Sensor Arrays for NDE and Robotics. *Review of Progress in Quantitative Nondestructive Evaluation*, Vol. 6, D. O. Thompson and D.E. Chimenti, Plenum Press, New York. 1987, pp. 454-462.

Binns, K. J. and Lawrenson, P. J. *Analysis and Computation of Electric Field Problems*, 2nd eddition. Oxford. Pergamon Press. 1973.

Boast, Warren. *Principle of Electric and Magnetic Fields*. Harper and Brothers, New York. 1956.

Cardenas-Garcia, J. F., Peters, R. D. and Moulder, J. C. Finite Element Modeling of 3D Capacitive Sensors for NDE Applications. *Review of Progress in Quantitative Nondestructive Evaluation*, Vol. 10A, D. O. Thompson and D.E. Chimenti, Plenum Press, New York. 1991, pp. 927-934.

Esselle, K. P. A. P. and Stuchly, S. S. Capacitive Sensors for in-vivo Measurements of the Dielectric Properties of Biological Materials. *IEEE Transactions of Instrumentation and Measurement*, Vol. 37. 1988, pp. 101-105.

Freziger, J. H. *Numerical Method for Engineering Applications*. John Wiley, New York. 1981.

Gimple, M. *Capacitive Arrays for Robotic Sensing*. Ph.D. Dissertation, Stanford University. 1987.

Gimple, M. and Auld, B. A. Capacitive Arrays for Robotic Sensing. *Review of Progress in Quantitative Nondestructive Evaluation*, Vol. 6A, D. O. Thompson and D.E. Chimenti, Plenum Press, New York. 1987, pp. 737-743.

Gimple, M. and Auld, B. A. Position and Sample Feature Sensing with capacitive array probes. *Review of Progress in Quantitative Nondestructive Evaluation*, Vol. 7, D. O. Thompson and D.E. Chimenti, Plenum Press, New York. 1988, pp. 1-7.

Gimple, M. and Auld, B. A. *Variable Geometry Capacitive Probes for Multipurpose Sensing*. Res. Nondestr. Eval., Springer-Verlag New York. 1989, pp 111-132.

Gonzalez, Rafael C. and Wood, Richard. *Digital Image Processing*. Addison-Wesley, Reading, MA. 1993.

Heyligher, P. R., Moulder, J. C. and Nakagawa, N. Simulation of Capacitive Sensors Using Finite and Infinite Elements. *International Journal of Numerical Modeling*. John Wiley and Sons, New York. Vol. 2. 1989, pp. 117-129.

Heyligher, P. R., Moulder, J. C., Shull, P. J., Gimple, M., and Auld, B. A. Numerical Modeling of Capcitive Array Sensors Using the Finite Element Method. *Review of Progress in Quantitative Nondestructive Evaluation*, Vol. 7A, D. O. Thompson and D.E. Chimenti, Plenum Press, New York. 1988, pp. 501-508.

Kong, J. A. *Electromagnetic Wave Theory*. John Wiley, New York. 1986.

Lapidus, L. and Pinder, G. *Numerical Solutions of Partial Differential Equations in Science and Engineering*. John Wiley, New York. 1982.

Libby H. L. *Introduction to Electromagnetic Nondestructive Methods*. Wiley-Interscience, New York. 1971.

Matiss, I. G. A New Capacitive Technique for Quality Control of Nonmetallic Materials and Structures. *Material Evaluation*. March, 1982, pp 128-156.

Ramo, S., Whinnery, J. R. and Van Duzer, T. *Fields and Waves in Communication Electronics*, John Wiley, New York. 1984.

Sadiku, Matthew N. O. *Elements of Electromagnetics*. Saunder College, a Division of Halt, Rienhart and Winston, Orlando, Florida. 1989.

Shull, P. J., Moulder, J. C., Heyligher, P. R., Gimple, M., and Auld, B. B. Applications of Capacitive Array Sensors to Nondestructive Evaluation. *Review of Progress in Quantitative Nondestructive Evaluation*, Vol. 7A, D. O. Thompson and D.E. Chimenti, Plenum Press, New York. 1988, pp. 517-523.

Shull, P. J., Clark, A. V., Heyligher, P. R., Moulder, J. C., and Auld, B. B. Characterization of Capacitive Array for NDE Applications. *Res. Nondestr. Eval.*, Vol.2. 1990, pp. 11-27.

Vendelin, G. D. *Design of Amplifiers and Oscillators by S-Parameter Method*, John Wiley, New York. 1982.